

AD-A048 669

NAVAL POSTGRADUATE SCHOOL MONTEREY CALIF
THE EFFECTS OF VELOCITY ON CORROSION OF GALVANIC COUPLES IN SEA--ETC(U)
SEP 77 G A STORM

F/G 13/10

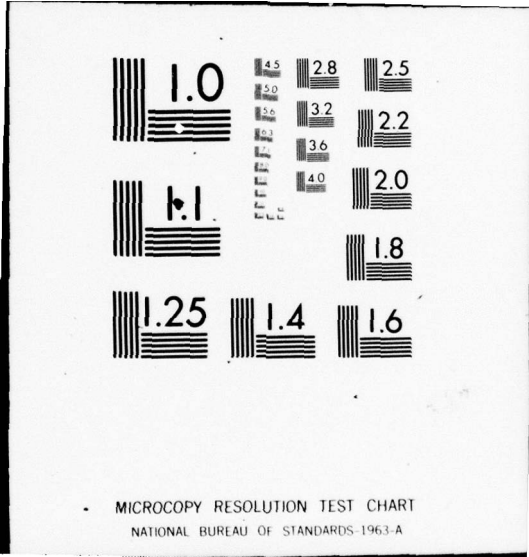
UNCLASSIFIED

NL

172

ADAO48 669





AD A 0 48669

2

NAVAL POSTGRADUATE SCHOOL

Monterey, California



9 Master's **THESIS**

6 THE EFFECTS OF VELOCITY ON CORROSION OF GALVANIC COUPLES IN SEAWATER.

by

10 Gary Alan/Storm 12 139 p.

11 Sep 1977

Thesis Advisor: A. J. Perkins

Approved for public release; distribution unlimited.

AD No.
DDC FILE COPY

DDC
RECEIVED
JAN 17 1978
B

251 450

mt.

REPORT DOCUMENTATION PAGE		READ INSTRUCTIONS BEFORE COMPLETING FORM
1. REPORT NUMBER	2. GOVT ACCESSION NO.	3. RECIPIENT'S CATALOG NUMBER
4. TITLE (and Subtitle) THE EFFECTS OF VELOCITY ON CORROSION OF GALVANIC COUPLES IN SEAWATER		5. TYPE OF REPORT & PERIOD COVERED Master's Thesis September 1977
7. AUTHOR(s) Gary Alan Storm		6. PERFORMING ORG. REPORT NUMBER
9. PERFORMING ORGANIZATION NAME AND ADDRESS Naval Postgraduate School Monterey, California 93940		8. CONTRACT OR GRANT NUMBER(s)
11. CONTROLLING OFFICE NAME AND ADDRESS Naval Postgraduate School Monterey, California 93940		10. PROGRAM ELEMENT, PROJECT, TASK AREA & WORK UNIT NUMBERS
14. MONITORING AGENCY NAME & ADDRESS (if different from Controlling Office)		12. REPORT DATE September 1977
		13. NUMBER OF PAGES
		15. SECURITY CLASS. (of this report) Unclassified
		15a. DECLASSIFICATION/DOWNGRADING SCHEDULE
16. DISTRIBUTION STATEMENT (of this Report) Approved for public release; distribution unlimited.		
17. DISTRIBUTION STATEMENT (of the abstract entered in Block 20, if different from Report)		
18. SUPPLEMENTARY NOTES		
19. KEY WORDS (Continue on reverse side if necessary and identify by block number)		
20. ABSTRACT (Continue on reverse side if necessary and identify by block number) The effects of velocity on the corrosion of galvanic couples (70/30 Cu-Ni/plain carbon steel and K-Monel/plain carbon steel) in synthetic seawater electrolyte were studied. A unique experimental apparatus was designed and built, employing a foil-shaped specimen holder rotating in a tank, and the hydrodynamic flow conditions within the test system were carefully characterized. Galvanic current measurements were taken at various velocities and corrosion product formation and dissolution		

patterns were studied. A model is developed which considers both hydrodynamic and electrochemical boundary layer effects, and the role of the polarization characteristics of the individual metals is discussed. The development of corrosion products, protective oxide films, and surface metal removal are discussed. A corrosion product growth/removal cycle and consequent surface metal removal sequence is hypothesized under dynamic conditions.

ACCESSION for		
NTIS	White Section	<input checked="" type="checkbox"/>
DDC	Buff Section	<input type="checkbox"/>
UNANNOUNCED		<input type="checkbox"/>
JUSTIFICATION _____		
BY _____		
DISTRIBUTION/AVAILABILITY CODES		
Dist.	AVAIL. and/or	SPECIAL
A		

Approved for public release; distribution unlimited

The Effects of Velocity
on Corrosion of
Galvanic Couples
in Seawater

by

Gary Alan Storm
Lieutenant, United States Navy
B.S., United States Naval Academy, 1968

Submitted in partial fulfillment of
the requirements for the degree of

MASTER OF SCIENCE IN MECHANICAL ENGINEERING

from the
NAVAL POSTGRADUATE SCHOOL
September 1977

Author

G. A. Storm

Approved by:

Jeff Perkins Thesis Advisor

Allen E. Fuhs
Chairman, Department of Mechanical Engineering

Robert L. ...
Dean of Science and Engineering

ABSTRACT

The effects of velocity on the corrosion of galvanic couples (70/30 Cu-Ni/plain carbon steel and K-Monel/plain carbon steel) in synthetic seawater electrolyte were studied. A unique experimental apparatus was designed and built, employing a foil-shaped specimen holder rotating in a tank, and the hydrodynamic flow conditions within the test system were carefully characterized. Galvanic current measurements were taken at various velocities and corrosion product formation and dissolution patterns were studied. A model is developed which considers both hydrodynamic and electrochemical boundary layer effects, and the role of the polarization characteristics of the individual metals is discussed. The development of corrosion products, protective oxide films, and surface metal removal are discussed. A corrosion product growth/removal cycle and consequent surface metal removal sequence is hypothesized under dynamic conditions.

TABLE OF CONTENTS

I. INTRODUCTION	15
A. GALVANIC CORROSION	15
B. CORROSION VARIABLES	23
1. Electrolyte pH	24
2. Temperature	24
3. Marine Organisms	25
4. Salinity	25
5. Time	26
6. Mechanical Factors	26
7. Ohmic Factors	27
8. Solid Structure Stability	27
9. Thermodynamic Feasibility	28
10. Area Effect	30
11. Metallic Structure	30
C. INFLUENCE OF VELOCITY OF THE ELECTROLYTE	30
D. THE KINEMATICS OF THE FLUID FLOW	33
E. PREVIOUS RESEARCH	38
II. EXPERIMENTAL PROCESS	49
A. APPARATUS	49
1. Static Exposure Tank	49
2. Dynamic Exposure Assembly	51
3. Scanning Electron Microscope and X-ray Analyzer	61

B.	PROCEDURE	64
1.	Static Exposures	70
2.	Dynamic Flow Characterization	72
3.	Dynamic Exposures	80
III.	EXPERIMENTAL RESULTS AND DISCUSSION	86
A.	CHARACTERIZATION OF SINGLE METAL CORROSION BEHAVIOR	86
1.	Polarization Characteristics	86
2.	Single Metal Exposures	89
B.	PREDICTIONS OF COUPLED METAL BEHAVIOR	97
1.	Expected Effects of Velocity and Coupling on Polarization of Test Metals	97
2.	Expected Effects of Velocity and Coupling on Corrosion Distribution and Morphology	99
C.	COUPLES	100
1.	Electrical Couples	100
a.	Galvanic Current Measurements	100
b.	Surface Observations	107
c.	Interpretations	113
2.	Proximate Couples	117
D.	SUMMARY OF RESULTS	129
1.	Static vs. Dynamic Exposures	129
2.	Electrical vs. Proximate Couples	130
IV.	CONCLUSIONS	132
V.	RECOMMENDATIONS	134
	APPENDIX A: Preparation of Artificial Seawater	135
	LIST OF REFERENCES	136
	INITIAL DISTRIBUTION LIST	139

LIST OF TABLES

1. Electromotive-Force Series [2] (77°F).....	19
2. Galvanic Potentials in Flowing Seawater [4] (Velocity = 13 ft per sec except where noted).....	20
3. Corrosion of Metals by Seawater moving at Different Velocities [15]	34
4. Galvanic Corrosion Rates as a Function of Velocity for Aluminum Hull Alloys Uncoated [18].....	46
5. Spectrographic Analysis of Cu-Ni 70/30 Specimens	66
6. Spectrographic Analysis of K-Monel Specimens	67
7. Thermo-Mechanical History of Cu-Ni 70/30 Thermo-Mechanical History of K-Monel	68
8. Experimentally Determined Values of Turbulence Intensity over the Foil Surface (5 ft/sec = 1.52 m/sec and 10 ft/sec = 3.02 m/sec)	79
9. Experimental Parameters	84
Experimental Parameters, cont	85

LIST OF FIGURES

1. Corrosion Cell formed by two Dissimilar Metals [2]	16
2. General Polarization Diagram	22
3. Simplified Potential - pH diagram for the Fe-H ₂ O System (M. Pourbaix, "Atlas of Electrochemical Equilibria in Aqueous Solutions", p. 307-321, Pergamon Press, New York, 1966) [5].....	29
4. The Effects of Velocity on Corrosion Rate of Steel by Seawater	32
5. Apparatus to Rotate Specimen Discs in Seawater. Test Specimens Mounted on Periphery of Large Discs in a Test for Erosion Corrosion. Apparatus for Aspirator Type Jet Tests. Equipment used in H.R. Copson's Study [14].....	39
6. Nozzle Assembly [15].....	41
7. High Speed Water Wheel [18] (Test area is 6 in x 18 in).....	44
8. Specimen Designs for (a) Zero Velocity Tests, (b) Wedge Specimens, and (c) Small Area Specimens [18].....	45
9. Experimental Apparatus showing Dynamic Exposure Tank, Rotating Foil Assembly, Digital Voltmeter, Digital Counter, Strip Chart Recorder, and Motor Controller	50
10. Static Exposure Stand with Single Specimen Mounted in Place	52
11. Detail of Specimen-Carrying Foil (1 in = 2.54 cm).....	53
12. Detail of Vertical and Horizontal Support Arm	55
13. Illustration of the Location of Specimens when Mounted in Foil	56
14. Section AA: Detail of Specimen Hole	57
15. Detail showing Platinum Discs used in Electrically Connecting Mounted Specimens	58
16. Slip Ring and Brush Arrangement	60

17.	Cambridge Model S4-10 Scanning Electron Microscope (SEM) and Princeton-Gamma-Tech PGT-1000 X-ray Analyzer.....	62
18.	Plain Carbon Steel normalized by Austenitizing at approximately 900°C and air cooled, 400x.....	65
19.	Scanning Electron Microphotograph of Initial Polished Specimen Surface, 580x.....	69
20.	Illustration of Specimens, Couple Types and Tool used for Couples. From left-to-right, top-to-bottom: Torque Wrench used to apply standard Torque, Unmounted Specimens, Couple Specimens in Special Aluminum Ring showing system used to apply Torque, finished Galvanic Couple, finished Single Metal Mount (Centerline), finished Single Metal Mount (Inboard/Outboard).....	71
21.	Foil with Hot-Film Probe mounted over Centerline Hole.....	74
22.	Detail of a Hot-Film Probe.....	76
23.	Plots of \sqrt{V} vs. e^2 for each Specimen position on the Foil (Note extrapolated value for V_0 on each plot).....	78
24.	Foil configuration for Dynamic Exposure run.....	81
25.	70/30 Cu-Ni/PCS Polarization Curves.....	87
26.	K-Monel/PCS Polarization Curves.....	88
27.	(a) Surface of PCS Specimen after 24 hours exposure, Static, 610x. (b) Surface of PCS Specimen at 24 hours exposure, 5 ft/sec (1.52 m/sec), 10x.....	91
28.	(a) Surface of PCS Specimen after 24 hours exposure at 10 ft/sec (3.02 m/sec), 130x. (b) Surface of PCS Specimen after 24 hours exposure at 10 ft/sec (3.02 m/sec), 1210x. Note the "Mud-Cracking" appearance of the Corrosion Product Formation.....	92
29.	(a) Surface of PCS Specimen after 24 hours exposure at 5 ft/sec (1.52 m/sec), 115x. (b) Cleaned Surface of PCS Specimen after 24 hours exposure at 5 ft/sec (1.52 m/sec), 240x.....	95
30.	(a) Cleaned Surface of PCS Specimen exposed for 24 hours at 10 ft/sec (3.02 m/sec), 235x. (b) Clean Surface of PCS Specimen exposed for 24 hours at 10 ft/sec (3.02 m/sec), 560x. Note the pits within the pits.....	96

31.	Plot of Current Density vs. Time for 70/30 Cu-Ni/PCS Couple (5 ft/sec = 1.52 m/sec and 10 ft/sec = 3.02 m/sec)	101
32.	Plot of Current Density vs. Time for K-Monel Couple (5 ft/sec = 1.52 m/sec and 10 ft/sec = 3.02 m/sec).....	102
33.	Plot of Velocity vs. MPY for 70/30 Cu-Ni/PCS Couple	104
34.	Plot of Velocity vs. MPY for K-Monel/PCS Couple	105
35.	(a) PCS Surface of 70/30 Cu-Ni/PCS Elec. Couple exposed at 5 ft/sec (1.52 m/sec) for 24 hours, 600x. (b) PCS Surface of 70/30 Cu-Ni/PCS Elec. Couple exposed at 10 ft/sec (3.02 m/sec) for 24 hours, 550x	109
36.	(a) Cleaned Surface of PCS Half of 70/30 Cu-Ni/PCS Elec. Couple exposed at 5 ft/sec (1.52 m/sec) for 24 hours, 610x. (b) Cleaned Surface of PCS Half of 70/30 Cu-Ni/PCS Elec. Couple exposed at 10 ft/sec (3.02 m/sec) for 24 hours, 1225x	110
37.	(a) PCS Surface of K-Monel/PCS Elec. Couple exposed at 5 ft/sec (1.52 m/sec) for 24 hours, 225x. (b) PCS Surface of K-Monel/PCS Elec. Couple exposed at 10 ft/sec (3.02 m/sec) for 24 hours, 1225x	111
38.	(a) Cleaned Surface of PCS Half of K-Monel/PCS Elec. Couple exposed at 5 ft/sec (1.52 m/sec) for 24 hours, 225x. (b) Cleaned Surface of PCS Half of K-Monel/PCS Elec. Couple exposed at 10 ft/sec (3.02 m/sec) for 24 hours, 240x	112
39.	(a) PCS Half of K-Monel/PCS Elec. Couple exposed at 5 ft/sec (1.52 m/sec) for 24 hours, 10x. (b) PCS Half of K-Monel/PCS Elec. Couple exposed at 10 ft/sec (3.02 m/sec) for 24 hours, 10x	114
40.	(a) Cleaned Surface of PCS Half of 70/30 Cu-Ni/PCS Proximate Couple, Static Exposure for 30 minutes. Note onset of pitting corrosion, 240x. (b) Cleaned Interface of K-Monel/PCS Proximate Couple, Static Exposure for 30 minutes. Note pitting corrosion not as severe as in 39(a), 240x	118
41.	(a) Interface of 70/30 Cu-Ni/PCS Proximate Couple (PCS on left), Static Exposure for 30 minutes, 225x. (b) Interface of 70/30 Cu-Ni/PCS Proximate Couple (PCS on left), 10 ft/sec (3.02 m/sec) for 30 minutes, 130x	119

42. (a) Surface of PCS Half of 70/30 Cu-Ni/PCS Proximate Couple, Static Exposure for 24 hours, 550x. (b) Cleaned Surface of PCS Half of 70/30 Cu-Ni/PCS Proximate Couple, Static Exposure for 24 hours, 240x....121
43. (a) Cleaned Surface of PCS Half of K-Monel/PCS Proximate Couple, Static Exposure for 24 hours, 600x. (b) Cleaned Surface of PCS Half of K-Monel/PCS Elec. Couple, Static Exposure for 24 hours, 600x....122
44. (a) Cleaned Surface of PCS Half of 70/30 Cu-Ni/PCS Proximate Couple, exposed at 5 ft/sec (1.52 m/sec) for 30 minutes, 600x. (b) Cleaned Surface of PCS Half of K-Monel/PCS Proximate Couple, exposed at 10 ft/sec (3.02 m/sec) for 30 minutes, 600x.....124
45. (a) Surface of PCS Half of 70/30 Cu-Ni/PCS Proximate Couple exposed at 5 ft/sec (1.52 m/sec) for 24 hours, 20x. (b) Cleaned Surface of PCS Half of 70/30 Cu-Ni/PCS Proximate Couple exposed at 5 ft/sec (1.52 m/sec) for 24 hours, 600x.....125
46. (a) Surface of PCS Half of 70/30 Cu-Ni/PCS Proximate Couple exposed at 10 ft/sec (3.02 m/sec) for 24 hours, 250x. (b) Cleaned Surface of Interface between 70/30 Cu-Ni and PCS in Proximate Couple exposed at 10 ft/sec (3.02 m/sec) for 24 hours, 235x.....126
47. (a) Surface of PCS Half of K-Monel/PCS Proximate Couple exposed at 5 ft/sec (1.52 m/sec) for 24 hours, 25x. (b) Cleaned Surface of PCS Half of K-Monel/PCS Proximate Couple exposed at 5 ft/sec (1.52 m/sec) for 24 hours, 60x.....127
48. (a) Surface of PCS Half of K-Monel/PCS Proximate Couple exposed at 10 ft/sec (3.02 m/sec) for 24 hours, 25x. (b) Cleaned Interface of K-Monel/PCS Proximate Couple exposed at 10 ft/sec (3.02 m/sec) for 24 hours, 125x.....128

LIST OF SYMBOLS

A	Arrhenius constant
a_{H^+}	hydrogen ion activity
$a_{\text{Q}}^{\text{q}}, a_{\text{R}}^{\text{r}}$, etc	elemental ionic activities
	density
δ_{d}	diffusion boundary layer thickness
μ	dynamic viscosity
δ_{h}	hydrodynamic boundary layer thickness
E	electrode potential
E°	standard reference potential
E_{corr}	corrosion potential of couple
e	D.C. bridge voltage
e^{r}	RMS voltage
emf	electromotive force
exp	exponential function
F	Faraday constant (96,500 coulombs)
$\text{Fe}(\text{OH})_3$	ferric hydroxide (rust)
i	current density
i_{corr}	corrosion current density
ipy	inches per year
ν	kinematic viscosity
l	liter
ln	natural logarithm
log	logarithm (base 10)
M	metal

M^+	metal ion
mA	milliamp
ml	milliliter
mmho	millimho
mpy	mils per year
μA	microampere
μm	micrometer
mv	millivolts
n	number of electrons in cell reaction (faraday/mole)
N·cm	Newton centimeters
nm	nanometers
pH	standard hydrogen potential
Q	activation energy
R	universal gas constant (8.314 joules/degree·mole)
Re	Reynolds number
rpm	revolutions per minute
Sc	Schmidt number
S.C.E.	saturated calomel electrode
SEM	scanning electron microscope
T	temperature
U	corrosion rate
u	fluid velocity
V	foil velocity
V_0	extrapolated value from plot of \sqrt{V} vs. e^2
$\frac{v'}{V}$	turbulence intensity
v	volts

ACKNOWLEDGEMENT

The author wishes to express his sincere gratitude for assistance from Professor Jeff Perkins, as the faculty advisor, throughout the course of this study. His suggestions during the final editing phase were especially helpful toward the development of a clear and concise manuscript.

Numerous consultations with Professor Turgut Sarpkaya helped to shed light on several complex fluid dynamic problems.

Mechanical Engineering Department Technician, George Bixler, warrants special praise for the high quality craftsmanship and invaluable advice in construction of the testing apparatus, while technician Tom Christian assisted and helped develop the electronic instrumentation used during experimentation.

Last but certainly not least, the author is indebted to Material Science Laboratory Technician, Roy Edwards, for his untiring assistance in the setup of all experimental equipment and his devotion to upkeep of microscopy equipment.

I. INTRODUCTION

A. GALVANIC CORROSION

Corrosion can be generally defined as the destruction of a metal by chemical or electrochemical reaction with its environment. This represents the view most engineers would attach to the word, and since it is derived from the Latin verb "CORRODO" - to gnaw to pieces, to wear away - it is superficially correct [1].

Nearly all metals are inherently unstable and it is their natural tendency to seek self-destruction by reacting with their environment to attain a state of lower energy. The result of this reaction is the formation of a corrosion product.

The corrosion of metals can generally be divided into two classes: 'dry' and 'wet'. This paper is concerned with the latter, in which the interface is metal/solution. The electrochemical corrosion rate of a metal frequently can be changed by the properties of the corrosion products. An example is the passivation of zinc anodes in a marine environment. The types of corrosion that have been defined and studied are far too numerous to be discussed here. Coverage of only one aspect of the electrochemical corrosion reaction will be treated in detail, namely galvanic corrosion.

When two dissimilar metals are in contact with each other (or otherwise electrically connected) and exposed to a conductive fluid, a potential is set up between these two metals and a current flows, as represented in Figure 1. Corrosion of the less-corrosion-resistant metal is usually increased and attack of the more-resistant metal is

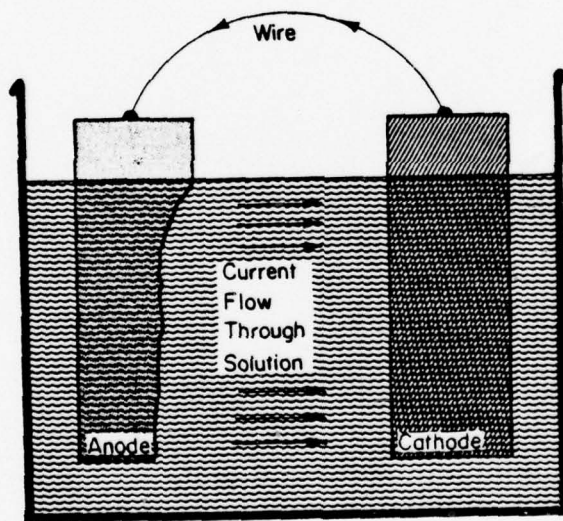


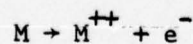
FIGURE 1
CORROSION CELL FORMED BY TWO
DISSIMILAR METALS [2].

decreased, as compared to the behavior of the metals when they are not in contact. The less-resistant metal becomes anodic and the more-resistant metal cathodic [2]. "Oxidation" is said to occur at the anode, and "reduction" at the cathode. Because of the electric currents and dissimilar metals involved, this form of corrosion is called galvanic, or two-metal, corrosion. It is electrochemical in nature and the current that flows is called the galvanic current. The driving force for the current flow and corrosion is the potential or voltage developed between the two metals. This reaction can occur only if the corroding metal passes into solution, during which process the atom loses one or more electrons and becomes an ion. A corrosion reaction is always accompanied by a flow of electricity from one metallic site to another through an electrolytic solution.

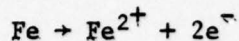
A cell's electromotive force (emf) is the algebraic sum of its electrode potentials. The Nernst equation [3]:

$$E = E^{\circ} - \frac{RT}{mF} \ln \frac{a_Q^q \cdot a_R^r}{a_L^l \cdot a_M^m}$$

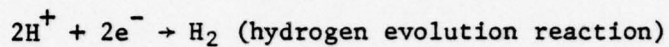
is used to calculate the potential of each electrode and ultimately the cell emf. Oxidation of an anode can be written in general terms as:



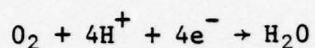
where M is the metal dissolved. The resulting ions enter into solution. The reaction for an iron anode can be written as:



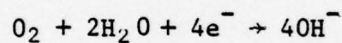
There are three reactions of particular importance that occur at cathodes, in acidic solutions;



or



, while in alkaline or neutral solutions:



[1]. This latter reaction is known as the 'oxygen reduction reaction' and predominates when iron is corroding in seawater.

Sometimes when the products of the anode and the cathode meet they enter into further mutual reactions. A well-known example is the reaction of hydroxyl ions from the cathodic process with the ferrous ions of the anodic dissolution. This occurs when steel corrodes in seawater; the result - rust.

The electromotive-force series shown in Table 1 and the galvanic potentials of metals in flowing seawater shown in Table 2 are examples of the potentials set up when dissimilar metals are coupled or placed in electrical contact with each other. In general, the potentials of base metals and their alloys are reasonably well-correlated in such series.

TABLE 1

Element	Electrode Reaction	Standard Electrode Potential, v ^a
(Active end)		
Sodium	$\text{Na} \rightarrow \text{Na}^+ + e$	-2.712
Magnesium	$\text{Mg} \rightarrow \text{Mg}^{++} + 2e$	-2.34
Beryllium	$\text{Be} \rightarrow \text{Be}^{++} + 2e$	-1.70
Aluminum	$\text{Al} \rightarrow \text{Al}^{+++} + 3e$	-1.67
Manganese	$\text{Mn} \rightarrow \text{Mn}^{++} + 2e$	-1.05
Zinc	$\text{Zn} \rightarrow \text{Zn}^{++} + 2e$	-0.762
Chromium	$\text{Cr} \rightarrow \text{Cr}^{+++} + 3e$	-0.71
Iron	$\text{Fe} \rightarrow \text{Fe}^{+++} + 3e$	-0.44
Cadmium	$\text{Cd} \rightarrow \text{Cd}^{++} + 2e$	-0.402
Cobalt	$\text{Co} \rightarrow \text{Co}^{++} + 2e$	-0.277
Nickel	$\text{Ni} \rightarrow \text{Ni}^{++} + 2e$	-0.250
Tin	$\text{Sn} \rightarrow \text{Sn}^{++} + 2e$	-0.136
Lead	$\text{Pb} \rightarrow \text{Pb}^{++} + 2e$	-0.126
Hydrogen	$\text{H} \rightarrow 2\text{H}^+ + 2e$	0.000 (reference)
Copper	$\text{Cu} \rightarrow \text{Cu}^{++} + 2e$	+0.345
Copper	$\text{Cu} \rightarrow \text{Cu}^+ + e$	+0.522
Silver	$\text{Ag} \rightarrow \text{Ag}^+ + e$	+0.800
Platinum	$\text{Pt} \rightarrow \text{Pt}^{++} + 2e$	+1.2
Gold	$\text{Au} \rightarrow \text{Au}^{+++} + 3e$	+1.42
(Noble end)		

ELECTROMOTIVE-FORCE SERIES [2]
(77°F)

TABLE 2

METAL OR ALLOY	TEMPERATURE, °C	VOLT' VS. SATURATED CALOMEL
Zinc	26	-1.03
Mild steel	24	.61
Gray cast iron	24	.61
Austenitic cast iron ^a	14	.47
Copper	24	.36
Admiralty brass	24.6	.36
Gunmetal	24	.31
Aluminum brass	24.6	.29
Admiralty brass	11.9	.30'
Lead-Tin Solder (50-50)	17	.28
90/10 copper-nickel alloy (1.4 Fe)	6	.24
90/10 copper-nickel alloy (1.4 Fe)	17	.29
90/10 copper-nickel alloy (1.5 Fe)	24	.22
70/30 copper-nickel alloy (0.51 Fe)	6	.22
70/30 copper-nickel alloy (0.51 Fe)	17	.24
70/30 copper-nickel alloy (0.51 Fe)	26.7	.20
Nickel-copper alloy 400	22	.11
Nickel	25	.10'
Titanium	27	-.10
Graphite	24	+.25
Platinum	18	+.26'

Notes: 1. Seawater velocity = 7.8 ft. per sec.
 2. Austenitic nickel ductile cast iron Type D-2 (3.0 C, 1.5-3 Si, 0.7-1.25 Mn, 18-22 Ni, 1.75-2.75 Cr).
 3. All values negative vs. saturated calomel reference electrode except those for graphite and platinum.

GALVANIC POTENTIALS IN FLOWING SEAWATER [4]
 (VELOCITY = 13 ft per sec EXCEPT WHERE NOTED)

A distance effect also enters the picture. The extent of distance from the junction to which appreciable galvanic corrosion occurs is dependent on the conductivity of the electrolyte, the path of the current flow, and the resistance of the circuit. As the conductivity is increased, corrosion extends farther away from the junction.

Also, the potential generated by a galvanic cell consisting of dissimilar metals typically changes with time. The potential change causes a flow of current and corrosion to occur at the anode, the amount of corrosion being directly proportional to the current flow. As corrosion progresses, reaction products are generated at the anode and cathode, and there is a reduction in the rate at which corrosion continues; the potential of the anode tends to drift toward that of the cathode and vice versa. These changes in potential are referred to as "polarization". Polarization is defined as the displacement of electrode potential resulting from the effects of current flow, measured with respect to either equilibrium (reversible) or steady-state potentials [2]. A general polarization diagram is illustrated in Figure 2.

In most corrosion reactions, cathodic polarization is more predominant; however, the degree of cathodic polarization can be quite different for various metals and alloys. It is therefore necessary to know something about their polarization characteristics before predicting the extent of galvanic corrosion for a given couple under a given set of conditions.

There are a number of procedures or practices that can be used to combat and minimize galvanic corrosion. Among these are [2]:

- (1) Select metals as close together as possible in the galvanic series.

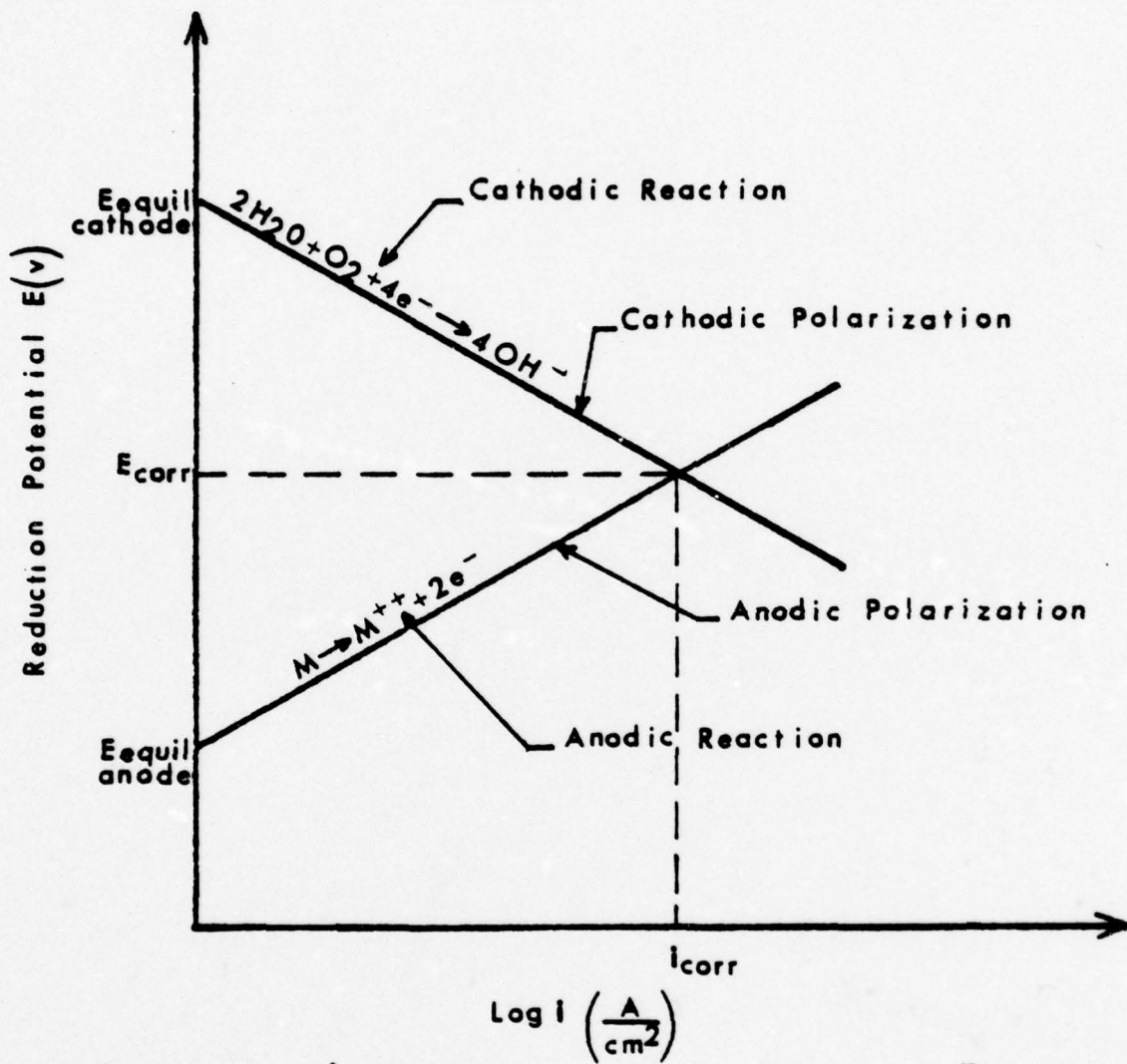


FIGURE 2

GENERAL POLARIZATION DIAGRAM

(2) Avoid adverse area combinations between anode and cathode (large cathode, small anode); this problem will be discussed in a later section.

(3) Insulate dissimilar metals.

(4) Add chemical inhibitors to the corrosive solutions if possible.

(5) Install relatively small replaceable sections of the less noble material at joints and increase its thickness in such regions.

(6) Keep the dissimilar metals physically as far apart as possible if they cannot be insulated from one another.

(7) Avoid joining materials well apart in the galvanic series by threaded connection.

Finally, it must be stressed that any galvanic series simply indicates the tendency of the more anodic member of the couple to corrode, in terms of the probably emf of the corrosion cell formed; such series do not predict the rate at which attack occurs. "The rate depends on the current that flows in the cell" [1].

B. CORROSION VARIABLES

Seawater is an extremely complex, heterogeneous solution. It contains a large amount and diversity of dissolved material, dissolved gases, and biological matter. Although the effect of electrolyte velocity on corrosion rates was the primary purpose of this research, it is necessary to understand that corrosion is a function of several variables other than velocity. The most important of these are pH, temperature, marine organisms and salinity. Other variables such as time, mechanical factors, ohmic factors, solid solution feasibility, area effect and metallic structure also play a role in determination of

corrosion rates and mechanisms [5]. All of these variables are explained in some detail below in the interest of clarity as well as to explain how and if they were controlled during experimentation.

1. Electrolyte pH

The pH value of a solution is represented by

$$\text{pH} = -\log [\text{H}^+]$$

the negative value of the logarithm of the hydrogen ion concentration. The pH value influences the corrosion rate in a varied manner, depending on whether the metal is noble, and whether its oxide is soluble in acid or in both acid and alkali. Noble metals such as platinum and gold are stable in acid or alkaline solutions and their corrosion behavior is independent of pH. At the other end of the scale metals such as zinc and aluminum have a parabolic dependence of rate of corrosion on pH, dissolving rapidly in both acid and alkalis [6].

In the marine environment values of pH remain relatively constant, with average values of 8.0 to 8.3 near the seawater surface [7]. For the purposes of experimentation in this study, synthetic seawater pH values were kept within the above range.

2. Temperature

For most electrochemical reactions, the reaction rate increases with increasing temperature. This increased reaction rate can be expressed mathematically by the Arrhenius Rate equation:

$$U = A \cdot \exp - (Q/RT)$$

where U is the corrosion rate and T is the absolute temperature [5]. Temperature affects the corrosion rate of metals in electrolytes primarily through its effect on factors which control the diffusion rate of oxygen. For every 30°C rise in temperature, corrosion rates generally double when they are controlled by the diffusion of oxygen [3]. When the temperature reaches 80°C the rate then falls off in an open system because the decrease in oxygen solubility becomes the dominant factor. Temperature can also effect the corrosion rate by changing the nature of the corrosion film.

Thus the effect of temperature on the corrosion rate of metals is quite complicated, and small temperature changes can have a marked effect on corrosion rates. The temperature of the synthetic seawater in the present experiments was kept at 20°C ± 1°C.

3. Marine Organisms

It is estimated that as much as one third of all corrosion may be traced to the destructive role played by micro-organisms [2]. Many micro-organisms adhere to metal surfaces, causing discontinuities which can result in localized corrosion of the remaining uncovered metal. Additionally, many micro-organisms can cause an accumulation of acids and dissolved gases at or near the surface of the metal, thereby speeding up the corrosion process. Another natural consequence of micro-organisms collecting on the metal surface is the formation of an oxygen concentration cell, associated with the organic buildups. The use of synthetic seawater in the present experiments eliminated the effect of organisms as a corrosion variable.

4. Salinity

The total salt content (salinity) of seawater may show variations

with geography, depth and temperature, however, these variations are small in the ocean environment. The average salinity of seawater is considered to be about 34 parts per thousand [8]. Thus in the natural seawater environment, the normally small variation encountered exerts a minimum affect on the corrosion rates of metal. This factor was kept constant during experimentation by the addition of small amounts of distilled water as electrolyte evaporated.

5. Time

Regardless of the corrosion mechanism, the amount of corrosion is very definitely time dependent. In these experiments, time was a variable, and was very closely controlled.

6. Mechanical Factors

It is possible to differentiate five distinct characteristic causes of the deterioration of metals by the action of the mechanical factor. They are [9]:

- (1) General corrosion of a stressed metal.
- (2) Corrosion cracking.
- (3) Corrosion fatigue.
- (4) Cavitation erosion.
- (5) Corrosion-erosion.

All of the above listed mechanisms involve the addition of energy to the metal, and tend to lower the thermodynamic stability or cause a breach in the continuity of a passive and protective film [5].

The action of induced or residual stresses in conjunction with a corrosive media can promote cracking of metals since resistance to cracking is destroyed by the corrosive action. A complete thermomechanical history of the test materials used in this research was obtained and is detailed in a later section.

7. Ohmic Factors

Metals possess an electric conductivity thousands and tens of thousands times higher than that of typical electrolytes. Therefore it can be stated that the electrical resistance of a galvanic cell primarily exists in the current path through the electrolyte. Factors to be considered when considering the internal resistance of a galvanic cell are the specific resistivity of the electrolyte, the ratio of anodic-to-cathodic areas, and the geometric configuration and relative position of the regions [5]. During these experiments the conductivity of the electrolyte was maintained at a fairly constant value, the area ratio was held constant, and the relative positions of the specimens to each other was the same at all times, with several different configurations being investigated.

8. Solid Solution Stability

The composition of alloys of course determines to some extent their general corrosion resistance. If an active metal or an alloy composed of active elements is under consideration, its corrosion resistance is due chiefly to its ability for forming and maintaining a protective film. It is known that a gradual increase in the concentration of the noble component in an alloy will cause the chemical stability to also increase gradually [5]. It is stated by Uhlig that regardless of environment, it is generally necessary to add between 25 and 50 atomic percent of the more noble component to the solid solution to ensure some corrosion resistance [3]. However, it is not mandatory that one of the components of a solid solution be a noble metal. It is sufficient if it is stable in the given corrosive environment. Alloying is not beneficial in all cases. Parting or dezincification is a type of corrosive attack

resulting from the addition of alloying elements, Selective dissolution of one of the solid solution elements results in a porous matrix rendered weak and prone to early failure.

9. Thermodynamic Feasibility

As stated earlier, nearly all metals are inherently unstable and as a result tend to react with their environments to reach a state of lower energy. Their spontaneous tendency to return to their stable state is the basic cause of the corrosion of metals [1].

The thermodynamic tendency for electrochemical corrosion is simply a prerequisite for the galvanic corrosion reaction to actually occur. If the cell proceeds at a very slow rate, then the metal will be for all practical purposes inert. For example, if corrosion product on the metal surface forms a continuous film which isolates the metal from its corrosive environment, then the rate of corrosion will be impeded. The above discussion leads us to formulate a criterion for corrosion as follows. Corrosion will not occur unless the spontaneous direction of the reaction indicates metal corrosion, and the time for the reaction to occur will vary from metal to metal since barriers of different types may impose various rates for the processes.

The application of thermodynamics to corrosion has been generalized by means of Pourbaix diagrams. These diagrams are potential-pH plots and are used in (1) predicting the spontaneous direction of reactions, (2) estimating the composition of corrosion products, and (3) predicting environmental changes which will prevent or reduce corrosive attack [9]. Figure 3 illustrates a simplified Pourbaix diagram for the Fe-H₂O system.

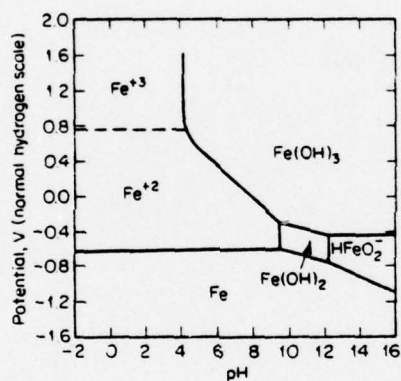


FIGURE 3

SIMPLIFIED POTENTIAL - pH DIAGRAM
 FOR THE Fe-H₂O SYSTEM (M. POURBAIX,
 "ATLAS OF ELECTROCHEMICAL EQUILIBRIA
 IN AQUEOUS SOLUTIONS", p. 307-321,
 PERGAMON PRESS, NEW YORK, 1966) [5]

10. Area Effect

Another important factor in galvanic corrosion is the ratio of anode-to-cathode area. An unfavorable (adverse) area ratio consists of a large cathode and a small anode. The greater the current density of the current leaving an anodic area, the greater is the corrosion rate. During the present experiments the cathode-to-anode area ratio was constant for all couples at one-to-one.

11. Metallic Structure

The microstructure of a metal or alloy can have a marked affect on its tendency to corrode. Grain boundaries are generally anodic regions and are in many instances a gathering place for alloying elements or impurities. The conglomeration at grain boundaries may lead to intergranular attack causing a serious reduction in mechanical properties such as strength and ductility.

Surface inclusions and non-uniformities such as scratches on a finely ground surface can also be relatively anodic and cause an increase in the rate of attack [5]. For purposes of experimentation all specimen surfaces were prepared in the same manner to avoid any variation in surface characteristics.

C. INFLUENCE OF VELOCITY OF THE ELECTROLYTE

Velocity often strongly influences the mechanisms of corrosion reactions. The study of its effects on corrosion is extremely difficult because laboratory tests can rarely duplicate service conditions. Perhaps the major problem is the inability to precisely control the rate and nature of flow [9].

As a result of electrolyte velocity several types of corrosion may result, such as uniform attack, corrosion-erosion and cavitation. There is not a clear-cut dividing line between these types of corrosion as a function of electrolyte velocity, but rather a continuum of attack with one mechanism leading into the other. As a consequence, because there is no real dividing line and because the flow characteristics or rates of flow have been difficult to determine, little or no correlation exists from one test method to another.

Increases in velocity generally result in increased attack, particularly if substantial flow rates are involved. Figure 4 illustrates the effect of velocity on the corrosion rate of steel by seawater. It is essential that one realize that velocity will generally increase the corrosion rate, but not always. Velocity increases can in some cases lead to decreases in the rate of attack. The controlling factors for the overall corrosion reaction are the rates of mass transport of reactants and products to and from the metal surface, known as diffusion control; or by the rate of reaction at the anode or cathode, known as chemical control. In the corrosion of iron for example, the overall rate of attack is controlled by the rate of diffusion of oxygen from the bulk of the electrolyte to the metal surface. With more noble metals such as copper, the rate is partially controlled by diffusion of metal ions away from the surface.

The effect of velocity on corrosion rates will typically be nil, or increase slowly until a critical velocity is reached, and then attack may increase at a rapid rate. In other cases, increased velocity may initially reduce attack, depending on its effect on the corrosion mechanism involved. For example, velocity can decrease attack by increasing the supply of, and thus effectiveness of, inhibitors [9].

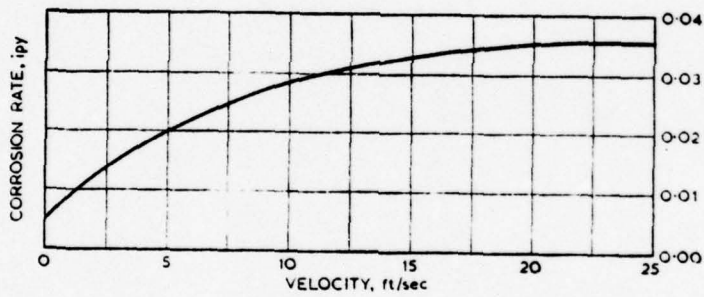


FIGURE 4 [1]

THE EFFECT OF VELOCITY
ON CORROSION RATE OF
STEEL BY SEAWATER.

Increased velocity may increase attack on some metals by providing an increased supply of oxygen in contact with the metal surface, or velocity may increase diffusion or transfer of ions by reducing the thickness of the stagnant film at the surface. Higher velocities may also cause a scouring effect on the metal surface, thus destroying protective oxide films.

Some typical corrosion rates, for metals in flowing seawater under different conditions, are given in Table 3. It must be noted that the data in Table 3 is collected from three different types of velocity effects tests, and cannot be directly compared. Only very general ideas can realistically be drawn from the grouped data of Table 3. However, if there had been characterization of the flow conditions for the respective experiments, data such as that shown in Table 3 would be much more useful. The ability to correlate data with other test results is one of the most desirable features of any corrosion experiment [10], and this was one of the primary objectives in the design of velocity effects experiments in this work.

D. THE KINEMATICS OF THE FLUID FLOW

At relatively low relative velocities between metal and electrolyte, flow is laminar. Above a critical velocity flow becomes turbulent; a small element of water chosen at random may be moving in any direction, although averaged over the entire cross-section, the net movement is in a given direction. The transition from one type of flow to the other does not occur at any precisely definable velocity but over a range of velocities. The actual flow is dependent on such factors as surface roughness and mechanical vibrations, and is also a function of the geometry of the system [6].

TABLE 3

Material	Typical corrosion rates, mdd		
	1 ft/sec*	4 ft/sec†	27 ft/sec‡
Carbon steel	34	72	254
Cast iron	45	—	270
Silicon bronze	1	2	343
Admiralty brass	2	20	170
Hydraulic bronze	4	1	339
G bronze	7	2	280
Al bronze (10% Al)	5	—	236
Aluminum brass	2	—	105
90-10 Cu Ni (0.8% Fe)	5	—	99
70-30 Cu Ni (0.05% Fe)	2	—	199
70-30 Cu Ni (0.5% Fe)	<1	<1	39
Monel	<1	<1	4
Stainless steel type 316	1	0	<1
Hastelloy C	<1	—	3
Titanium	0	—	0

* Immersed in tidal current.

† Immersed in seawater flume.

‡ Attached to immersed rotating disk.

SOURCE: International Nickel Co.

CORROSION OF METALS BY
SEAWATER MOVING AT
DIFFERENT VELOCITIES [5]

In order to differentiate between the two flow regimes (laminar or turbulent) a dimensionless parameter called the Reynold's Number, Re , is used [11]:

$$Re = ux\rho/\mu = ux/\nu$$

where,

u = fluid velocity

x = a characteristic dimension, such
as length for a flat plate

ρ = density of fluid

μ = dynamic viscosity

ν = kinematic viscosity

In this study, the critical Reynold's Number corresponding to a flat plate approximation in a uniform flow field was used. In this case, the critical Reynold's Number at which the transition from laminar to turbulent flow occurs is assumed to be $Re = 5 \times 10^5$.

Whatever the type of flow, there will be a laminar layer in immediate contact with the metal. Even when the flow is turbulent there will still be a thin laminar sublayer caused by viscous drag on the water by the metal surface. Within this hydrodynamic boundary layer is a diffusional boundary layer, in which the relative velocity is small or nearly zero. In this inner boundary layer reactions will be either entirely by molecular or ionic diffusion. Outside this layer increased velocity means convective diffusion will be the predominate mode of mass transport. This mass-transport boundary layer is related to the

hydrodynamic boundary layer by [12]:

$$\frac{\delta_h}{\delta_d} \equiv Sc$$

where δ_h is the thickness of the hydrodynamic boundary layer given by [13]:

$$\delta_h = \frac{x \cdot 0.38}{Re^{0.2}}$$

and

x = distance from leading
edge of flat plate

Re = Reynold's Number

and δ_d is the thickness of the diffusional boundary layer. The dimensionless relationship, Sc is known as the Schmidt Number and is given by [12]:

$$Sc = \frac{\nu}{D}$$

where

ν = kinematic viscosity

D = the diffusion coefficient
of the reacting species

The larger the value of Sc , the thinner the diffusional layer and the more rapidly it develops [12].

Thus in many instances, the rate of mass transfer across the diffusional boundary layer is inversely proportional to the hydrodynamic boundary layer thickness. Since the magnitude of the surface shear stress gives a direct measure of δ_h , it would often be more appropriate to report corrosion rates in terms of shear stress, than in terms of velocity [12]. If the two boundary layers start to form at the same location, their relative thickness is constant. The thickness of the diffusion boundary layer is generally about 0.5 mils or less for turbulent flow [6].

Surface roughness is a very important factor in characterizing the flow regime. It can be caused by projections, grooves, or buildup of corrosion products. If the flow is laminar and the height of the projection is small in comparison with the thickness of the diffusion boundary layer, then the flow over the surface will be virtually unaffected. If, on the other hand, the flow velocity is greater than some critical value the projection will cause localized turbulence on the downstream surface of the body.

The geometry presented by the metal specimen or moving form to the flow can and will greatly affect the resulting flow regime. A wedge-shaped body, for example, will cause the flow to transition from laminar to turbulent at a much lower velocity or Reynold's Number than, say, a hydrodynamically designed and streamlined foil.

As has been emphasized, the type of flow obtained is dependent on the rate and quantity of fluid handled as well as the geometry and design of the experimental equipment. In addition to high velocities, ledges,

crevices, deposits, obstructions, sharp changes in cross-section and other devices that disturb the flow patterns may result in an increased rate of corrosion and in many cases in erosion or cavitation corrosion.

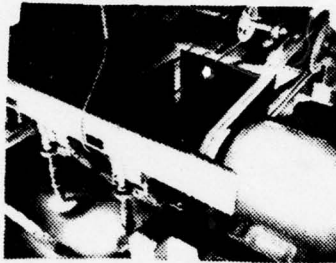
The design of all experimental equipment as well as all experimental parameters used to produce the desired flow characteristics are detailed in a later section of this work. The methods used to characterize the flow over the specimen surfaces are also detailed.

E. PREVIOUS RESEARCH

Significant research into the effects of electrolyte velocity on corrosion rate started in the late 1950's and early 1960's. In 1959, H.R. Copson did a study on the effects of velocity on corrosion, dealing with a variety of metals and couple combinations [14]. Tests were conducted over a range of velocities and different flow environmental conditions; some of the various experimental setups used are shown in Figure 5. For tests conducted below the cavitation range, Copson concluded that motion generally increases total weight loss by supplying the corrosives at a faster rate. It appeared as though the effects of velocity and oxygen concentration were inter-related; an increase in velocity tends to supply more oxygen and thus tends to increase the corrosion rate. Copson's results, though useful, cannot be exactly correlated with other results because of differences in environmental and test conditions. Additionally, Copson made no attempt to characterize the flow regime or rate of flow within the test system. Without this characterization, the procedure is not reproducible, nor are results predictable in other tests.

In the early 1960's, research conducted at the U.S. Naval Engineering Experiment Station by J.L. Basil studied high velocity effects and the

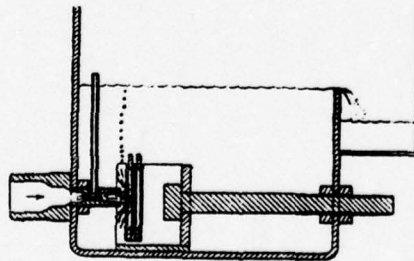
FIGURE 5



APPARATUS TO ROTATE SPECIMEN
DISCS IN SEAWATER



TEST SPECIMENS MOUNTED ON
PERIPHERY OF LARGE DISCS IN A
TEST FOR EROSION CORROSION



APPARATUS FOR ASPIRATOR
TYPE JET TESTS

EQUIPMENT USED IN H.R. COPSON'S STUDY [14]

effect of seawater velocity on selected alloy groups [15, 16], In the first experimental study a method of exposure was chosen that moved the seawater past the specimen. This allowed the velocity relative to the stationary specimen to be controlled and measured with precision. The equipment designed, Figure 6, consisted of six nozzles threaded into a nylon flange. The nylon flange was in turn bolted to a copper-nickel pipe. Alloys studied were nickel base, stainless, titanium copper base, aluminum, and carbon and low alloy steels. Tests were run up to 80 knots with the following results [15]:

(1) Nickel alloys, titanium alloys, and stainless steels had excellent corrosion resistance at high velocities.

(2) Copper alloys, aluminum alloys and steels exhibited poorer corrosion resistance by a factor of 100 or more at high velocities.

For the second study, three alloy groups were chosen; stainless steels, copper alloys, and nickel alloys. Tests were run over a range of velocities from two feet per second to 117 feet per second (.61 m/sec to 35.7 m/sec). Test results showed that of the three types of alloys considered, the nickel-copper alloys offered the best resistance to seawater corrosion over the range of velocity conditions. The corrosion resistance of copper-based alloys was limited to relatively low velocity conditions. The results obtained by Basil showed that increased velocity did in fact increase the corrosion rate of some metals. Unfortunately, the turbulence level over the test specimens was not characterized, nor was the velocity profile over the test surface. Therefore it is not clear how much metal loss could be attributed to the action of corrosion and how much to the effect of turbulence (shear forces) and cavitation.

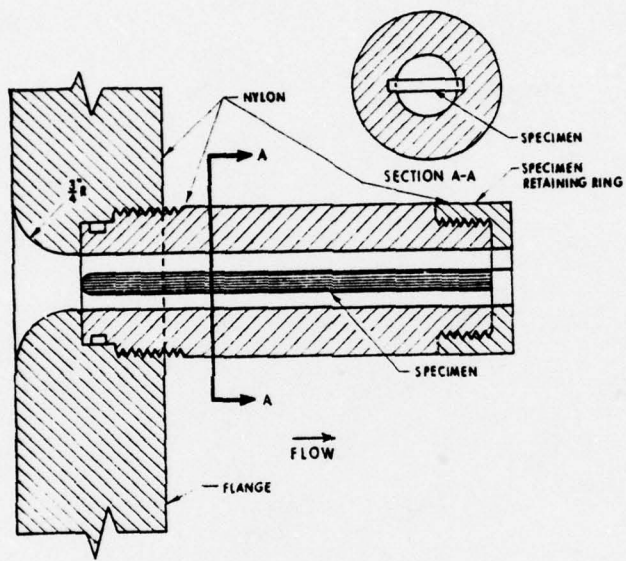


FIGURE 6
NOZZLE ASSEMBLY [15]

As mentioned previously, without information as to the test system, no comparisons can be accurately made or results predicted.

Further studies into the effect of seawater velocity on the corrosion behavior of metals was carried out by G.J. Danek, Jr., at the U.S. Navy Marine Engineering Laboratory, Annapolis, Maryland [17]. Data was collected at three discrete velocities in the range of 0 - 120 ft/sec (0 - 36.6 m/sec). The apparatus used for the low velocity tests was a trough where the specimens were mounted and exposed to velocities of 1 - 2 ft/sec (.30 m/sec - .61 m/sec). For the intermediate velocity studies, specimens were attached radially to the periphery of a 30.5 cm (12 in) diameter wheel. The assembly rotated vertically in seawater [17]. One shortcoming of this assembly is that the true velocity is somewhat unknown, due to the stirring effect in the tank.

High velocity studies were also conducted by Danek using the nozzle assembly designed by Basil. Again, because the true velocity of the seawater could not be determined, hydrodynamic considerations could not be included in the final results. No quantitative correlation was made by Danek to relate velocity and corrosion behavior for several reasons [17]:

- (1) Different testing techniques were used at different velocities.
- (2) Only three discrete velocities were considered over a wide range.
- (3) Tests were conducted at different times under different conditions.

None-the-less, Danek did come to some definite conclusions. The alloys investigated were classified into three distinct groups according to their film forming characteristics [17]:

(1) Alloys in the first group had excellent corrosion resistance at all velocities. Titanium alloys were an example.

(2) Alloys in the second group exhibited excellent resistance at intermediate and high velocities, but were attacked at low velocities. Nearly all passive-film forming alloys are in this group.

(3) Alloys in the third group exhibited excellent corrosion resistance at low velocity, but were attacked by corrosion-erosion at high and intermediate velocities. Copper based alloys were an example.

Additionally, it was observed that by adding small amounts of certain alloying elements to alloy types, their corrosion behavior improved. For example, a small amount of iron added to copper-nickel alloys improved the corrosion resistance of the alloys [17].

As the U.S. Navy Surface Effect Ship (SES) program became a reality, the need for additional information concerning a wide variety of metals and their behavior in a moving environment became apparent. In 1972 the Bell Aerospace Company conducted a program with the purpose of experimentally obtaining the design data required for a cathodic protection system for surface effect ships at high speeds [18]. Tests were conducted at six speeds (0, 10, 20, 30, 60 and 90 knots) using the high speed water wheel shown in Figure 7. Test periods ranged from 16 weeks for zero velocity to 20 hours for tests at 30, 60 and 90 knots. Three basic specimen designs were used as shown in Figure 8. The wedge-shaped specimens were aero-dynamically designed for test velocities from 10 to 90 knots, but no data was available as to the flow characteristics of the test system. Tests determined that galvanic corrosion rates of aluminum hull alloys galvanically coupled to appendage materials increased as the velocity increased. See Table 4. Additionally, protective current

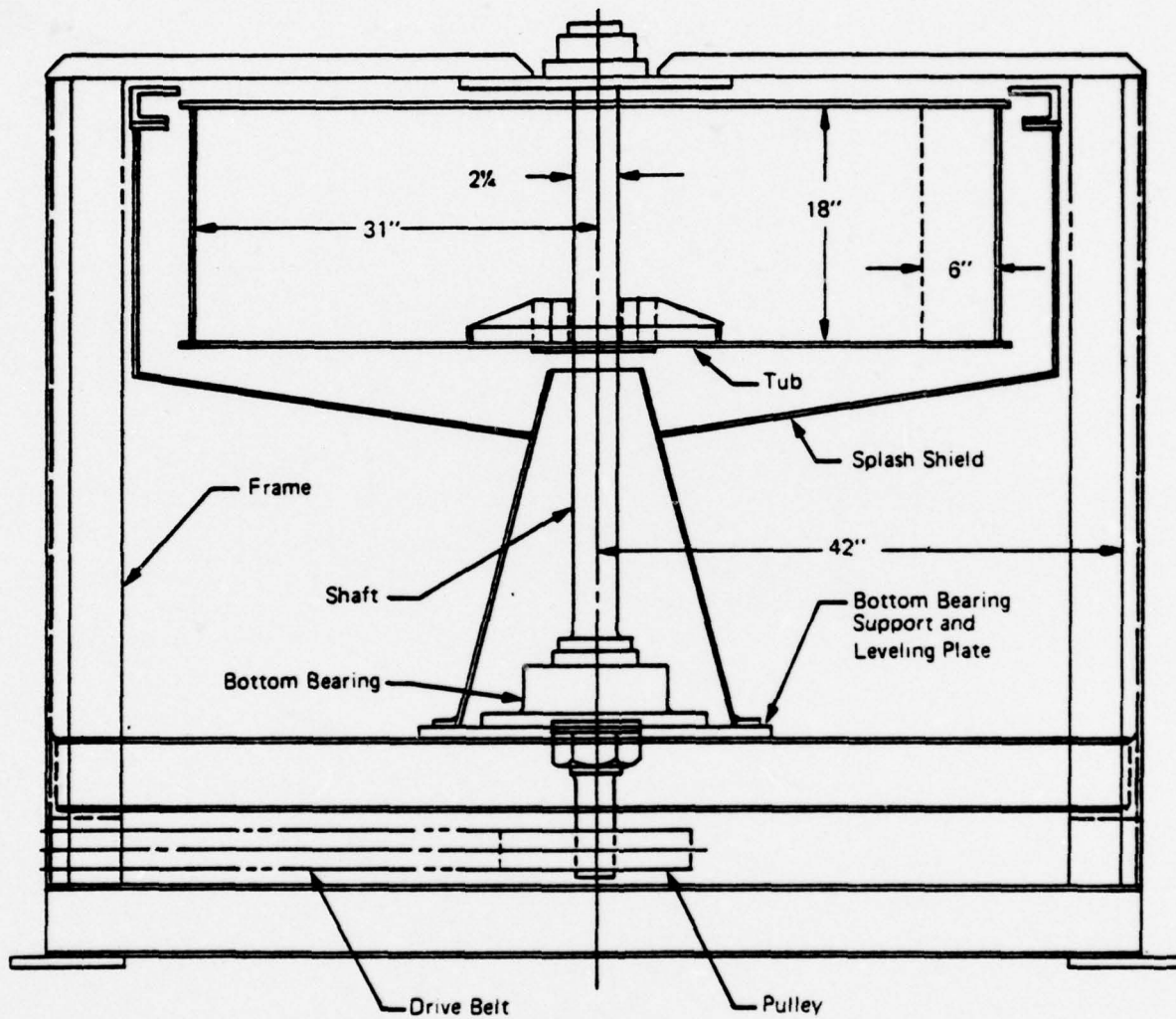
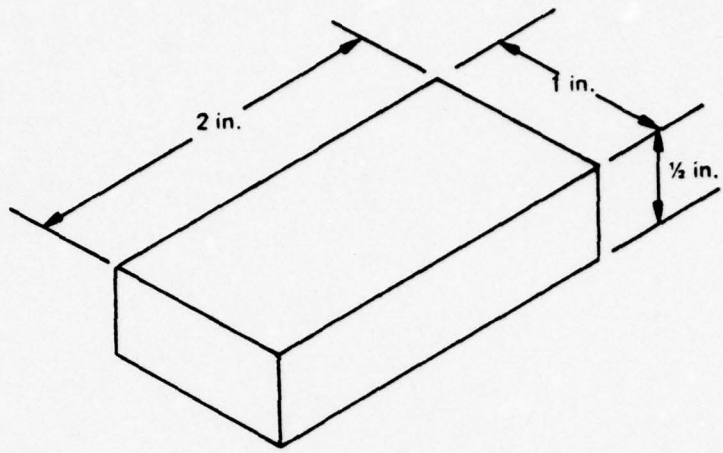
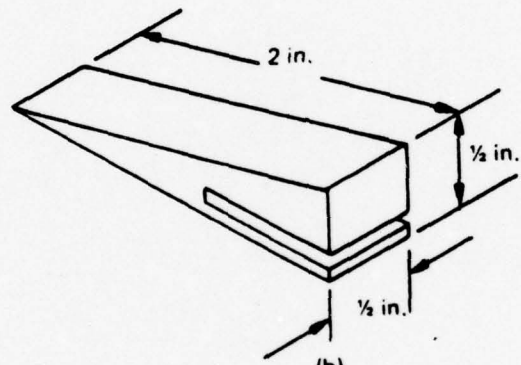


FIGURE 7

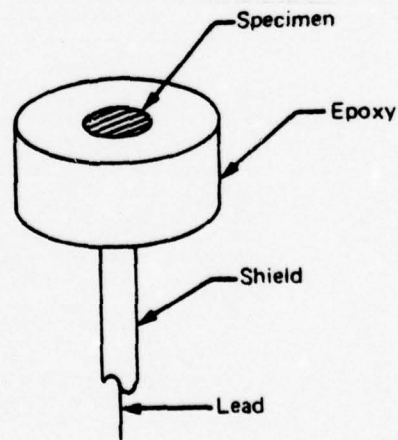
HIGH SPEED WATER WHEEL [18]
 (TEST AREA IS 6 in x 18 in)



(a)



(b)



(c)

FIGURE 8: SPECIMEN DESIGNS FOR (a) ZERO VELOCITY TESTS, (b) WEDGE SPECIMENS, AND (c) SMALL AREA SPECIMENS [18]

TABLE 4 [18]
 GALVANIC CORROSION RATES AS A FUNCTION OF VELOCITY FOR
 ALUMINUM HULL ALLOYS UNCOATED

Materials	Area Ratio	Velocity (Knots)					
		0	10	20	30	60	90
5086:Ti-6Al-4V	50:1	0.04	0.04	0.10			
	200:1	0.02	0.02	0.14			
	6:1				2.7	4.1	18.0
	24:1				2.0	4.1	3.6
5456:Ti-6Al-4V	50:1	0.03	0.12	0.20			
	200:1	0.01	0.01	0.01			
	6:1				5.4	3.4	18.0
	24:1				5.9	12.2	4.1
5086:17-4PH	12:1	0.6	0.7	1.2			
	150:1	0.1	0.1	0.03			
	1:1				15.3	17.2	32.0
	18:1				3.6	8.2	11.0
5456:17-4PH	12:1	0.3	0.1	0.65			
	150:1	0.04	0.1	0.5			
	1:1				15.8	17.2	24.8
	18:1				7.7	9.3	19.6
5086:Inconel 625	12:1	0.3	1.1	1.8			
	150:1	0.05	0.12	0.3			
	1:1				11.3	3.3	58.6
	18:1				12.6	9.8	14.0
5456:Inconel 625	12:1	0.3	1.1	0.4			
	150:1	0.05	0.13	0.2			
	1:1				10.6	14.7	27.0
	18:1				8.8	13.1	6.3

densities required to control galvanic corrosion increased with increasing velocity [18].

Davis and Gehring, in 1975, described measurements of corrosion currents for various marine materials as a function of seawater velocity [19, 20, 21]. Measurements were made using the same high speed water wheel shown in Figure 7 and the same specimen types shown in Figure 8.

In 1976, B.C. Syrett reviewed the environmental and metallurgical variables affecting erosion-corrosion of copper-nickel alloys in seawater [12]. After comparison of all current test methods, Syrett reached the same conclusion that most discriminating researchers had already come to. The test results in the area of erosion-corrosion and velocity effects varied widely from one researcher to another. Some of the variation in results may be correctly attributed to metallurgical variations, thermo-mechanical history of alloys tested, or seawater composition; but for the most part, variations in experimental technique were considered to be most responsible for inconsistencies in reported corrosion rates.

It is obvious that before a feasible, experimental model may be used to predict corrosion rates, several areas need special attention. The first is obviously the geometry of the test system. Since fluid flow characteristics are dependent upon the system geometry, it is essential that the geometry of the test system allows modeling of the geometry of the real system of interest. It is also of great value if the flow characteristics are reproducible in other test systems. If the real system geometry cannot be accurately modeled, then the test flow system should be one that most nearly approximates the actual in-service conditions to be encountered, yet lends itself to simple analysis and characterization [12].

Another important area is in the reporting of data. Consideration should be given to reporting corrosion test results in terms of dimensionless numbers. Given the right dimensional analysis, a dimensionless corrosion rate might be determined in the laboratory that could be related to such dimensionless groups as a Reynold's Number or Schmidt Number (these parameters were defined earlier). Using this information and a thorough knowledge of the fluid flow characteristics of the test system, corrosion rates under actual in-service conditions could be predicted directly and accurately modeled [12].

Endeavors of the sort discussed above are rare in this country [22, 23, 24, 25], while efforts to correlate hydrodynamic effects and corrosion rates have received extensive attention in Western Europe in the last decade [26, 27, 28, 29, 30]. As long as the fluid mechanics aspects of determining corrosion rates are given only qualitative consideration, corrosion rate data will continue to be reported with wide scatter and variation, leaving little chance of accurately predicting in-service corrosion behavior.

The bulk of the present work was concerned with systematically and accurately modeling and designing a system that closely approximated the in-service flow conditions. The experimental apparatus (discussed in a later section) was designed taking into account the hydrodynamic parameters involved, and great care was taken to characterize the flow field within the test system. Corrosion rate data was gathered only after a complete knowledge of the fluid flow in the test tank was obtained and analyzed.

II. EXPERIMENTAL PROCESS

The purpose of the experimental process used in this work was to develop an apparatus to closely control conditions which approximate those encountered by commonly used metals in a dynamic marine environment. Previous work on velocity effects at the Naval Postgraduate School was concerned primarily with the behavior of zinc sacrificial anode materials [31, 32, 33]. The present work sought to simulate conditions encountered by the actual structural materials. In this initial work, galvanic couples of 70/30 copper-nickel and K-Monel with plain carbon steel (PCS) were studied. Corrosion product morphology was studied macroscopically as well as microscopically throughout the experiment in order to observe the behavior of metallic couples under conditions of varying velocity and time of exposure. Additionally, the galvanic corrosion current of the couples was monitored at the different test velocities and later converted to a corrosion rate (in MPY).

A. APPARATUS

The apparatus used included a small static exposure tank, a large dynamic exposure tank, rotating foil assembly, a digital voltmeter, frequency counter, timer and calibrated strip chart recorder, and an electric motor controller as depicted in Figure 9.

1. Static Exposure Tank

The static exposure tank, which contained the synthetic seawater electrolyte, was designed and used by Luebke [32] in his work. The tank was 45.72 cm (18 in) in diameter and filled to a level of approximately 15.2 cm (6 in) to hold 23.5 liters (6 gallons). The tank bottom was

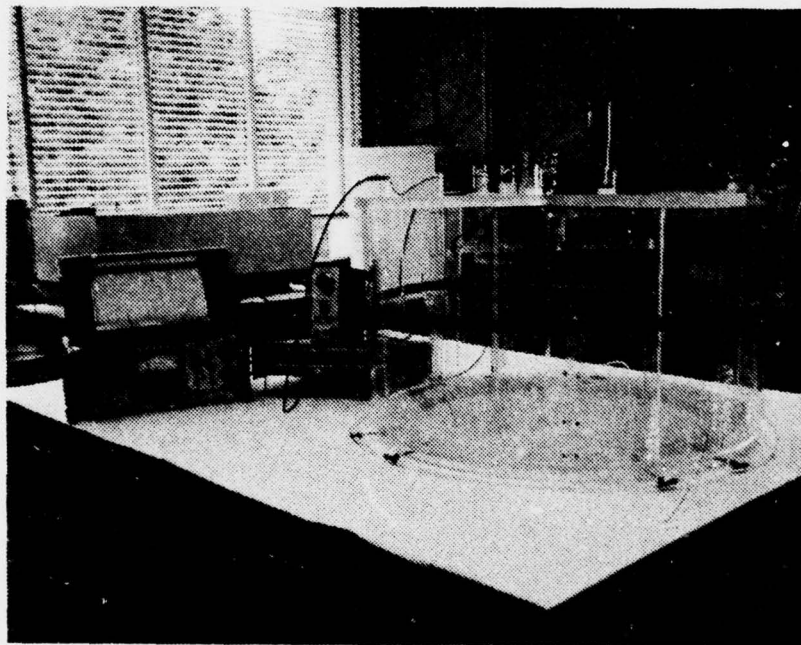


FIGURE 9

EXPERIMENTAL APPARATUS SHOWING
DYNAMIC EXPOSURE TANK, ROTATING
FOIL ASSEMBLY, DIGITAL VOLTMETER,
DIGITAL COUNTER, STRIP CHART
RECORDER, AND MOTOR CONTROLLER.

fitted with a 35.36 cm (14 in) diameter aeration canal which allowed compressed air to be bubbled through the fluid from an array of 12 equally spaced air holes. An attached regulator and air filter insured a precise flow of clean air into the electrolyte. The specimens were mounted on a plexiglass stand as shown in Figure 10. The specimen stand was then placed in the tank in a horizontal position. All specimens had an exact one-to-one ratio to ensure reproducibility.

2. Dynamic Exposure Assembly

The dynamic exposure tank, which contained synthetic seawater electrolyte, was constructed entirely of plexiglass. The tank was 91.44 cm (36 in) in diameter, 45.75 cm (18 in) in height and filled to a level of approximately 30.48 cm (12 in) to hold 189.27 liters (50 gallons). A system of plexiglass baffle strips was installed symmetrically along its interior sides and bottoms in an attempt to keep the electrolyte from stirring during velocity measurements. The tank bottom was fitted with an embedded 60.96 cm (24 in) diameter aeration canal which allowed air to be bubbled through the electrolyte from an array of 12 air holes spaced 30° apart. Compressed air was provided by a bottle of carbon dioxide free air with an attached regulator to provide for precise control of the aeration.

Mounted over and in the exposure tank was the rotating foil assembly used to expose the various specimens studied. The assembly consisted of a specimen-carrying foil suspended 10.16 cm (4 in) below the surface of the electrolyte by a 21.59 cm (8.5 in) vertical plexiglass support arm. Figure 11 details the specimen-carrying foil, constructed entirely of plexiglass. The vertical support arm was streamlined to reduce drag and keep the stirring effect to a minimum.

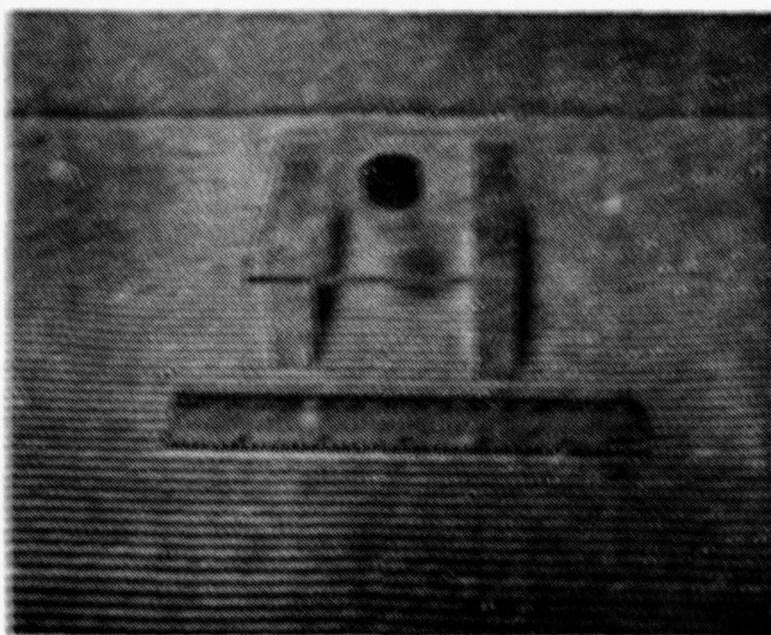


FIGURE 10

STATIC EXPOSURE STAND WITH SINGLE
SPECIMEN MOUNTED IN PLACE

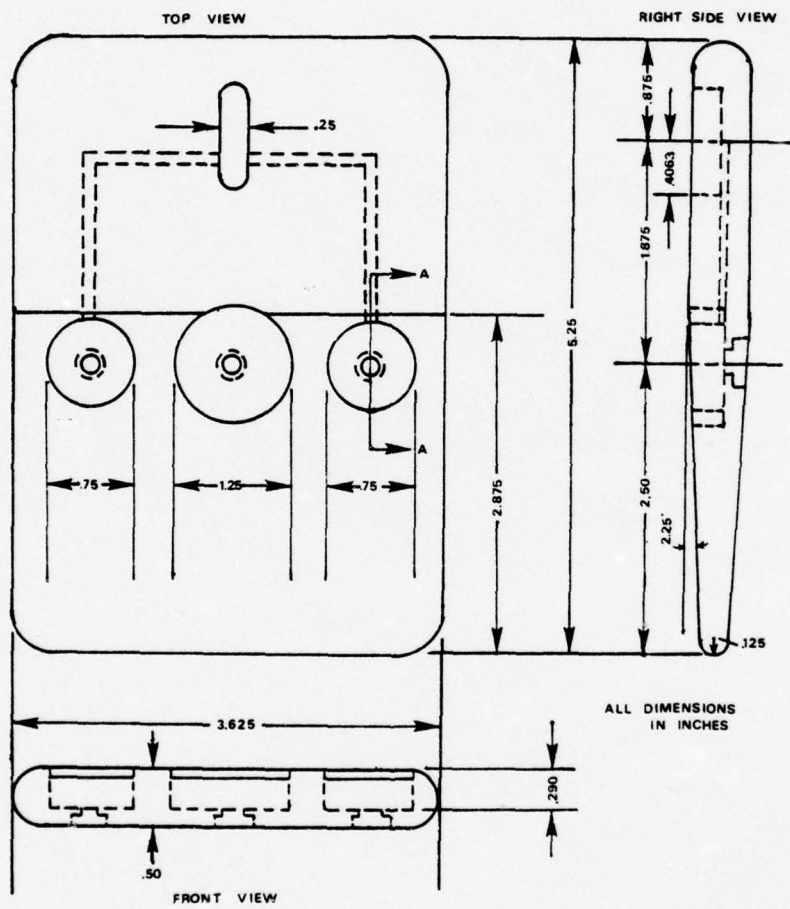


FIGURE 11

DETAIL OF SPECIMEN-CARRYING FOIL
 (1 inch = 2.54 cm)

The vertical support arm was attached to a 50.80 cm (20 in) horizontal plexiglass support arm suspended below a 3.175 cm (1.25 in) diameter plexiglass shaft, Figure 12. The shaft was connected via a pulley arrangement to an electric motor. The entire rotating foil assembly was statically balanced to reduce shaft and bearing wear. The assembly was supported by a large cross-piece that was connected to the top edge of the tank at four places to ensure lateral stability.

Each metallic couple was located topside in the foil, in round holes as shown in Figure 13. Proximate couples, in which the metals were in physical contact, were placed in the 3.175 cm (1.25 in) diameter centerline hole. Couples that were electrically coupled but not in physical contact with one another were placed in the 1.90 cm (.75 in) inboard and outboard holes. The specimen holes were machined to accommodate the specimens with minimum tolerance so that once in place, they were flush with the foil surface. A tight circumferential, watertight fit was also gained by this scheme. By mounting the specimens in this manner, a minimum of solution disturbance was realized.

Figure 14 is a detailed blowup of one of the specimen holes. As is shown, specimens were set in the top of the foil and held in place by a tight press fit and a thin layer of liquid paraffin applied around the circumference of the specimen before placement. Figure 15 reveals that electrical contact was accomplished by using a platinum disc fitted into the bottom of the specimen hole. The platinum disc was connected by solder to an electrical lead of low resistance copper wire. As the specimen was pressed into the hole, it was forced down upon the platinum disc to complete the circuit. Specimens were removed from the foil by pushing them out from the bottom (see Figure 14). When a specimen or

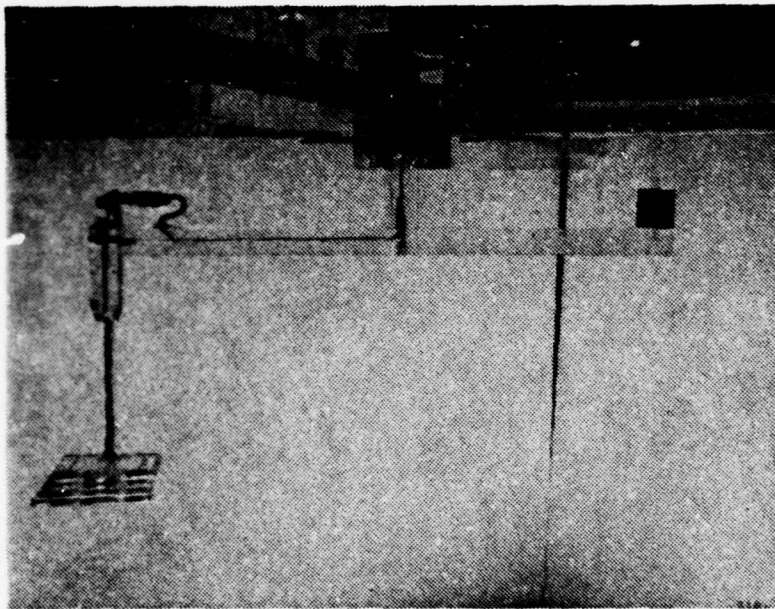


FIGURE 12

DETAIL OF VERTICAL AND
HORIZONTAL SUPPORT ARMS.

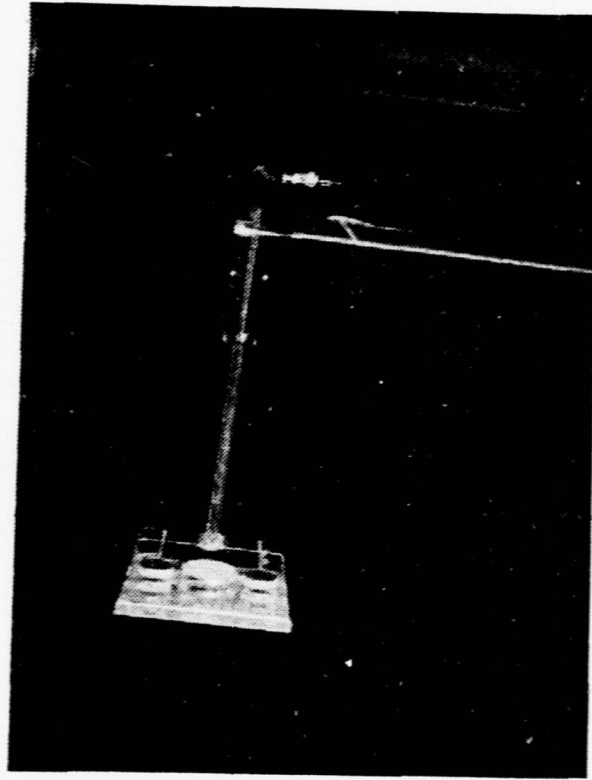


FIGURE 13

ILLUSTRATION OF THE LOCATION
OF SPECIMENS WHEN MOUNTED IN FOIL

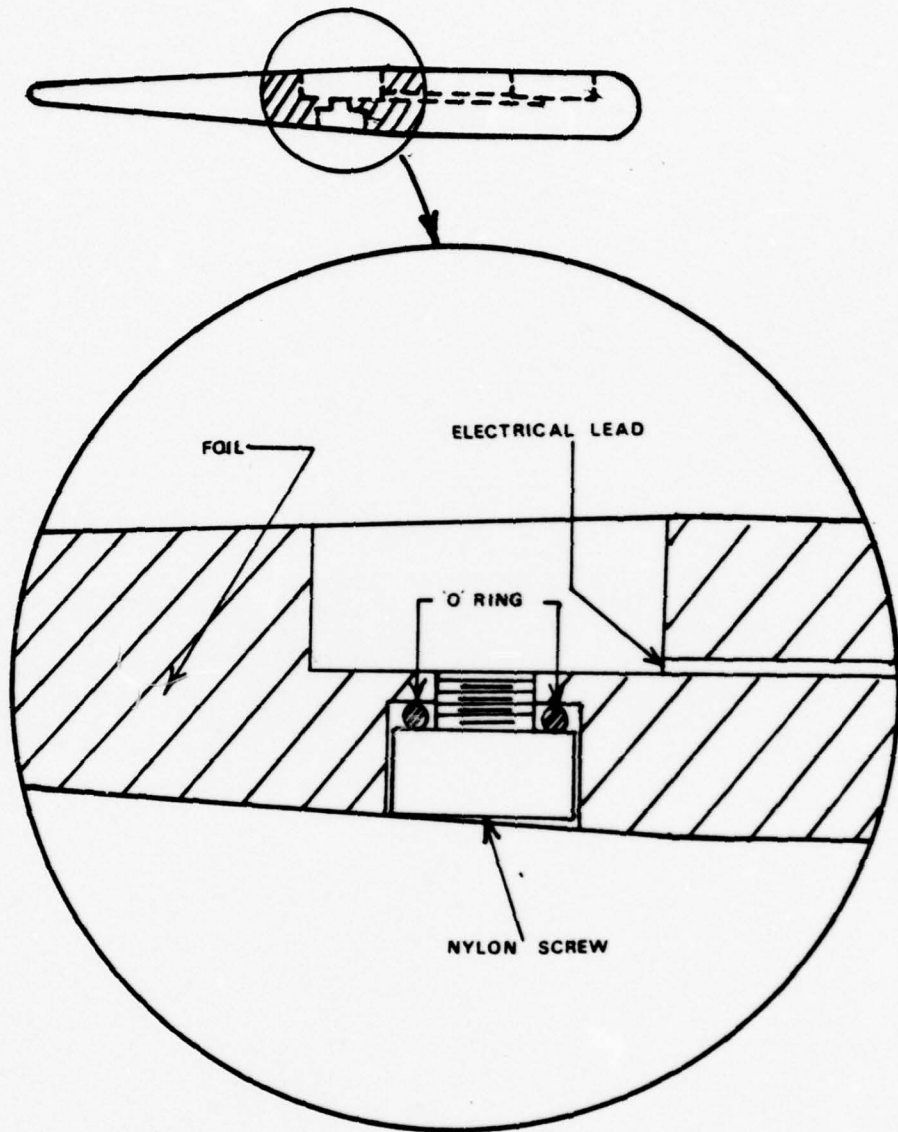


FIGURE 14

SECTION AA: DETAIL
OF SPECIMEN HOLE

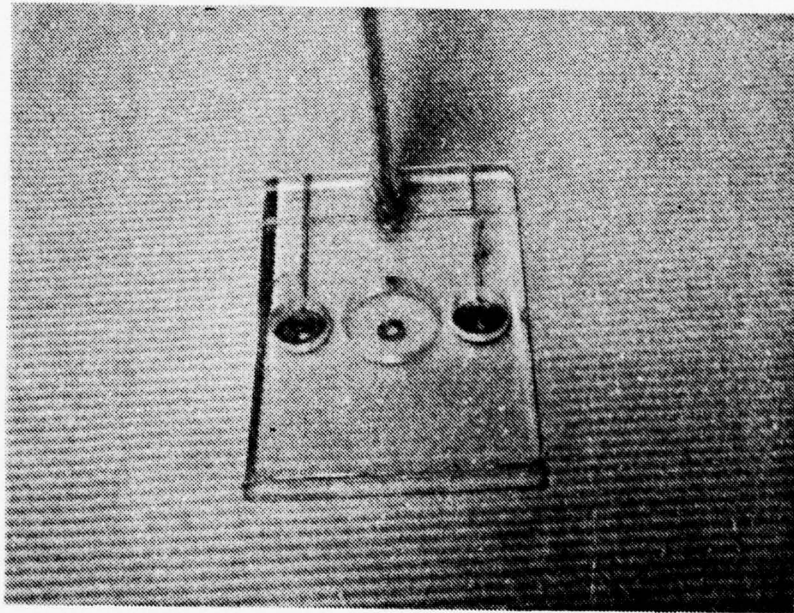


FIGURE 15

DETAIL SHOWING PLATINUM DISCS
USED IN ELECTRICALLY
CONNECTING MOUNTED SPECIMENTS

specimens were mounted, and before the foil was immersed in electrolyte, the access hole in the bottom of the foil was sealed watertight by means of a nylon screw and rubber o-ring.

The galvanic current between two specimens when moving at various velocities was monitored by means of a Hewlett-Packard 7100 B strip chart recorder. A resistor of known value (999.1 ohms) was placed across the input terminals of channel A, and the measured potential drop converted to current. The electrical circuit was completed by a sealed wire running through the foil, up the vertical support arm, through the center of the horizontal plexiglass support arm and up through the center of the plexiglass shaft. The foil and vertical support arm were detachable from the horizontal support arm by way of a BNC electrical connector shown in Figure 12. All joints and access points were sealed with Silaster 732 RTV general purpose sealant to ensure a watertight route. In order to transmit the electrical signal from the internal system circuit to the external strip chart recorder, on top of the plexiglass shaft was located an arrangement of two brass rings and brushes as detailed in Figure 16. The brass brushes were positioned to rest against the brass rings, to which were soldered the copper wires from the interior of the shaft.

In addition to the brass ring arrangement, the top of the shaft was also fitted with a pulley wheel, providing a 5 to 1 speed reduction, and a 60-tooth gear. A magnetic pickup, positioned near the gear and attached to a digital counter, sensed a magnetic flux as each tooth passed during shaft rotation. These flux signals were instantaneously converted into rpm and displayed by the counter. The shaft was driven via a pulley and V-belt drive arrangement by a 1/15 HP variable rpm

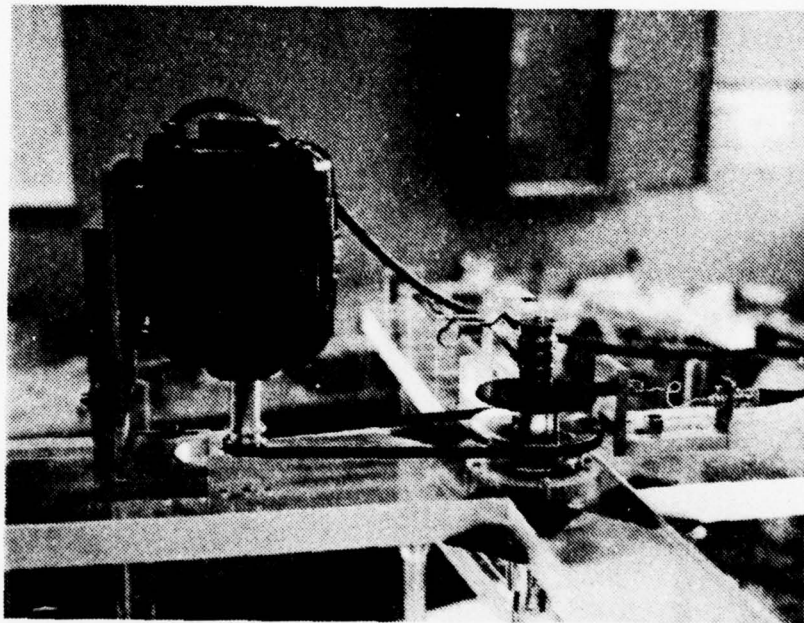


FIGURE 16

SLIP RING AND BRUSH ARRANGEMENT

D.C. motor capable of speeds up to 1725 rpm. The motor was controlled by a Minarik Speed Control model SH-63AH. This arrangement allowed the shaft speed to be controlled to within ± 1 rpm at all times under any condition of loading.

Where the shaft passed through the plexiglass cross-piece, which supported the entire assembly, two sealed, self-lubricating precision roller bearings coupled the shaft to the cross-piece. The bearings allowed for low-friction motion of the shaft at all speeds and prevented shaft wobble and vibration to the maximum possible extent.

Figure 16 illustrates the assembly.

3. Scanning Electron Microscope and X-Ray Analyzer

After exposure to varying velocity conditions in the corrosive environment, the surface morphology of each metallic couple was examined with a Cambridge model S4-10 Stereoscan Scanning Electron Microscope (SEM), Figure 17. It enables the examination of surfaces whose roughness or other characteristics render their observation extremely difficult or impossible by means of a conventional light microscope. The specimen detail resolution is always better than 10nm under satisfactory conditions, with a depth of focus that is at least 300 times greater than that of a light microscope [34]. The useful magnification is about 10,000x, but for the purposes of this study, magnification of up to only about 2500x were utilized.

The SEM focuses a beam of electrons to a fine spot on the surface of the specimen by a system of electromagnetic lenses. The lenses focus the beam which is scanned over an area of 0.25 cm^2 (0.04^2) or less on the sample surface, depending on magnification. Low-energy electrons, emitted from the surface of the specimen due to the action of bombarding

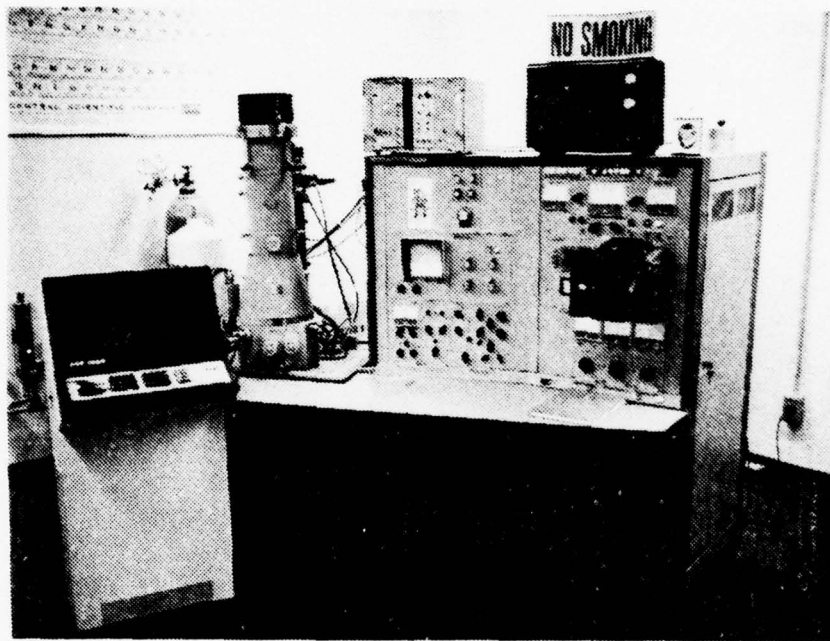


FIGURE 17

CAMBRIDGE MODEL S4-10 SCANNING
ELECTRON MICROSCOPE (SEM)
AND PRINCETON-GAMMA-TECH
PGT-1000 X-RAY ANALYZER.

electrons, are attracted towards the electron collection system. The electron collection system, which consists of a scintillator, a photomultiplier, and several amplifiers, delivers the signal to a cathode ray tube for display. The ratio of the length of a scan line on the cathode ray tube to the length of a scan line on the specimen is the magnification of the image scan [34]. In order that the image can be photographed, a second display unit is provided on which a camera is mounted.

Variation in the number of electrons emitted or reflected from different parts of the specimen result in an image that has a marked three-dimensional appearance. Light and dark areas on a SEM display indicate variations on topography as well as conductivity of the surface.

The specimen is situated in a region of weak magnetic and electrostatic fields and is not subjected to severe heating by the electron beam. The standard specimen stage allows objects of up to 1.27 cm (0.50 in) in diameter and about 0.64 cm (.25 in) in thickness to be manipulated in any required orientation whilst under observation [34].

Coupled to the Naval Postgraduate School SEM is a Princeton Gamma Tech 1000 energy-dispersive x-ray analyzer (spectrometer). This device energy-analyzes fluorescent x-rays emitted by atoms in the specimen surface. The x-rays are collected by a lithium-drifted silicon semiconductor detector located in the SEM specimen chamber. The analyzer processes the detector signals and displays an energy spectrum, $(N(E) \text{ vs. } E)$. Specific elements can be identified from the characteristic energies of the peaks displayed.

B. PROCEDURE

Metals studied included 70/30 copper-nickel, K-Monel and plain carbon steel. The specimens were coupled or considered individually as follows:

- (1) 70/30 Cu-Ni: carbon steel
- (2) K-Monel: carbon steel
- (3) Single metal exposure specimens

The plain carbon steel specimens used were cut from bars with a 1 cm x 1 cm (.394 in x .394 in) cross-section. The steel had been normalized by austenitizing at about 900°C and air cooled. See Figure 18.

The 70/30 copper-nickel and K-Monel specimens were cut from the ends of tensile test specimens provided by Mare Island Naval Shipyard. A spectrographic analysis of these specimens is contained in Tables 5 and 6 and the thermomechanical history is outlined in Table 7.

All specimens were cut to 1 cm x 1 cm x .75 cm (.394 in x .394 in x .295 in) and milled on all sides and surfaces. Prior to mounting, the surface of each specimen underwent a standard preparation sequence, so as to minimize the effects of surface roughness variations and cleanliness on the reproducibility of data. Each specimen was ground with 180-grit paper, ultrasonically cleaned in distilled water for 5 minutes, rinsed with alcohol and dried. Immediately after drying the specimens were mounted. Figure 19 shows a typical surface, ready to be exposed.

Since specimens were to be exposed physically coupled, electrically coupled, and singly, three different mount types and sizes were required. All mounting was done in a cold-type quickmount for ease in grinding, polishing and mounting in the specimen-carrying foil.



FIGURE 18

PLAIN CARBON STEEL NORMALIZED
BY AUSTENITIZING AT APPROXIMATELY
900°C AND AIR COOLED, 400x.

TABLE 5

SPECTROGRAPHIC ANALYSIS OF 70/30 Cu-Ni SPECIMENS

<u>METAL</u>	<u>% REQ'D*</u>	<u>% COMP. (ACT.)</u>
COPPER	65.0 (MIN)	67.98
SULFUR	0.02 (MAX)	0.007
PHOSPHORUS	0.02 (MAX)	0.008
MANGANESE	1.0 (MAX)	0.78
LEAD	0.05 (MAX)	<0.01
IRON	0.40 - 0.70	0.56
ZINC	1.0 (MAX)	0.06
NICKEL	29.0 - 32.0	30.60
SUM OF NAMED ELEMENTS	99.50 (MIN)	>99.50

* MIL-SPEC: MIL-C-15726E

TABLE 6
SPECTROGRAPHIC ANALYSIS OF K-MONEL SPECIMENS

<u>METAL</u>	<u>% REQ'D*</u>	<u>% COMP. (ACT.)</u>
NICKEL & COBALT	63.0 - 70.0	65.58
CARBON	0.25 (MAX)	0.15
SULFUR	0.010 (MAX)	<0.005
PHOSPHORUS	0.02 (MAX)	0.006
MANGANESE	1.50 (MAX)	0.75
SILIVON	0.50 (MAX)	<0.10
ALUMINUM	2.30 - 3.15	3.00
TITANIUM	0.35 - 0.85	0.54
IRON	2.0 (MAX)	1.03
COPPER	REM	28.95

* MIL-SPEC: QQ-N-286 CLASS A

TABLE 7

THERMO-MECHANICAL HISTORY OF 70/30 Cu-Ni

- 1) HEAT TREATED TO 1300°F
- 2) HELD FOR 4.5 HOURS AT 1300°F
- 3) WATER COOLED

	<u>YIELD (.5%) (KSI)</u>	<u>TENSILE STRENGTH (KSI)</u>	<u>ELONG % (2 in)</u>
MIN	18.0	45.0	30.0
ACTUAL	20.0	54.0	50.0

THERMO-MECHANICAL HISTORY OF K-MONEL

- 1) HEAT TREATED TO 1100°F
- 2) HELD FOR 16 HOURS AT 1100°F
- 3) COOLED AT REDUCTION OF 15°F/HR
- 4) TEMPERED AT 900°F

	<u>YIELD 0.2% OFFSET (KSI)</u>	<u>TENSILE STRENGTH (KSI)</u>	<u>ELONG % (2 in)</u>
MIN	100.0	140.0	20.0
ACTUAL	126.0	166.0	22.0

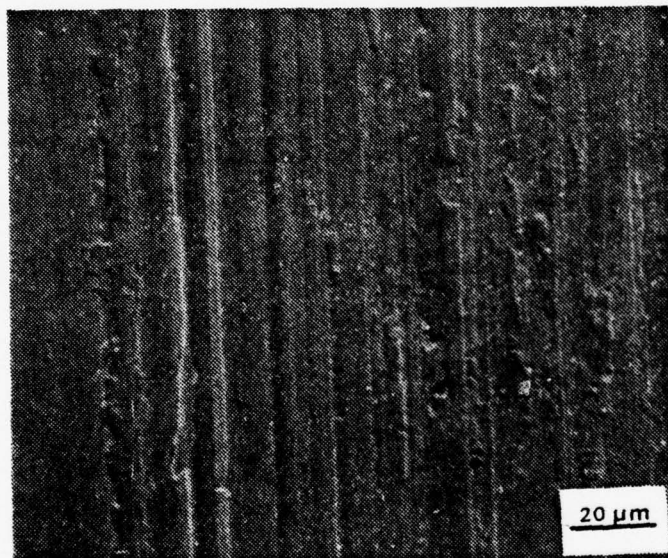


FIGURE 19

SCANNING ELECTRON MICROPHOTOGRAPH
OF INITIAL POLISHED SPECIMEN
SURFACE, 580x.

For specimens to be physically separated but electrically coupled during exposure, mounts 1.9. cm (.75 in) in diameter were used. These specimens would be placed in the inboard and outboard specimen holes in the foil and also used for static testing. After mounting in "quick-mount", the specimens were ground to a thickness of exactly .75 cm (.295 in) on 180-grit paper. The mounted specimens were then ultrasonically cleaned in distilled water for 5 minutes, rinsed in a mixture of alcohol and water, and dried.

Specimens to be exposed singly were mounted, ground and cleaned exactly as stated above except that 3.18 cm (1.25 in) diameter mounts were used. These specimens would be placed in the centerline specimen hole on the foil.

For specimens to be physically coupled during exposure, moulding was done in specially designed aluminum mounting rings 3.18 cm (1.25 in) in diameter. Small holes .476 cm (.1875 in) in diameter were drilled and tapped on opposite sides of the rings. Screws were placed in the holes and used to apply 0.7 N·cm (2 in-oz) of torque to the couple placed in the ring. The use of constant torque assured reproducibility of the contact stress for all couples. After mounting, the screws were removed and the remaining holes filled with parafin. Grinding, polishing and cleaning was accomplished in the same manner as the previous specimen. Figure 20 illustrates the three types of mounts used and the tool used to apply the constant torque. All specimens were kept in a vacuum chamber until exposed to prevent formation of oxide films or corrosion products.

1. Static Exposures

Experimental runs involving static conditions were conducted in the following manner: Specimens were mounted on the plexiglass stand

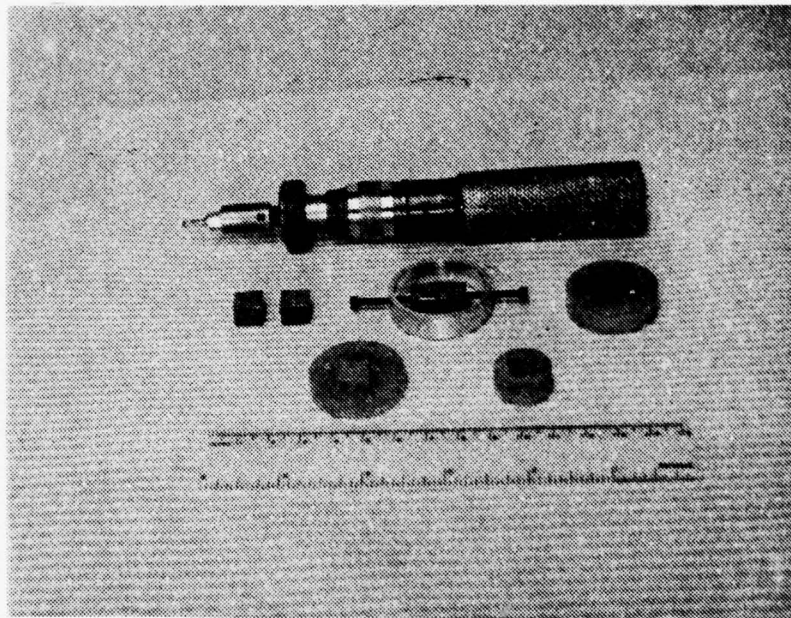


FIGURE 20

ILLUSTRATION OF SPECIMENS, COUPLE TYPES AND TOOL USED FOR COUPLE. FROM LEFT-TO-RIGHT, TOP-TO-BOTTOM: TORQUE WRENCH USED TO APPLY STANDARD TORQUE, UNMOUNTED SPECIMENS, COUPLED SPECIMENS IN SPECIAL ALUMINUM RING SHOWING SYSTEM USED TO APPLY TORQUE, FINISHED GALVANIC COUPLE, FINISHED SINGLE METAL MOUNT (CENTERLINE), FINISHED SINGLE METAL MOUNT (INBOARD/OUTBOARD).

assemblies and placed in the static exposure tank. Two specific exposure times were involved, 30 minutes and 24 hours. Prior to each exposure, the conductivity, temperature and pH of the synthetic seawater electrolyte was tested and recorded to ensure that they were within the prescribed limits [35]. Exposures were made using physically coupled specimens, single metal specimens, and specimens electrically coupled for the times previously indicated. The potential between the electrically coupled specimens was monitored on a calibrated strip chart recorder. It was discovered that the pH of the electrolyte could be properly maintained by bubbling clean air through the aeration canal in the bottom of the tank.

On removal of the specimens from the static exposure tank, they were air dried and mounted on a SEM stub for observation. Initially, on removal of the specimens from the tank, they were gently rinsed in distilled water. This rinse resulted in the removal of approximately 80 percent of the accumulated corrosion product, and for this reason the rinse step was deleted, but this left the likelihood of sea-salt deposits drying. The specimens were then characterized for surface corrosion product morphology and subsequent photographing. These photomicrographs provided the initial basis of information to which further corrosion product behavior would be related.

2. Dynamic Flow Characterization

Before dynamic exposure tests could be conducted it was necessary to determine the flow characteristics within the test system. The reason for this characterization was three-fold. Firstly, it was necessary to know the level of turbulence around the foil and specimens. The flow was turbulent at all test velocities by reason of foil design

(and the placement of a platinum trip wire .0508 cm (.020 in) in diameter at a distance of .3175 cm (.125 in) from the leading edge of the foil); but knowledge of the level of turbulence was important in order to properly evaluate surface corrosion product morphology, surface damage, and corrosion rates. The rate of corrosion, as stated earlier, is a function of the mass-transfer and hydrodynamic boundary layer thicknesses. It was crucial that these parameters be accurately determined for the dynamic system in use. Thirdly, in spite of efforts to streamline the foil and vertical support arm, solution disturbance was inevitable and steady flow patterns developed within the tank. It was necessary to know the extent of these disturbances and their effect on the actual velocity over the specimens surface.

In order to accurately determine the character of the flow around the foil a hot-film probe was mounted over each hole on the foil for consecutive runs. Data was then obtained for the area over each specimen hole and over the foil. Figure 21 illustrates the foil configuration for a run with the hot-film probe over the centerline hole. After the probe was mounted the dynamic exposure tank was filled with approximately 50 gallons of synthetic seawater electrolyte. Appendix A contains the specification standards followed and chemicals used in its preparation.

A hot-film probe or hot wire anemometer can be used to measure both the flow velocity and the turbulence intensity in a flow field. The principle of operation is relatively simple and straightforward. When an electrically heated wire is placed in a flowing stream, heat will be transferred between the wire and the stream, depending on a number of factors, including the flow rate. The sensing element

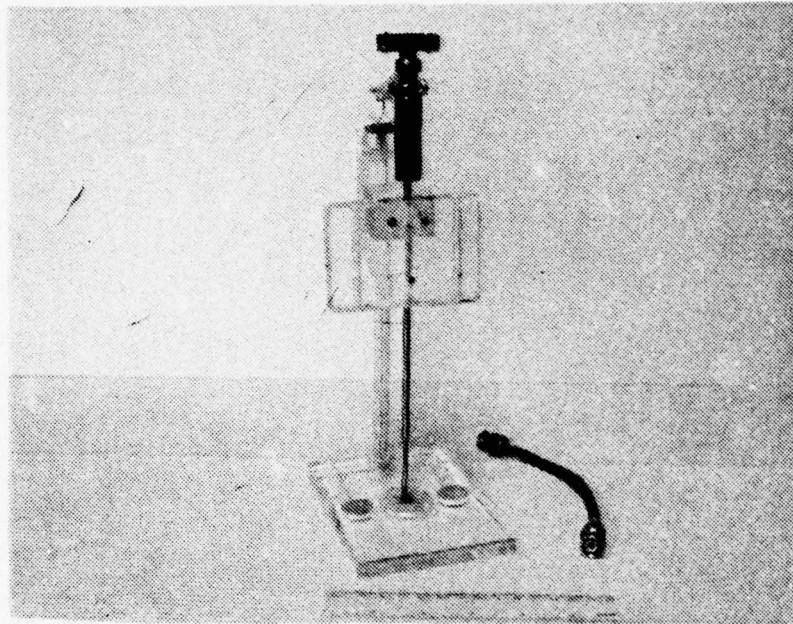


FIGURE 21

FOIL WITH HOT-FILM PROBE
MOUNTED OVER CENTERLINE HOLE

consists of a short length of fine wire stretched between two supports as shown in Figure 22. One measuring technique employs a constant current passing through the sensing wire. Variation in flow results in changed wire temperature, hence changed resistance, which thereby becomes a measure of flow. A second technique employs a servo-system to maintain wire resistance, hence wire temperature [36]. When the hot wire is placed in a flowing stream, heat will be transferred, primarily by convection. Radiation and conduction are normally negligible [36].

The sensing equipment used with the hot-film probe was a TSI model 1050 constant temperature anemometer, a TSI model 1051-1D monitor and power supply, and a TSI model 1060 RMS voltmeter. When foil was instrumented, runs were made starting at 20 rpm and going up to 120 rpm (at speeds greater than 120 rpm stirring in the tank became a dominant factor and the accuracy of the measurements became suspect). At each speed, the system was allowed to settle for 30 minutes before readings were taken. The parameters monitored were D.C. bridge voltage (e), RMS voltage (e') and rpm (ω).

For turbulence intensity the governing relations have been written as follows [37]:

$$\frac{V}{\bar{V}} = \frac{4e'V}{V^2 - V_0^2}$$

where $\frac{V'}{\bar{V}}$ is the turbulence intensity and

V = velocity in ft/sec, measured speed

e' = RMS voltage

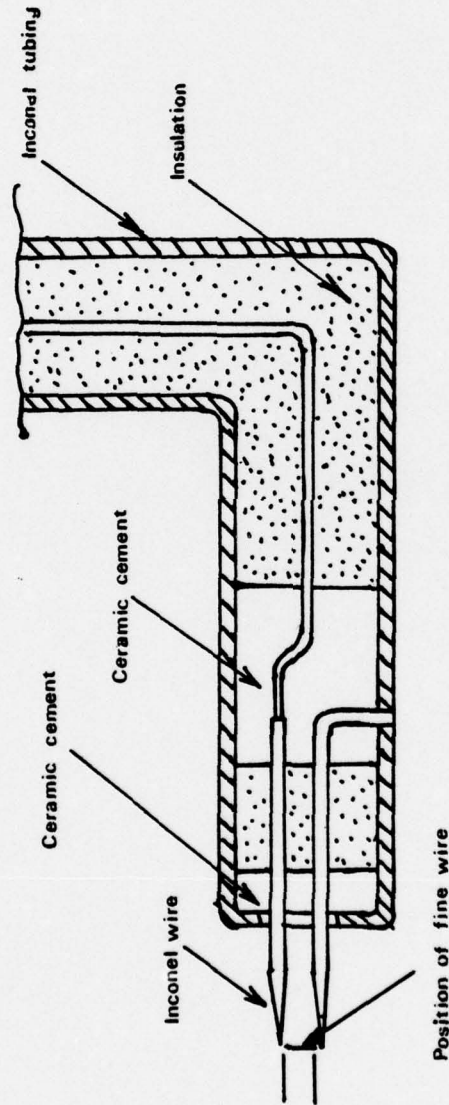


FIGURE 22
DETAIL OF A HOT-FILM PROBE [36].

e = D.C. bridge voltage

V_0 = extrapolated value from plot of e^2 vs. v

The value of V_0 was determined for each specimen position as shown in Figure 23. Once V_0 was known, the turbulence intensity could be calculated for each position. For the purposes of this experimentation it was necessary to know the turbulence intensity at 5 ft/sec (55 rpm) and 10 ft/sec (109 rpm) as these were the two speeds at which all dynamic exposures would be made. The results are tabulated in Table 8.

Upon completion of the first set of runs, the hot-film probe was raised 1 mm (0.0394 in) from its initial position on the surface of the foil and the data runs were repeated. The probe was then raised one more millimeter and the same procedure was again repeated. This was done in an attempt to establish a velocity profile over the foil as well as to determine the turbulence intensity with certainty. Comparison of the three data runs resulted in little if no variance in the turbulence intensity. Because the design of the hot-film probe allowed it to be placed no closer than 2.03 mm (0.08 in) from the surface of the foil and because the sensing area of the probe was about one mil, measurement of the same velocity at all three heights above the foil lead to the conclusion that the hydrodynamic boundary layer was 2.0 mm (.079 in) or less in thickness.

Theoretical prediction of the hydrodynamic boundary layer for turbulent flow over a flat plate is based on the equation [12]:

$$\frac{\delta_h}{x} = \frac{0.38}{Re^{0.2}}$$

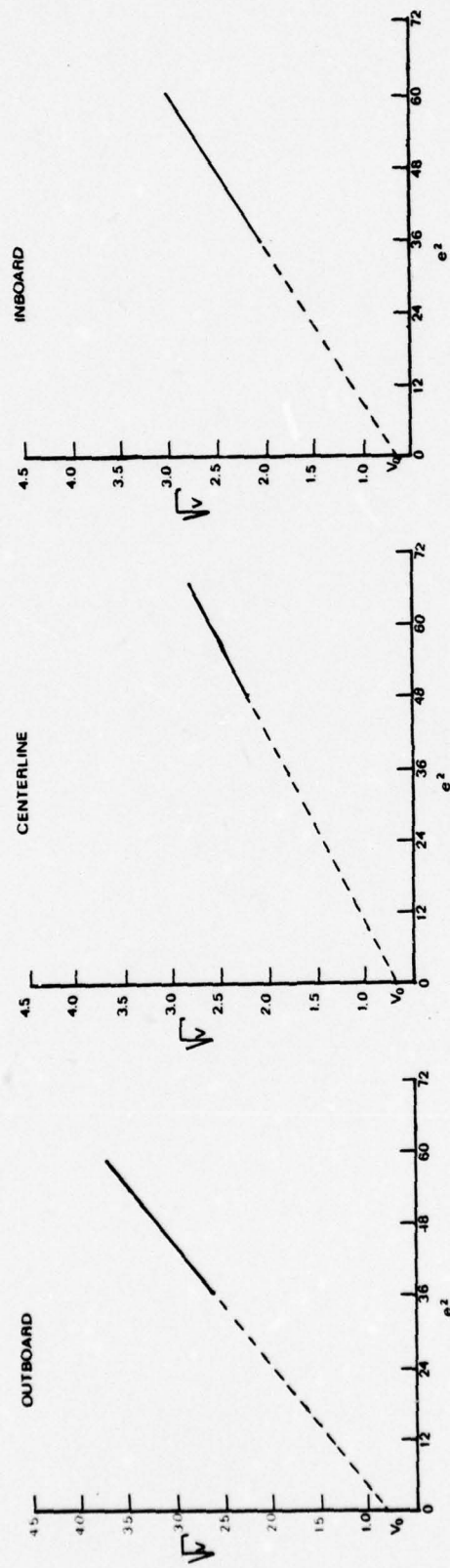


FIGURE 23

PLOTS OF \sqrt{V} vs. e^2 FOR EACH SPECIMEN POSITION ON THE FOIL
 (NOTE EXTRAPOLATED VALUE FOR V_0 ON EACH PLOT)

TABLE 8

	OUTBOARD	CENTERLINE	INBOARD
V	5 10 (ft/sec)	5 10 (ft/sec)	5 10 (ft/sec)
$\frac{v}{\bar{v}}$.093 .065	.094 .065	.097 .068

EXPERIMENTALLY DETERMINED VALUES OF
 TURBULENCE INTENSITY OVER THE
 FOIL SURFACE (5 ft/sec = 1.52 m/sec
 AND 10 ft/sec = 3.02 m/sec).

as stated in a previous section. Using the parameters of the actual foil and assuming a Reynold's Number of approximately 5×10^5 , the above equation predicts a boundary layer thickness of approximately 1.75 mm (.0689 in). This value supports the conclusions drawn from the experimental determination.

3. Dynamic Exposures

After characterization of the flow field within the test system was completed, the hot-film probe was removed and specimens were mounted for the first dynamic exposure. Figure 24 shows the foil configuration. Once mounted in the electrolyte, several checks were made to ensure a water-tight system and electrical continuity, if required.

It follows from the introductory discussion on galvanic corrosion that a metallic surface will undergo some corrosive activity the instant it is immersed in an electrolyte solution. Consequently, to minimize corrosion not induced by velocity, it was necessary to begin the run as soon as the assembly could be connected and checked in the exposure tank. Generally the time elapsed was approximately 45 seconds before the test velocity could be achieved. Before and after each run, the conductivity, temperature and pH were checked and recorded.

As the corrosion circuit was completed and the foil up to test velocity, an electric timer was started. The length of each run was timed to within an accuracy of one second. Simultaneously, for the test runs utilizing the electrically coupled specimens, the calibrated strip chart recorder was started in order to monitor and record the galvanic current between the two dissimilar metals. Because of the specimen and foil configuration, it was not possible to monitor the current between physically coupled specimens.

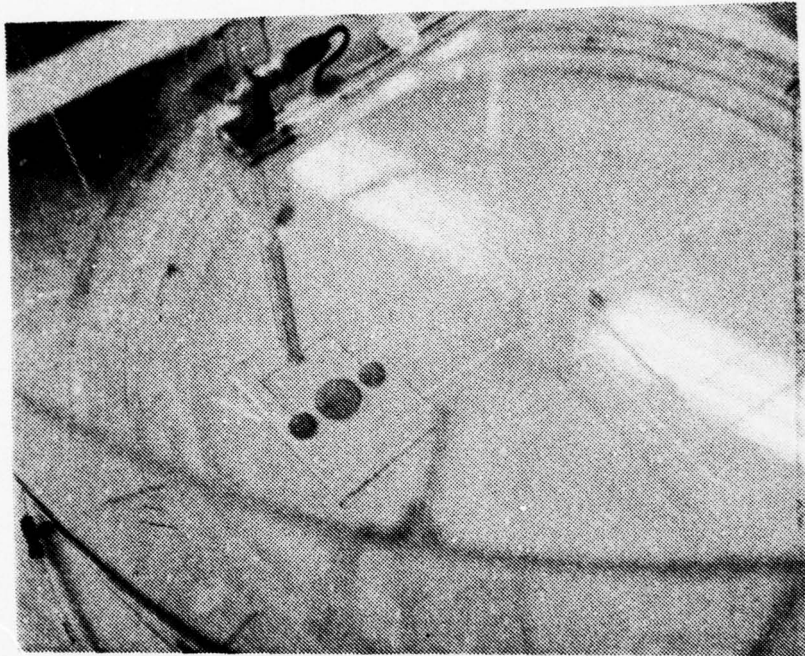


FIGURE 24

FOIL CONFIGURATION FOR
DYNAMIC EXPOSURE RUN

Coinciding with the expiration of each run, the strip chart recorder was disconnected and the foil immediately removed from the exposure tank. The removal process took 20 to 30 seconds on the average.

Once the foil had been removed from the exposure tank, the surface of each specimen was gently rinsed with distilled water. As the corrosion product was generally adherent to the metal surface (because of velocity effects to be discussed later), rinsing of the couple or specimen did not tend to damage or disturb the corrosion product as it might have for static specimens. Specimens were subsequently removed from their mounting hole(s) and allowed to dry naturally in air. This procedure avoided damage to the corrosion product structure while removing the electrolyte, but did not take into account the differences, if any, between the wet and dry states of the corrosion product. This study examined only the corrosion products in the dry state. Dried specimens were mounted on large aluminum SEM stubs, and the corroded metal surface was examined at various useful magnifications in an effort to compare the effects of velocity on corrosion product morphology and the actual metal surface. These results were then compared with the conditions on the stagnant exposure specimens.

A designated system will be utilized to identify specimens and exposure run conditions. The first number indicates the exposure time followed by the units of exposure time, minutes (M), or hours (H). Then the letter S for speed will be followed by either a 5 or a 10 designating 5 ft/sec or 10 ft/sec respectively. For static exposure runs the time of exposure will be followed by the designation ST. For example, 30MS10

indicates a 30 minute exposure at 10 ft/sec. A compilation of specimen exposure runs appears in Table 9.

TABLE 9

EXPERIMENTAL PARAMETERS **

<u>RUN #</u>	<u>COUPLE TYPE</u>	<u>EXPOSURE TIME</u>	<u>SPEED (ft/sec)</u>
2	Cu-Ni/PCS (E)*	24 (H)	ST
4	Cu-Ni/PCS (P)	24 (H)	ST
5	Cu-Ni/PCS (P)	24 (H)	5
6	K-Monel/PCS (P)	24 (H)	5
7	Cu-Ni/PCS (P)	24 (H)	10
8	K-Monel/PCS (P)	24 (H)	10
9	Cu-Ni/PCS (P)	30 (M)	5
10	Cu-Ni/PCS (P)	30 (M)	10
11	K-Monel/PCS (P)	30 (M)	5
12	K-Monel/PCS (P)	30 (M)	10
13	Cu-Ni/PCS (E)	24 (H)	5
14	K-Monel/PCS (P)	24 (H)	ST
15	K-Monel/PCS (E)	24 (H)	5
16	PCS (Single Metal)	24 (H)	5
17	Cu-Ni/PCS (P)	30 (M)	ST
18	K-Monel/PCS (P)	30 (M)	ST
19	Cu-Ni (Single)	24 (H)	5
20	Cu-Ni/PCS (E)	24 (H)	ST

* THE ABBREVIATION "PCS" STANDS FOR PLAIN CARBON STEEL. THE DESIGNATION 70/30 WILL BE OMITTED IN THE INTEREST OF SAVING SPACE. THE LETTER "E" MEANS ELECTRICALLY COUPLED, AND THE LETTER "P", PHYSICALLY COUPLED.

** ALL EXPERIMENTS PERFORMED AT APPROXIMATELY 20°C ± 1°C

TABLE 9 (cont.)

<u>RUN #</u>	<u>COUPLE TYPE</u>	<u>EXPOSURE TIME</u>	<u>SPEED (ft/sec)</u>
21	K-Monel/PCS (E)	24 (H)	ST
22	K-Monel (Single)	24 (H)	5
23	PCS (Single)	24 (H)	ST
24	PCS (Single)	24 (H)	10
25	Cu-Ni (Single)	24 (H)	ST
26	Cu-Ni (Single)	24 (H)	10
27	K-Monel (Single)	24 (H)	ST
28	K-Monel (Single)	24 (H)	10
29	Cu-Ni/PCS (E)	24 (H)	10
30	PCS (Single)	30 (M)	ST
31	K-Monel/PCS (E)	24 (H)	10
32	Cu-Ni/PCS (E)	24 (H)	10
33	Cu-Ni/PCS (E)	24 (H)	5
34	K-Monel/PCS (E)	24 (H)	5
35	Cu-Ni/PCS (E)	30 (M)	5
36	K-Monel/PCS (E)	30 (M)	5
37	Cu-Ni/PCS (E)	30 (M)	10
38	K-Monel/PCS (E)	30 (M)	10
39	Cu-Ni (Single)	30 (M)	ST
40	K-Monel (Single)	30 (M)	ST
41	Cu-Ni/PCS (E)	30 (M)	ST
42	K-Monel/PCS (E)	30 (M)	ST

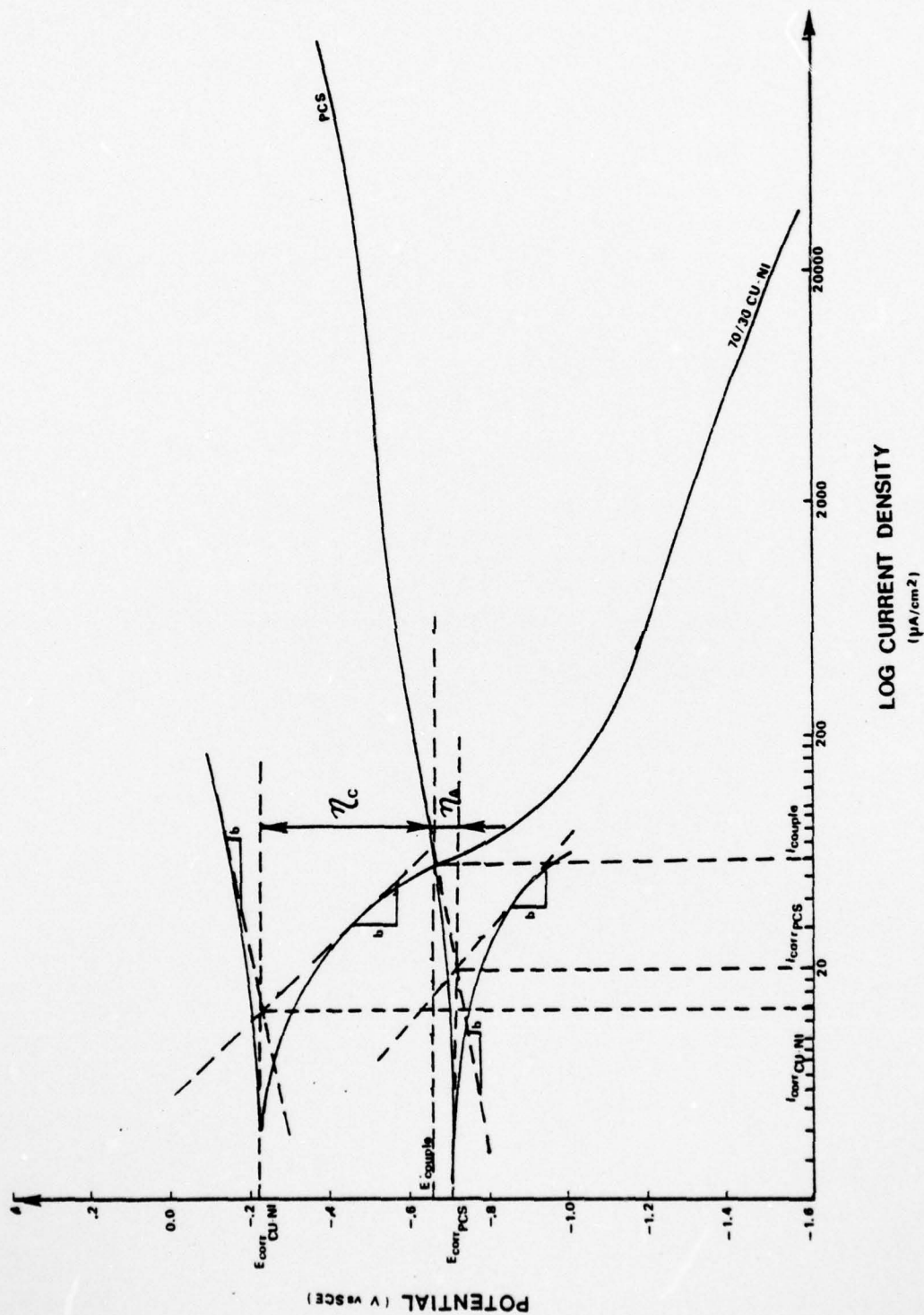
III. EXPERIMENTAL RESULTS AND CONCLUSIONS

A. CHARACTERIZATION OF SINGLE METAL CORROSION BEHAVIOR

1. Polarization Characteristics

It is incorrect to assume that the corrosion rate for a galvanic couple is determined simply by the difference in the potentials of the dissimilar metals on open circuit. When the metals are short circuited, as when bolted, riveted or welded together, other factors, such as polarization, relative areas and the conductivity of the solution play important roles. In the present experiments, the relative areas of the metals tested were the same, and the conductivity of the solution was relatively high and can be considered to have been constant. Therefore, these factors are considered to have not affected the corrosion rate to any significant extent. On the other hand, the polarization characteristics are distinctive for the respective metals (PCS, K-Monel and 70/30 Cu-Ni) and warrant careful consideration. Experimentally determined polarization curves for the single metals (PCS, K-Monel and 70/30 Cu-Ni) are presented in Figures 25 and 26.

Polarization refers to the change in electrode potentials that takes place as current passes. By definition, the polarization of the electrode, η , is the difference between the actual electrode potential and the calculated equilibrium electrode potential (the Nernst equation potential), and can be determined graphically from the Tafel slope, b , of the polarization curve. Examination of the polarization curves in Figures 25 and 26 shows that in both couple types (70/30 Cu-Ni/PCS and K-Monel/PCS), the reactions were under cathodic control, (with a greater



LOG CURRENT DENSITY
 ($\mu\text{A}/\text{cm}^2$)

FIGURE 25: 70/30 Cu-Ni/PCS POLARIZATION CURVES

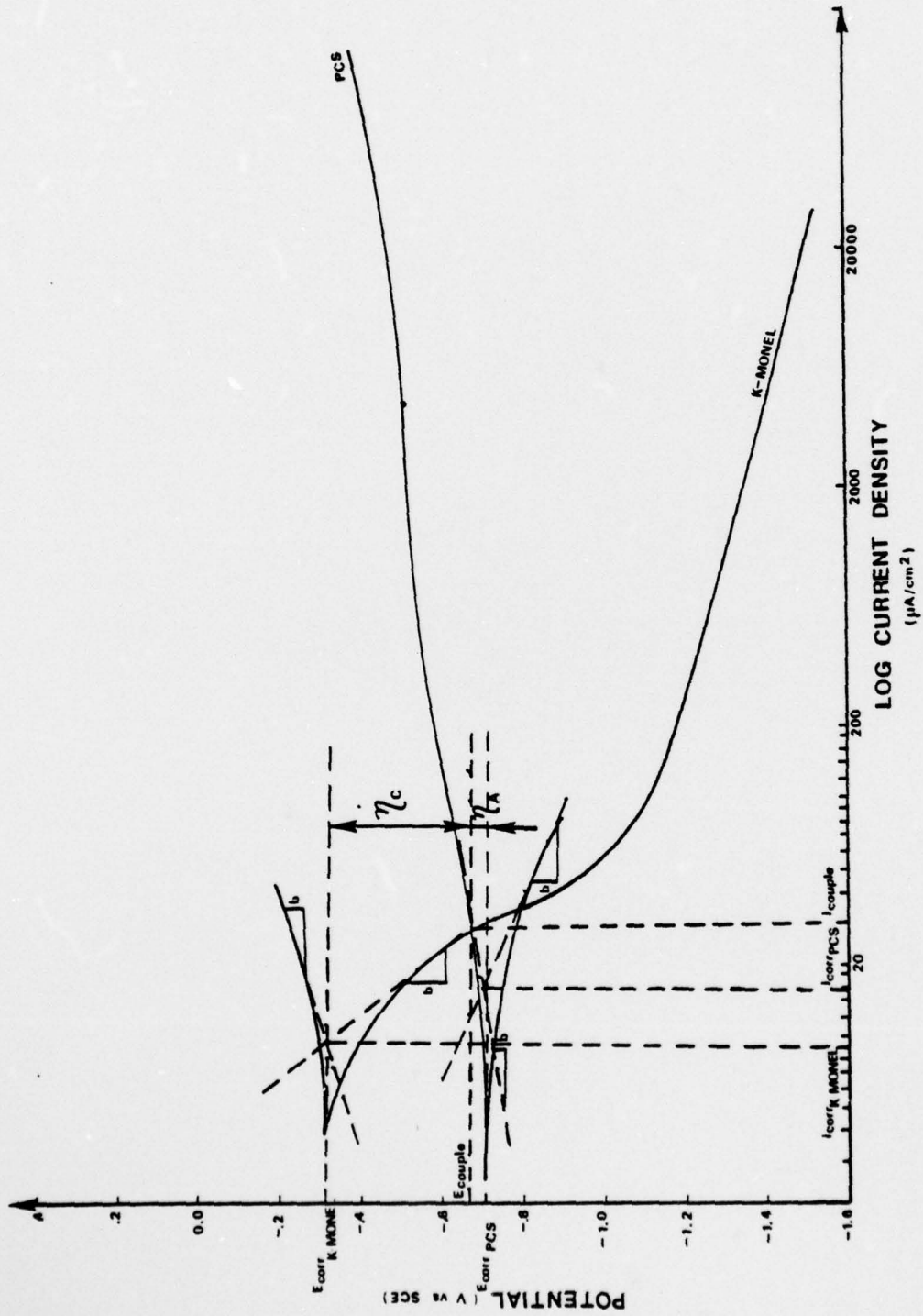


FIGURE 26: K-MONEL/PCS POLARIZATION CURVES

cathodic Tafel slope for the K-Monel than the 70/30 Cu-Ni). This means that most of the polarization in the couple occurred at the cathodic member, so that the net potential, E_{couple} , was near the open circuit anode potential, $E_{\text{corr}_{\text{PCS}}}$. In general, it is considered desirable to obtain greater polarization of both the anode (PCS) and the cathode (70/30 Cu-Ni and K-Monel) because it will decrease i_{couple} . It becomes obvious from the static polarization curves shown in Figures 25 and 26 that, under cathodic control, small changes in the cathodic Tafel slope will strongly influence i_{couple} , with cathodic de-polarization resulting in an increased rate. It should be noted that general shape and parameter values obtained for the polarization curves determined in the present study were in good agreement with previously obtained values [39, 42, 43].

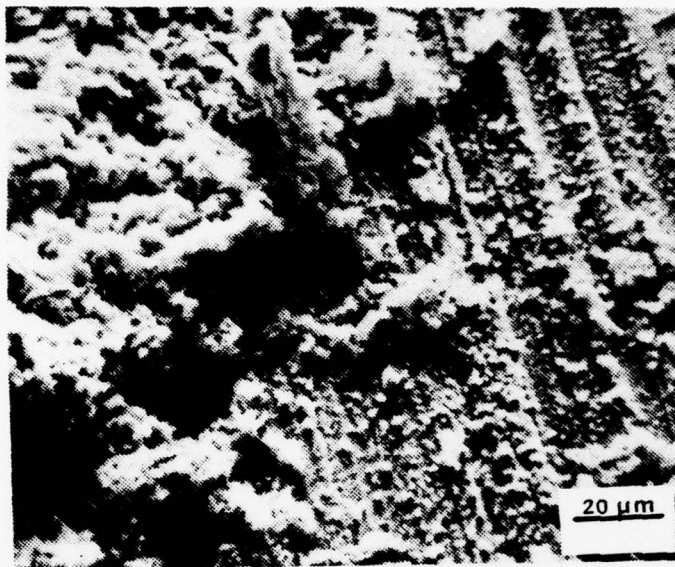
2. Single Metal Exposures

In order to establish a basis for comparison of velocity effects on corrosion product formation, morphology and corrosion rates in couples, single metal (uncoupled) specimens were studied under static and dynamic conditions. Two exposure times were considered, 30 minutes and 24 hours. The surface of both the 70/30 Cu-Ni and K-Monel specimens showed no evidence of corrosive attack under either static or dynamic conditions. Both metals are oxide film formers and since the period of exposure was relatively short, corrosive attack was neither hypothesized nor expected. The only noticeable surface feature which varied on either metal was the degree of oxide film formation, which seemed to be related to the exposure velocity. For example, 70/30 Cu-Ni specimens exposed at 5 ft/sec (1.52 m/sec) showed a normal (static-like) protective oxide film. At the relatively low velocity of 5 ft/sec (1.52 m/sec), few wake-induced air

bubbles were entrained in the electrolyte and the turbulence intensity was low. These conditions, along with the thickness of the hydrodynamic boundary at that velocity, probably account for the maintenance of this character for the surface film. At the test velocity of 10 ft/sec (3.02 m/sec) more air bubbles are entrained in the electrolyte and the turbulence intensity increased; these actions, and a reduction in the hydrodynamic boundary layer thickness might be associated with increased mechanical scrubbing effects, ultimately leading to breakdown of the protective oxide film on the metal surface. Visual and microscopic observations indicated a brighter surface on the 70/30 Cu-Ni exposed at 10 ft/sec (3.02 m/sec) than those exposed at 5 ft/sec (1.52 m/sec). On the other hand, K-Monel did not show any appreciable difference in surface luster at the various velocities. This result is consistent with the well known excellent corrosion resistance and oxide film formation characteristics of nickel-copper alloys under conditions of high turbulence in a dynamic system [5, 9, 39]. These subtle observations of the differences in the oxide film formation serve to demonstrate the importance of hydrodynamic effects and the need to characterize the flow regime in any test system.

The PCS, on the other hand, did display very graphic evidence of corrosion product formation and attack under both static and dynamic test conditions. The PCS exposed for the short time of 30 minutes showed, for all velocities, very slight evidence of corrosive attack, with discoloration only near surface irregularities. More noticeable attack occurred on specimens exposed for 24 hours, Figures 27 and 28.

The corrosion product shown in Figure 27(a) was light orange in color and covered approximately 30 percent of the exposed surface. The



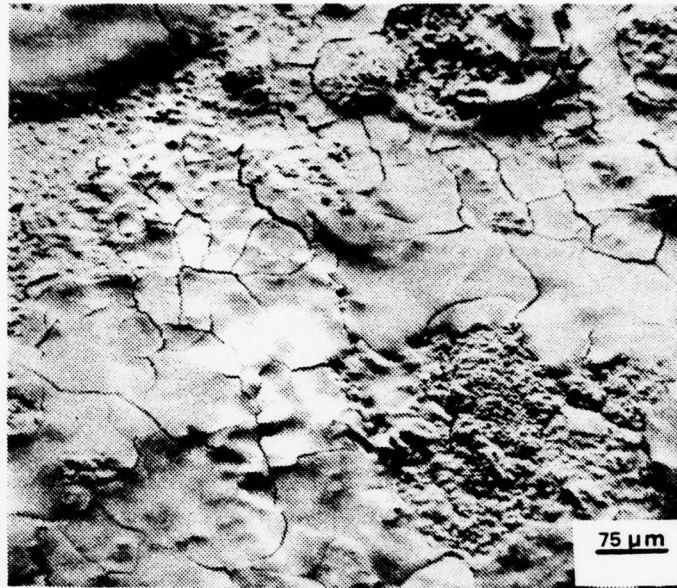
(a)



(b)

FIGURE 27

(a) SURFACE OF PCS SPECIMEN AFTER 24 HOURS EXPOSURE, STATIC, 610x. (b) SURFACE OF PCS SPECIMEN AT 24 HOURS EXPOSURE, 5 ft/sec (1.52 m/sec), 10x.



(a)



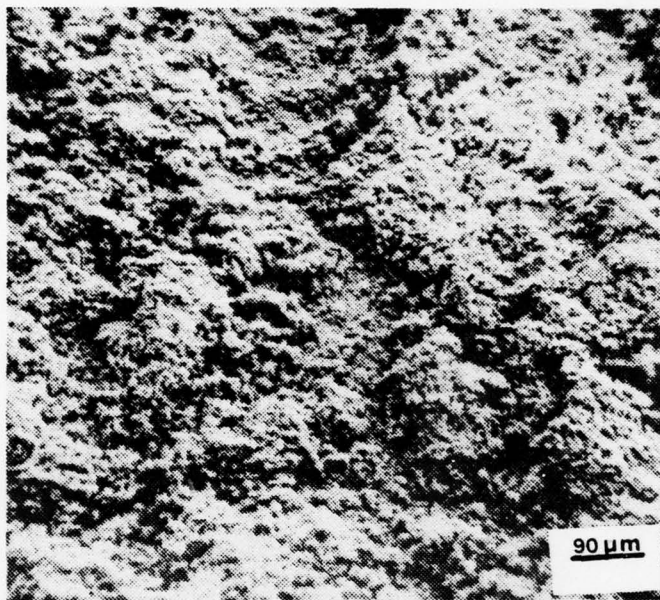
(b)

FIGURE 28: (a) SURFACE OF PCS SPECIMEN AFTER 24 HOURS EXPOSURE AT 10 ft/sec (3.02 m/sec), 130x. (b) SURFACE OF PCS SPECIMEN AFTER 24 HOURS EXPOSURE AT 10 ft/sec (3.02 m/sec), 1210x. NOTE THE "MUD-CRACKING" APPEARANCE OF THE CORROSION PRODUCT FORMATION.

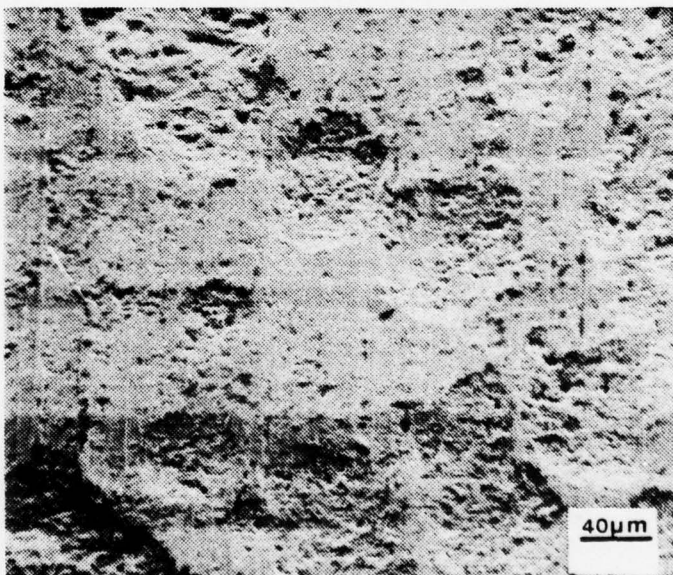
orange colored product was ostensibly ferric hydroxide ($\text{Fe}(\text{OH})_3$) [5]. Ferric hydroxide is a fairly insoluble iron corrosion product, yet appeared to cover only about 30 percent of the PCS surface. However, this does not mean that the process of electrochemical "rusting" had been suppressed when the film formed under static conditions [5]. It was observed that formation of rust corrosion product does not occur directly on the specimen surface but rather in the electrolyte directly adjacent to the corroding surface. This observation is well known as the reaction of hydroxyl ions from the cathodic process with the ferrous ions of the anodic dissolution when PCS is corroding in seawater. The two ions combine to form ferrous hydroxide which rapidly becomes oxidized and precipitates as the familiar rust [1]. In these stagnant seawater conditions, a corrosion product suspension appeared to float ever so slightly above the metal surface, and it was difficult to remove the PCS specimens from the static electrolyte environment without disturbing or partially losing the corrosion product. As the specimens were gently lifted from the electrolyte, the lightly adherent corrosion products were, in effect, washed away or shifted in position by the relative motion of the electrolyte. This is why some samples were observed with a coverage of only 30 percent or so.

Response of the PCS to dynamic conditions was readily observable. Specimens exposed for 24 hours at 5 ft/sec (1.52 m/sec), Figure 27(b), exhibited an adherent oxide film (rust) over about 40 percent of the exposed surface, bright orange in color. The corrosion product buildup was "streaked" in appearance with an obvious irregular topology. PCS specimens exposed for the same length of time at 10 ft/sec (3.02 m/sec), Figure 28, exhibited a very different corrosion product morphology, being

much darker in color, a red-brown, and more compact on the metal surface. The very obvious differences in the character of the corrosion products formed on the specimens at these two velocities may be explained in terms of differences in availability of oxygen and differences in diffusive mass-transfer rates. With increased velocity the hydrodynamic boundary layer becomes thinner, with a concurrent increase in the relative thickness of the diffusion mass-transfer boundary layer. At velocities such as the higher test velocities, convective diffusion predominates, bringing small elements of electrolyte containing dissolved oxygen towards the metal surface, thus increasing the available oxygen supply and speeding up corrosion product formation. As the velocity of the electrolyte increases, ferric hydroxide is formed in closer contact with the metal surface, giving a more compact form, whereas at lower velocities, ferrous products are precipitated more loosely on the surface [12]. Examination of the PCS specimen surfaces after cleaning revealed a uniform, general dissolution pattern over the entire exposed surface after exposure for 24 hours at 5 ft/sec (1.52 m/sec), Figure 29; some isolated pitting was observed. Specimens exposed at 10 ft/sec (3.02 m/sec) for the same length of time exhibited rather more severe corrosion attack and more localized dissolution pitting. Figure 30 illustrates rather large areas of metal removal; such areas were on the order of 80 to 120 μm wide over 65 percent of the specimen surfaces. Within the valleys large cavities, 40 to 60 μm in diameter, were observed and within these cavities were smaller pock-marks averaging 10 to 15 μm in diameter. These smallest pock-marks correspond approximately to the size of the pearlite regions in the PCS microstructure (see Figure 18). The attack noted above was predicted earlier by Rogers [38]. According to Rogers, all PCS's corrode



(a)



(b)

FIGURE 29: (a) SURFACE OF PCS SPECIMEN AFTER 24 HOURS EXPOSURE AT 5 ft/sec (1.52 m/sec), 115x. (b) CLEANED SURFACE OF PCS SPECIMEN AFTER 24 HOURS EXPOSURE AT 5 ft/sec (1.52 m/sec), 240x.

AD-A048 669

NAVAL POSTGRADUATE SCHOOL MONTEREY CALIF
THE EFFECTS OF VELOCITY ON CORROSION OF GALVANIC COUPLES IN SEA--ETC(U)
SEP 77 G A STORM

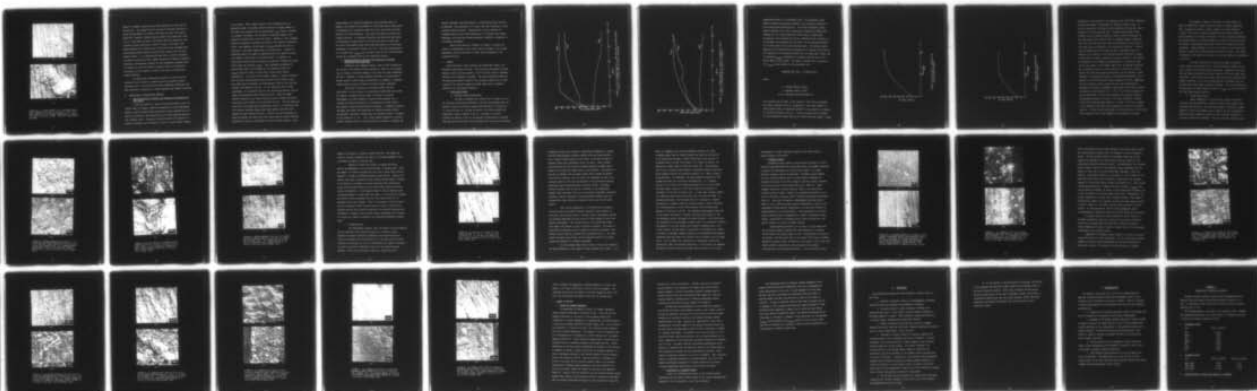
F/G 13/10

UNCLASSIFIED

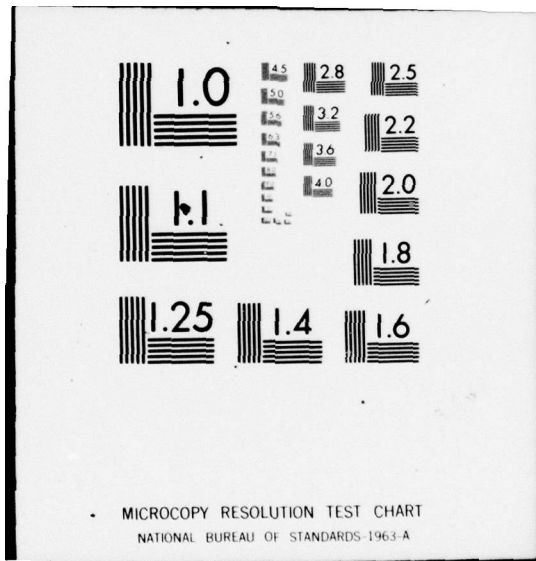
NL

292

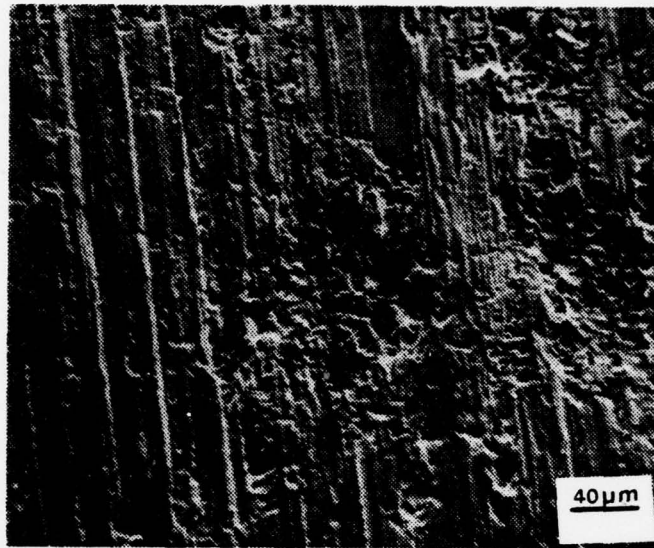
ADA048 669



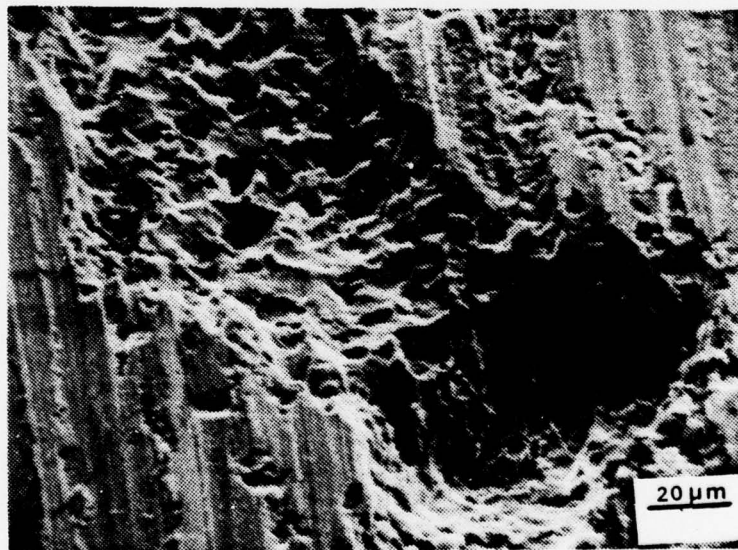
END
DATE
FILMED
2-78
DDC



MICROCOPY RESOLUTION TEST CHART
NATIONAL BUREAU OF STANDARDS-1963-A



(a)



(b)

FIGURE 30: (a) CLEAN SURFACE OF PCS SPECIMEN EXPOSED FOR 24 HOURS AT 10 ft/sec (3.02 m/sec), 235x. (b) CLEAN SURFACE OF PCS SPECIMEN EXPOSED FOR 24 HOURS AT 10 ft/sec (3.02 m/sec), 560x. NOTE THE "PITS WITHIN THE PITS".

rapidly in seawater unless they are well-protected (in this case the PCS was not). The overall rate of corrosion of PCS when used bare in slowly moving seawater is around 0.005 inches per year (0.13 cm/yr). These PCS's, however, undergo pitting corrosion and penetration rates of up to 0.04 inches per year (.102 cm/yr) should be allowed for thin sections in water velocities of about 10 ft/sec (3.02 m/sec) [38]. Rogers predicted the corrosion rate of PCS but did not determine what relationship existed between the electrolyte velocity and the fluid dynamic effects. It is hypothesized here that as velocity increases, the factors discussed earlier, namely entrained air bubbles, turbulence intensity, and decreased thickness of the hydrodynamic boundary layer, all combine to cause the observed corrosion effects of dissolution pitting and cavity formation in terms of the type of surface metal removal observed.

The single metal observations reported in this section are intended to form a basis for comparison with the galvanic couples discussed later. The next section briefly summarizes differences that might logically be expected for couples exposed under dynamic conditions.

B. PREDICTIONS OF COUPLED METAL BEHAVIOR

1. Expected Effects of Velocity and Coupling on Polarization of Test Metals

It was not possible to readily obtain polarization curves for couples under the dynamic conditions established in these experiments. However, using the single metal polarization curves obtained here as a basis for discussion, some predictions can be made regarding behavior and corrosion rates. Coupling of dissimilar metals and exposure to a dynamic environment can be expected to lead to several logical changes

in the system. First, simply because of the coupling of the two dissimilar metals, the anodic current passed by the anodic member of the couple will increase over the single metal i_{corr} values. Secondly, in a dynamic environment, the provision of dissolved oxygen in the system will increase due to the foil action. Oxygen is a very energetic cathodic de-polarizer (decreases the slope of the cathodic polarization curve), thus leading to an increase in i_{couple} and thus the rate of corrosion of the anodic member (PCS in all cases here). Another de-polarizing effect that might be expected would be the removal of metal ions formed by dissolution at the work surface. In general, de-polarization effects tend to decrease the respective cathodic and anodic Tafel slopes and increase i_{couple} . Also, depending on whether de-polarization effects are strongest at the cathode or anode, the E_{couple} value will shift, to more noble or more active values, respectively. In the case of the present couples, it would be expected that the major de-polarizing effects would be at the cathode, since even under static conditions the anode material (PCS) is not polarized strongly (see Figures 25 and 26). At the velocities used in these experiments, it is expected that the rate controlling reaction would be oxygen de-polarization under diffusion control. When the oxygen reduction reaction is not under diffusion control, flowing electrolyte should have little effect on the corrosion rate [6]. From the shape and character of the single metal polarization curves, it is predicted that the corrosion reactions taking place under dynamic conditions will probably be under diffusion control. Finally, the rate and manner in which the K-Monel and 70/30 Cu-Ni form their protective oxide films may determine the extent of polarization of the corrosion reactions. Even

though oxygen is a cathodic de-polarizer, the increased supply of oxygen to the surface of the K-Monel or 70/30 Cu-Ni aids to some extent in maintenance of a protective oxide film, and a more noble corrosion potential for these materials. This oxide film tends to polarize the cathodic reaction. At increased velocities and relatively high levels of turbulence the oxide film on the 70/30 Cu-Ni tends to break down, the film on the K-Monel being little affected because of its excellent resistance to electrolyte velocity [12, 39]. From this characteristic, it is evident that i_{couple} (and corrosion rate) for the 70/30 Cu-Ni/PCS couple will be greater than for the K-Monel/PCS couples.

2. Expected Effects of Velocity and Coupling on Corrosion Distribution and Morphology

Coupling of the dissimilar metals, since it will increase the net current in the system, would be expected to result in an increased rate of attack of the anodic member of the couple (in these experiments the PCS). Therefore, in given exposure intervals, one would expect a greater extent of attack might be manifested, for example, by expanded surface areas of attack and heavier corrosion product formation.

The effect of velocity on corrosion product form and distribution is less certain, but some general predictions can be made. For example, increased velocity might be expected to disfavor developments of loosely adherent corrosion product masses, and to increase the general distribution of dissolution; in other words, a more compact corrosion product might be expected. At higher velocities, one might also expect more exhibition of erosion-corrosion effects, with possibly concurrent pitting while the corrosion product is forming on the surface [5, 9, 12]. Also, under dynamic conditions, corrosion product formation may be a cyclical process of formation, cracking, and

removal (spalling), and fluctuations in current density with time may be expected. Such spalling, if it occurs, may also contribute to local erosion-corrosion activity. Qualitatively, one can conceive of a threshold velocity above which maintenance of a coherent film becomes impossible, with base metal being essentially constantly re-exposed to a turbulent environment.

These brief predictive comments are offered to prepare the reader for consideration of the actual results obtained in the present experiments, and the discussion of these results presented in the following sections.

C. COUPLES

During testing of 70/30 Cu-Ni/PCS and K-Monel/PCS couples, two different couple types were used. One type placed the metals in direct physical contact with one another to form the couple (this is hereafter referred to as "proximate" coupling). The other deployment scheme had the metals electrically coupled by low resistance copper wire in order to monitor the corrosion potential between them (this is hereafter referred to as "electrical" coupling).

1. Electrical Couples

a. Galvanic Current Measurements

In order to establish the relative rate or degree to which the corrosion process was proceeding in the test system being used, the galvanic current in electrical couples was monitored at 3 velocities, 0, 5 and 10 ft/sec (0, 1.52 and 3.02 m/sec), for 70/30 Cu-Ni/PCS and K-Monel/PCS couples, Figures 31 and 32. According to the data contained in Figures 31 and 32, the galvanic current density increased with time and with velocity; this correlates with visual and microscopic



FIGURE 31: PLOT OF CURRENT DENSITY vs. TIME FOR 70/30 Cu-NI/PCS COUPLE
 5 ft/sec = 1.52 m/sec AND 10 ft/sec = 3.02 m/sec



FIGURE 32: PLOT OF CURRENT DENSITY vs. TIME FOR K-MONEL/PCS COUPLE
 5 ft/sec = 1.52 m/sec AND 10 ft/sec = 3.02 m/sec

examinations which will be discussed later. The increased current density verifies the predicted behavior of the couples in relation to their polarization characteristics. The values of galvanic current density measured in the static electrically coupled test system when compared with the values predicted from the static, single metal polarization curves (Figures 25 and 26), differed by only 5 percent on the average; this indicates that the effect of the calibrated resistor in the test system circuit was relatively small. The current density measured in the coupled system corresponds to an increase in the rate of the reactions at the cathode and anode over the single metal values, and the measured i_{couple} corresponds to a greater corrosion rate of the anodic member of the couples. The anodic corrosion rate is related to the i_{couple} current density by the expression [42]:

$$\text{CORROSION RATE (MPY)} = 0.1288i(\mu\text{A}/\text{cm}^2)$$

where:

i = current density ($\mu\text{A}/\text{cm}^2$)

ρ = specimen density (g/cm^3)

eq wt = specimen equivalent weight (g)

The corrosion rate (in MPY) of PCS coupled to 70/30 Cu-Ni and K-Monel are shown in Figures 33 and 34, respectively. The results shown in these figures verify the predicted behavior of the couples as a function of relative electrolyte velocity. A lower corrosion rate is observed for the K-Monel/PCS couples than for the 70/30 Cu-Ni/PCS couples. Visual

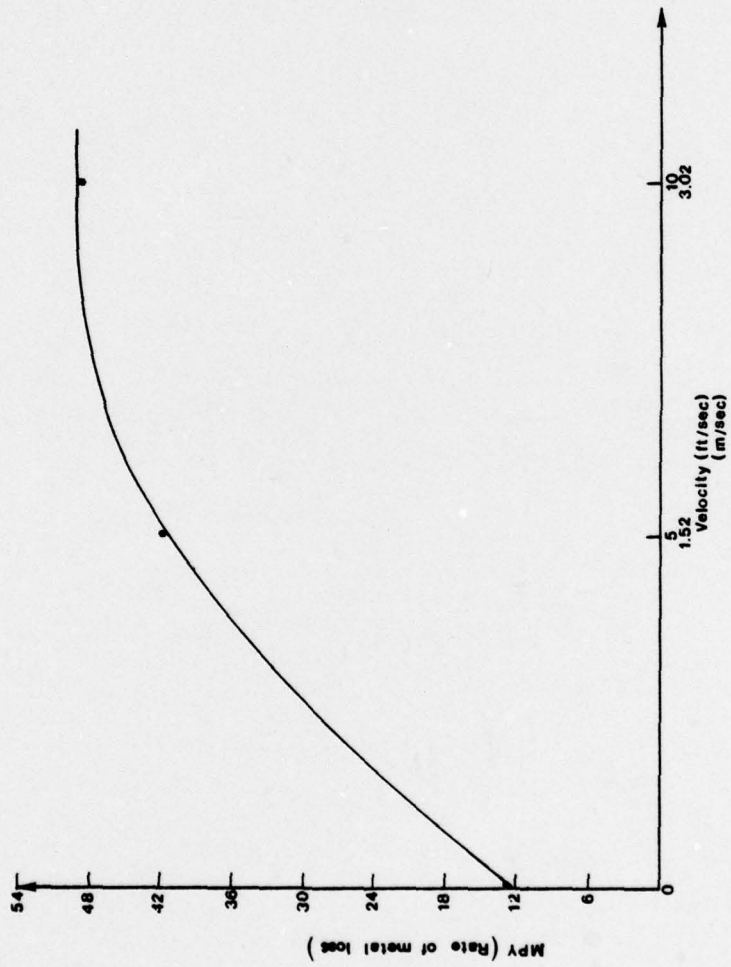


FIGURE 33: PLOT OF MPY vs. VELOCITY FOR
70/30 Cu-Ni/PCS COUPLE

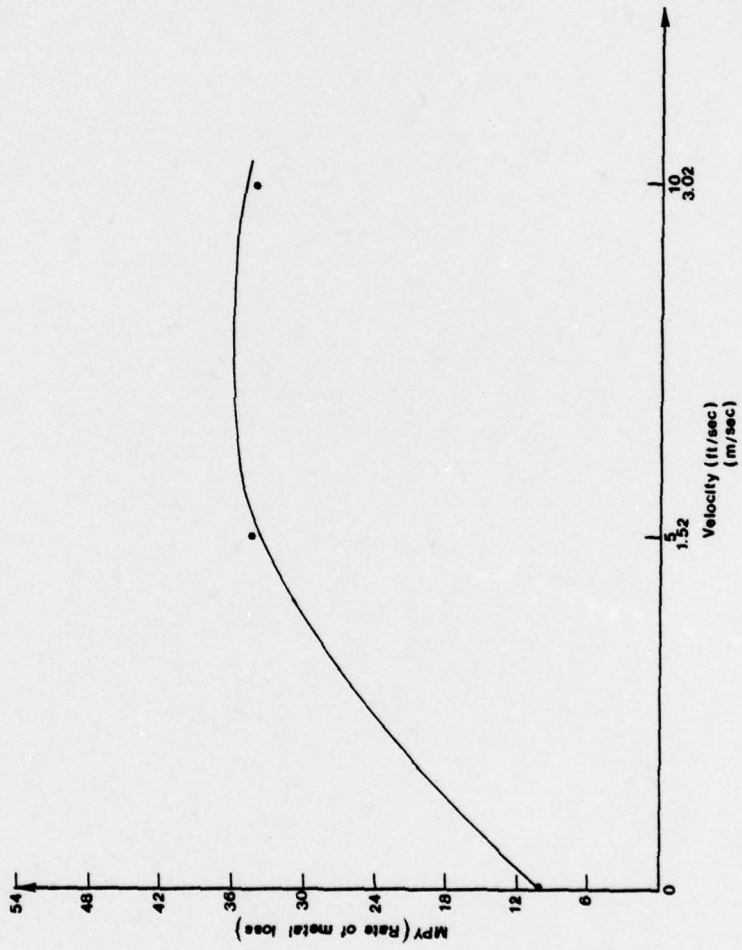


FIGURE 34: PLOT OF MPY vs. VELOCITY FOR
K-MONEL/PCS COUPLE

observation of the surfaces of the K-Monel and the 70/30 Cu-Ni components provide some insight to differences in observed corrosion rates. At all test velocities, the K-Monel surface exhibited the same dull luster, evidence of a protective oxide film. Although nickel-copper alloys (K-Monel) do not in general exhibit as good a corrosion resistance as the cupro-nickel alloys (70/30 Cu-Ni) in stagnant seawater conditions [17], they are still more noble than the PCS forming the other half of the couple and as a consequence are cathodically protected. A particularly valuable feature of K-Monel and most nickel-based alloys in seawater is the ability of the protective surface oxide film to remain in good repair in highly turbulent and erosive conditions. This ability was evidenced by the formation and maintenance of a protective oxide film on the surface of the K-Monel under static and dynamic conditions and the measured values of current density as a function of velocity. Because the oxide film remained undisturbed, the cell galvanic current remained at a relatively low level in the K-Monel/PCS galvanic cell, as compared to the 70/30 Cu-Ni/PCS couple (Figures 31 and 32), suggesting that the protective surface oxide film may be more susceptible to breakdown in turbulent environments, exposing bare metal and increasing the galvanic current density [12, 17, 39]. This idea was supported by visual observations of 70/30 Cu-Ni specimens after dynamic exposures. The specimens exposed at 10 ft/sec (3.02 m/sec) exhibited a brighter surface than those specimens exposed at 5 ft/sec (1.52 m/sec), leading to the conclusion that oxide film breakdown had occurred at the higher velocity. The very subtle differences in the surface luster on the 70/30 Cu-Ni specimens did not lend themselves to photographic recording.

With regard to Figure 31 (the plot of current density vs. time for K-Monel/PCS), several items are worthy of further explanation. First, although the values of current density for couples exposed at 5 ft/sec (1.52 m/sec) recorded are greater than the values observed for couples exposed at 10 ft/sec (3.02 m/sec), for the time period considered, the current density for couples running at 10 ft/sec (3.02 m/sec) had not yet reached a steady-state value after 24 hours of testing and was still increasing. Couples running at 5 ft/sec (1.52 m/sec), on the other hand, reached a steady-state current density value after 20 hours. This length of exposure in both cases was too short to allow any definitive conclusions to be drawn.

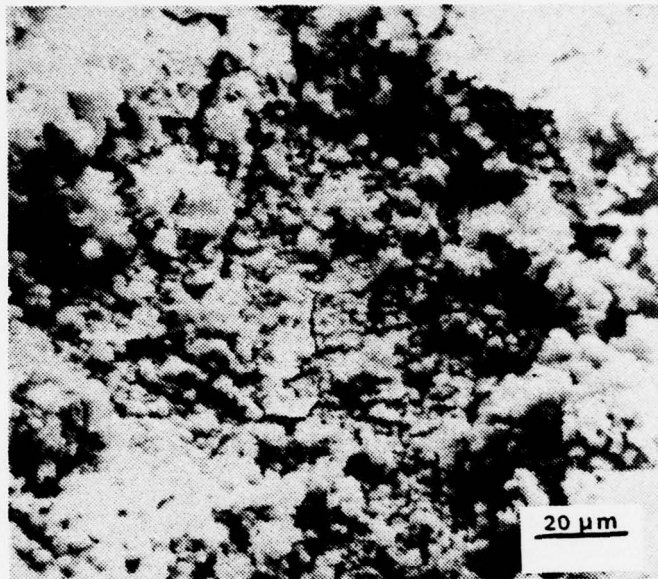
The final observation to be made with regard to galvanic current density and corrosion rate of the two different couples, was the rate at which the two cathodic metals polarized. Figures 25 and 26 show that the K-Monel polarizes more readily than the 70/30 Cu-Ni under static conditions. Since actual polarization curves could not be obtained under dynamic conditions it can only be predicted that the K-Monel will also polarize more rapidly under turbulent conditions. This is consistent with the observation of higher measured values of i_{couple} for the 70/30 Cu-Ni/PCS couple under dynamic condition.

b. Surface Observations

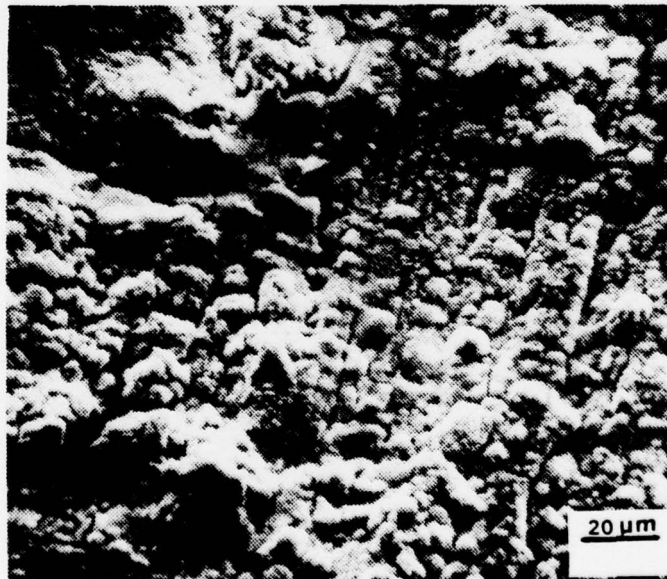
Visual examination of the electrical couples, both macroscopically and microscopically, revealed conditions that supported the reactions described above. The PCS anodic member of electrical couples exposed to a static environment did not exhibit any real differences in corrosion product formation, attack, or color from that exhibited on the static single metal specimens. The only noticeable difference was

that the proportion of exposed PCS surface covered by the product increased, when coupled, to about 80 to 90 percent. The most dramatic change in corrosion product formation, morphology, etc., was noted in the dynamically exposed specimens, Figures 35 through 38.

The amount and physical appearance of the corrosion products was different at the two test velocities. On the specimens exposed at the higher velocity of 10 ft/sec (3.02 m/sec), the accumulation of deposits was heavier and assumed a more compact character. Observation of the cleaned surfaces of the couples revealed dissolution pitting and evidence of erosion-corrosion metal removal of varying degree on the PCS surface, with higher velocity specimens exhibiting more surface attack and metal loss. The rather large areas of metal dissolution observed on the PCS are consistent with erosion-corrosion in a turbulent environment; these areas covered approximately 80 percent of the PCS surface at the higher velocity and about 30 percent of the PCS surface at the lower velocity. The degree of attack can be related to the level of turbulence over the metal surface (about 9% for 5 ft/sec (1.52 m/sec) and about 6% for 10 ft/sec (3.02 m/sec)), the actual electrolyte velocity and the thickness of the hydrodynamic boundary layer. As discussed earlier, as velocity increases, the hydrodynamic boundary layer becomes thinner. Additionally, with increased velocity, more air bubbles become entrained in the electrolyte. If the air bubbles have a diameter that is greater than a critical value (the thickness of the hydrodynamic boundary layer), the bubbles striking the boundary layer are not deflected and consequently are subjected to differential forces that disrupt them at the boundary layer; this enables the electrolyte to impinge directly on the metal surface at the point of bubble/boundary layer disruption, with possible

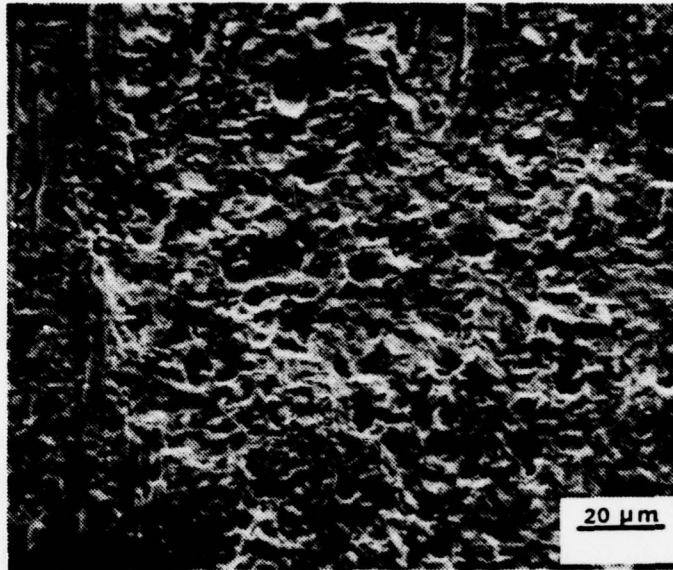


(a)

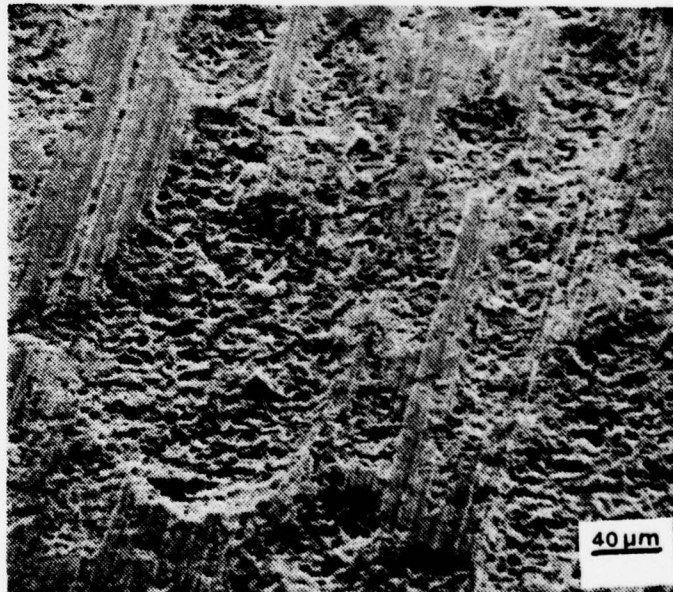


(b)

FIGURE 35: (a) PCS SURFACE OF 70/30 Cu-Ni/PCS ELEC. COUPLE EXPOSED AT 5 ft/sec (1.52 m/sec) FOR 24 HOURS, 600x. (b) PCS SURFACE OF 70/30 Cu-Ni/PCS ELEC. COUPLE EXPOSED AT 10 ft/sec (3.02 m/sec) FOR 24 HOURS, 550x.

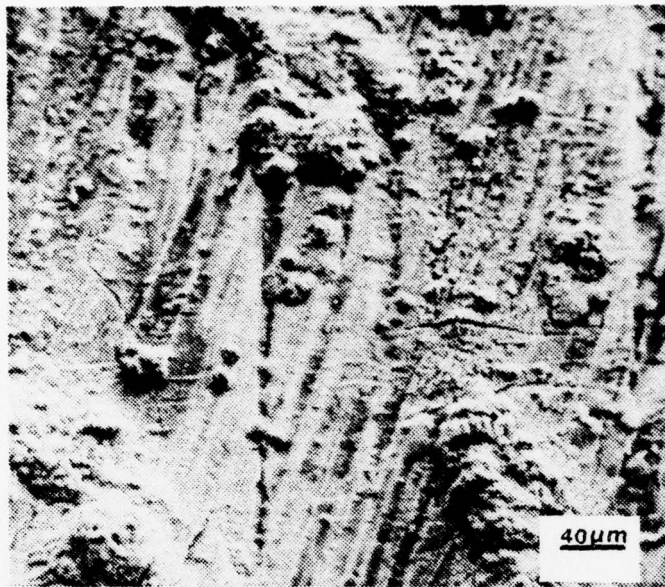


(a)

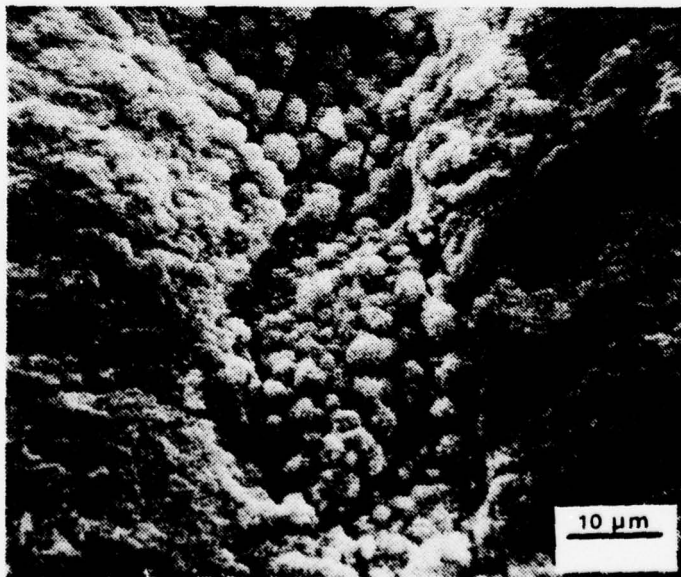


(b)

FIGURE 36: CLEANED SURFACE OF PCS HALF OF 70/30 Cu-Ni/PCS ELEC. COUPLE EXPOSED AT 5 ft/sec (1.52 m/sec) FOR 24 HOURS, 610x. (b) CLEANED SURFACE OF PCS HALF OF 70/30 Cu-Ni/PCS ELEC. COUPLE EXPOSED AT 10 ft/sec (3.02 m/sec) FOR 24 HOURS, 225x.

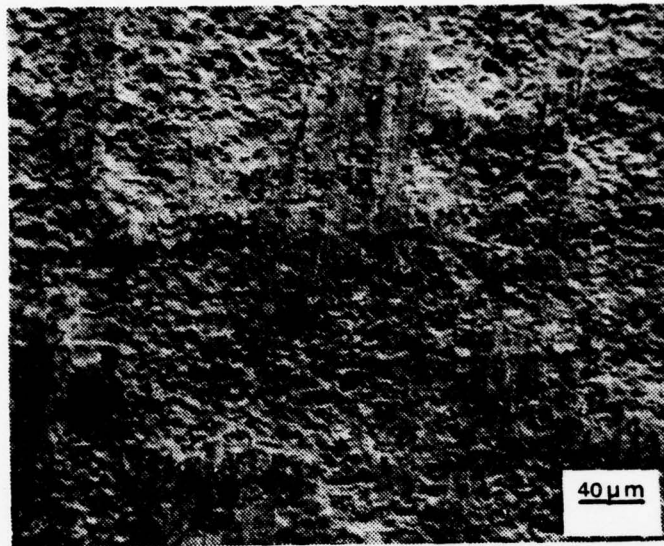


(a)

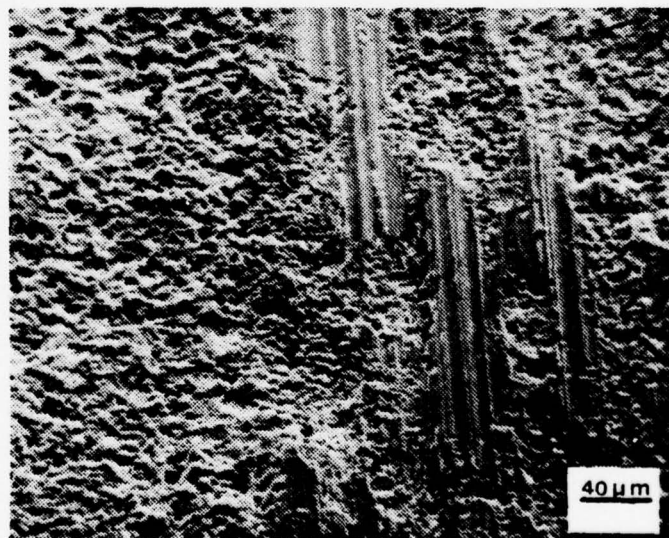


(b)

FIGURE 37: (a) PCS SURFACE OF K-MONEL/PCS ELEC. COUPLE EXPOSED AT 5 ft/sec (1.52 m/sec) FOR 24 HOURS, 225x. (b) PCS SURFACE OF K-MONEL/PCS ELEC. COUPLE EXPOSED AT 10 ft/sec (3.02 m/sec) FOR 24 HOURS, 1225x.



(a)



(b)

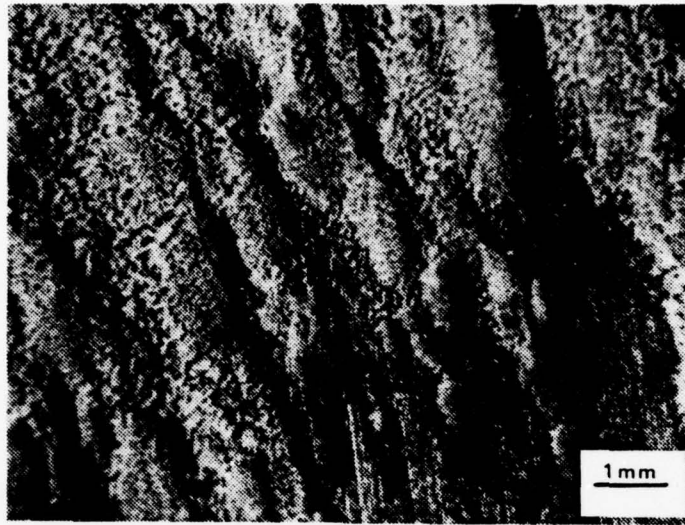
FIGURE 38: CLEANED SURFACE OF PCS HALF OF K-MONEL/
PCS ELEC. COUPLE EXPOSED AT 5 ft/sec (1.52 m/sec)
FOR 24 HOURS, 225x. (b) CLEANED SURFACE OF PCS
HALF OF K-MONEL/PCS ELEC. COUPLE EXPOSED AT 10
ft/sec (3.02 m/sec) FOR 24 HOURS, 240x.

removal of the metal or protective oxide film [39]. The higher the velocity, the more pronounced the effect of the above parameter, with a resultant increase in corrosion rate.

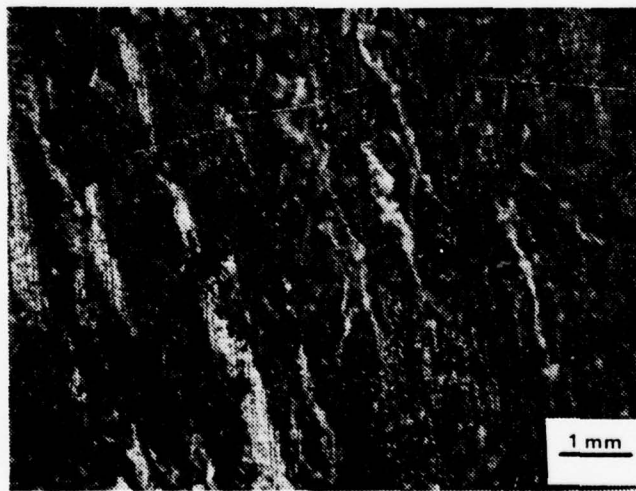
Exposure of electrical couples to varying velocities affects the appearance of the corrosion product in several ways. First, the number of "streaks" increases per unit area of anode (PCS) surface, Figure 39. Secondly, individual streaks are more narrow. Finally, the surface sites where individual streaks initiate became smaller. Reasons for increases in the number of streak initiation sites (dissolution sites) with increased velocity are not intuitively obvious and warrant further consideration. Fluid dynamics seems to play an important role concerning changes in streak number and width. As the velocity increases, electrolyte velocity gradients and thus local shear stress on the specimen surface are increased. Thus it is necessary to know the exact level of turbulence within the test system in order to correlate the observed results with in-service conditions or previously obtained data. Additionally, changes in the corrosion product morphology with increases in velocity are caused by changes in the existing hydrodynamic boundary layer.

c. Interpretations

The hydrodynamic boundary layer can modify the electrochemical factors involved in the corrosion reaction of a galvanic couple. Extensive discussion concerning fundamental electrode processes are offered by Gerisher [40] and Petrocelli [41], who agree that electrode reactions are affected not only by concentration and chemical conditions, but also by electrical conditions in and near the couple/electrode boundary. Near such an interface, oppositely charged particles



(a)



(b)

FIGURE 39: (a) PCS HALF OF K-MONEL/PCS ELEC. COUPLE EXPOSED AT 5 ft/sec (1.52 m/sec) FOR 24 HOURS, 10x. (b) PCS HALF OF K-MONEL/PCS ELEC. COUPLE EXPOSED AT 10 ft/sec (3.02 m/sec) FOR 24 HOURS, 10x.

accumulate as metal ions attempt to redistribute themselves to achieve an equal electrochemical potential between solid and solute metallic ions. Unequal currents exist as ions travel to and from the metal at different rates until equilibrium occurs (if ever). These currents cause the metal and the solution to become oppositely charged, which results in an electrical double layer at the interface. The ability of the ions to transfer from the metal surface (PCS) through the double layer and into solution, and vice versa, will determine the emf of the corrosion reaction, with the rate governed by the electrical potential differences near the metal/solution interface [35,40]. The metal/solution interface will in turn be a function of the hydrodynamic boundary layer thickness; that is, as the velocity increases, turbulence increases, causing a decrease in the hydrodynamic boundary layer and allowing more rapid diffusion of metallic ions to and from the metal surface.

After careful examination of corrosion product formation, corrosive attack on the metal surfaces, galvanic current density vs. time plots, and corrosion rate vs. velocity curves, some general notions are developed regarding the basic nature of these couples in static and dynamic environments. The corrosion product for coupled PCS becomes more compact and darkens in color as velocity increases. The extent of dissolution pitting and erosion is greater as velocity increases. Also galvanic current density increases with increasing velocity. All these results correlate quite nicely with the predicted behavior for metals coupled and deployed in a dynamic environment.

But even though these results could be fairly well predicted, the exact mechanisms at work remain in some instances quite vague. It is

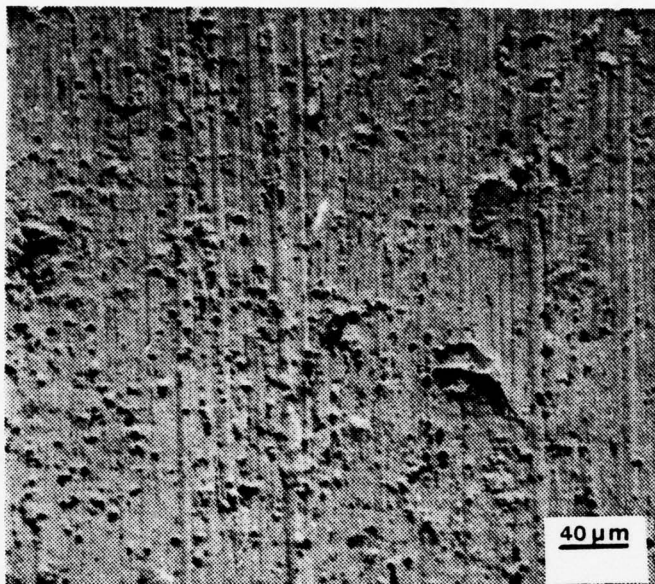
known, for example, that the electrochemical potential of freely corroding copper (and its alloys) becomes less noble as the velocity of the electrolyte increases. Syrett states that as the velocity is increased from 0.5 ft/sec (0.15 m/sec) to 13 ft/sec (4.0 m/sec), the potential of copper drops to 0.10 volts (SCE) [12]. This potential drop is due to the more rapid removal of anodically produced ions which would normally polarize the corrosion reaction, i.e., there is anodic de-polarization. By comparison, the electrochemical potential of PCS becomes more noble as the velocity increases [14]. At a seawater velocity of 0.5 ft/sec (0.15 m/sec) the potential is -0.70 volts (SCE) and rises almost linearly to -0.59 volts (SCE) as the velocity is increased to 13 ft/sec (4.0 m/sec) [12]. In this case, velocity affects the conditions under which the surface film on the PCS is formed. As discussed previously, the increased velocity, resulting in a greater availability of oxygen, causes the corrosion product (ferric hydroxide) to be precipitated as a hard closely adherent film, affording some degree of protection to the PCS. The changing electrochemical potential in the system, the degree of cathodic and anodic polarization of the two dissimilar metals, the degree of bubble formation in the electrolyte, the thickness of the hydrodynamic boundary layer, the turbulence intensity, the geometry of the test system, the constantly changing value of the current density, and the extent of protective film formation all combine to produce an extremely complex combination of experimental/environmental parameters which may affect the corrosion rate of couples such as studied here. It is no wonder that correlation of experimental results has historically been a hit-or-miss proposition. In this study, the emphasis has been on accurate control and proper characterization of the fluid

flow regime as a vitally important feature of any viable study of velocity effects on corrosion.

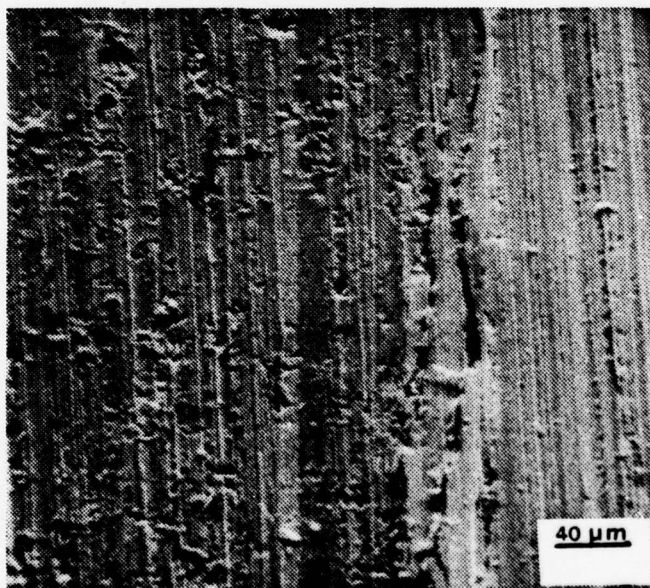
2. Proximate Couples

Proximate couples (metals in direct physical contact) of 70/30 Cu-Ni/PCS and K-Monel/PCS were tested under static and dynamic conditions in exactly the same manner as the electrical couples. Of course, galvanic currents could not be monitored. Proximate couples exposed for only 30 minutes showed little corrosion product formation but exhibited some signs of the early stages of pitting corrosion (defined as localized attack in depth rather than area), Figure 40. Under stagnant conditions, 30 minute exposure times do not produce much corrosion product buildup. However, by increasing the velocity to 10 ft/sec (3.02 m/sec) corrosion product formation was greatly accelerated, Figure 41. Note that the angular, diamond-shaped particles seen in Figure 41 are a chloride sea-salt deposit remaining as a result of the experimental drying process (composition of the particles inferred by energy-dispersive x-ray spectroscopy). The acceleration of corrosion product formation may be interpreted as a result of increased current density, associated with increased rates of ionic diffusion near the metal's surface as a result of higher velocity.

Couples exposed statically for 24 hours of course showed much more corrosion product formation than those exposed for 30 minutes. The PCS product was bright orange in color, covering about 95 percent of the surface. The more noble half of the couple (70/30 Cu-Ni or K-Monel) showed no corrosion product formation but did present a dull luster over their surfaces as predicted by their protective film forming characteristics and polarization behavior. The PCS corrosion product

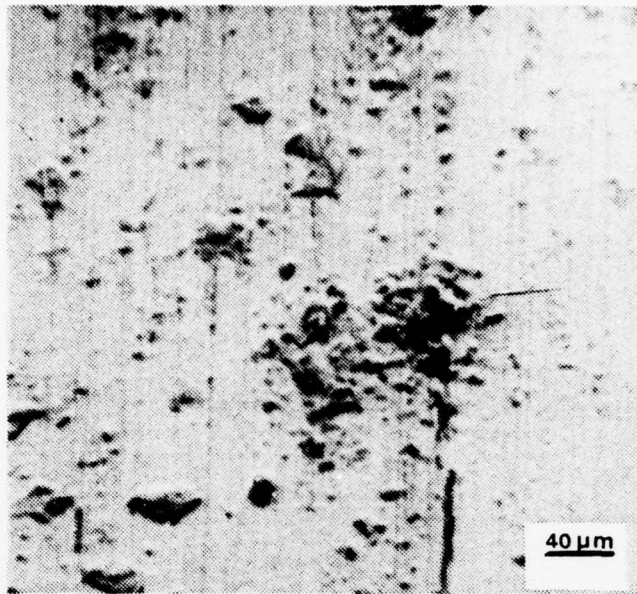


(a)

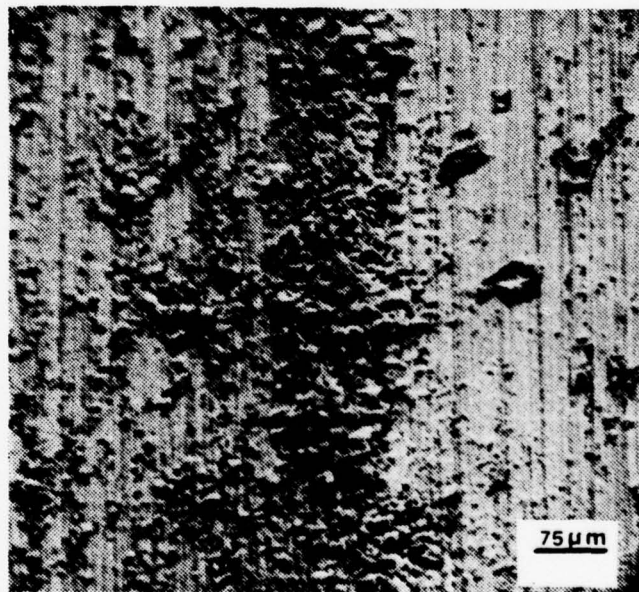


(b)

FIGURE 40: (a) CLEANED SURFACE OF PCS HALF OF 70/30 Cu-Ni/PCS PROXIMATE COUPLE, STATIC EXPOSURE, FOR 30 MINUTES. NOTE ONSET OF PITTING CORROSION, 240x. (b) CLEANED INTERFACE OF K-MONEL/PCS PROXIMATE COUPLE, STATIC EXPOSURE, FOR 30 MINUTES, NOTE PITTING CORROSION NOT AS SEVERE AS IN 39(a), 240x.



(a)



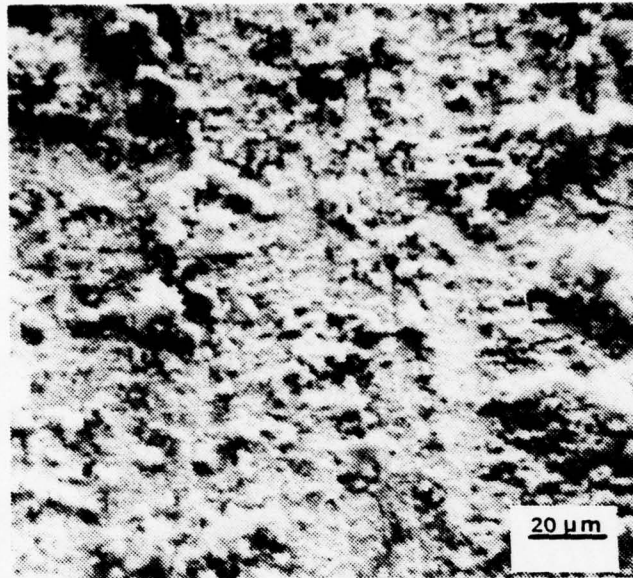
(b)

FIGURE 41: (a) INTERFACE OF 70/30 Cu-Ni/PCS PROXIMATE COUPLE (PCS ON LEFT), STATIC EXPOSURE, FOR 30 MINUTES, 225x. (b) INTERFACE OF 70/30 Cu-Ni/PCS PROXIMATE COUPLE (PCS ON LEFT), 10 ft/sec (3.02 m/sec), FOR 30 MINUTES, 130x.

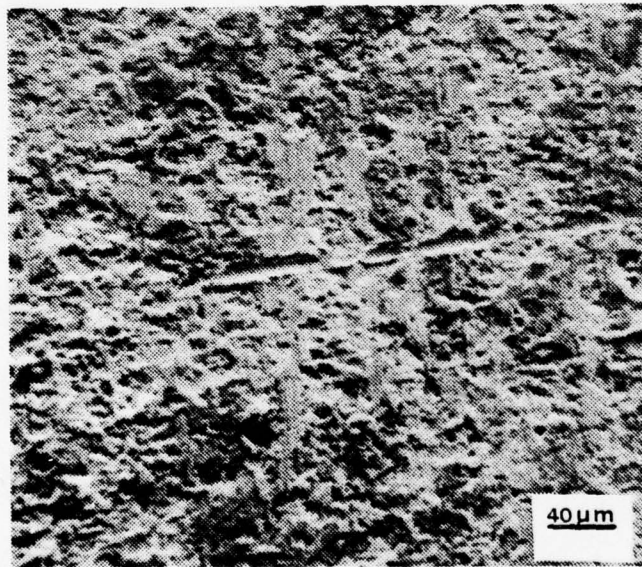
(ferric hydroxide) was very loosely adherent to the anodic (PCS) surface and concentrated more heavily near the interface of the two dissimilar metals. The PCS corrosion product for proximate couples was no more tenacious in adhering to the metal surface than that observed in the single metal exposures discussed earlier. The morphology of the corrosion product formed on the PCS in the proximate couple arrangement was very similar to that found on the PCS single metal specimens. There was, however, a noticeable difference in the amount of "rust" formed (for the same time period under static conditions), explained by the increased quantity of current that passes through the proximate cell. When coupled, the PCS anode polarizes to a higher corrosion potential (E_{couple}), the current density increases, the amount of metal dissolution increases, and so does the amount of corrosion product which forms. Examination of the couples (exposed for 24 hours) after cleaning revealed a high degree of surface metal removal due to general corrosion and some isolated pitting corrosion, Figure 42. The attack affected over 95 percent of the PCS surface. By such observation, the PCS surface damage was clearly distinguishable as being more severe than for PCS single metal specimens.

The degree and type of attack observed on the PCS surface in proximate couples was very nearly identical to the attack suffered by the electrical couples under the same static conditions, Figure 43. Careful examination of such as Figure 43 reveals little if no discernable differences in the corrosive attack.

Examination of proximate couples exposed to relative electrolyte velocities proved to be very informative. As for the electrical couples, changes in corrosion product morphology and type and distribution of attack were studied. The buildup of corrosion products in dynamic

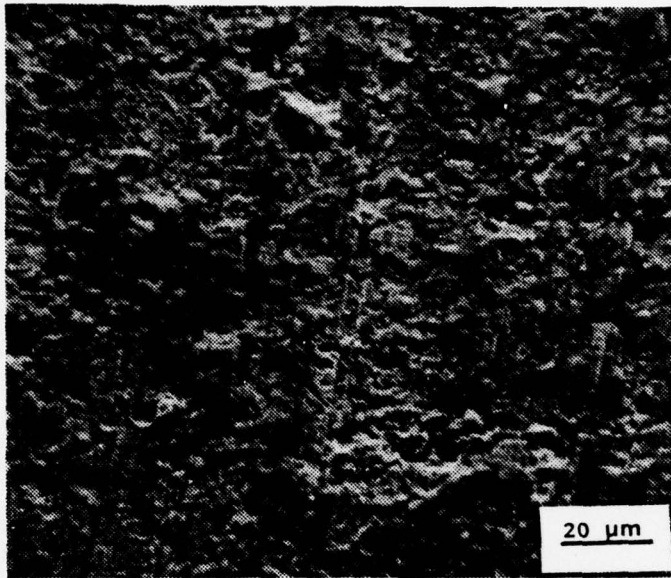


(a)

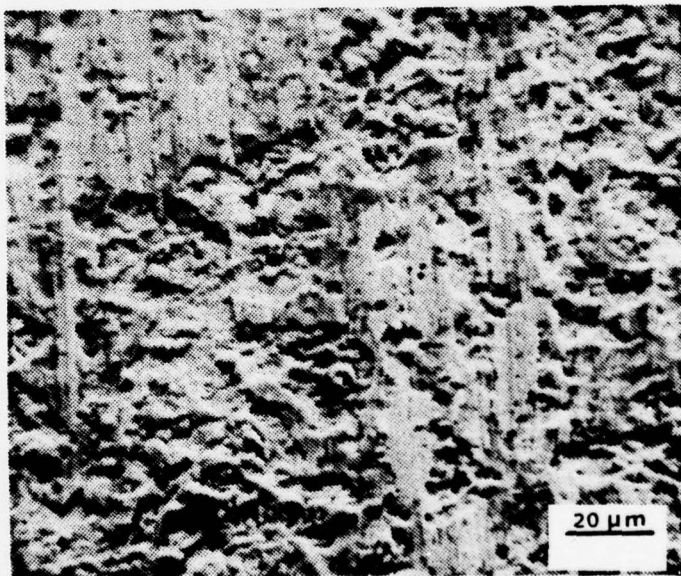


(b)

FIGURE 42: (a) SURFACE OF PCS HALF OF 70/30 Cu-Ni/
PCS PROXIMATE COUPLE, STATIC EXPOSURE, FOR 24 HOURS,
550x. (b) CLEANED SURFACE OF PCS HALF OF 70/30
Cu-Ni/PCS PROXIMATE COUPLE, STATIC EXPOSURE, FOR
24 HOURS, 240x.



(a)



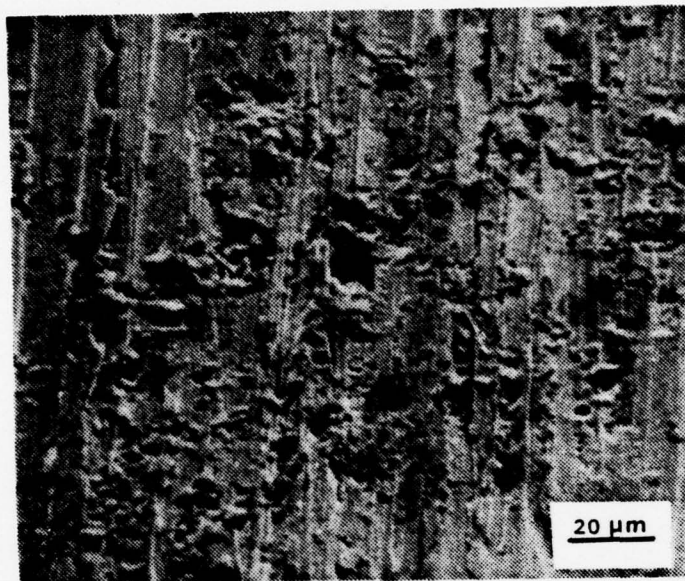
(b)

FIGURE 43: (a) CLEANED SURFACE OF PCS HALF OF K-MONEL/PCS PROXIMATE COUPLE, STATIC EXPOSURE, FOR 24 HOURS, 600x. (b) CLEANED SURFACE OF PCS HALF OF K-MONEL/PCS ELEC. COUPLE, STATIC EXPOSURE, FOR 24 HOURS, 600x.

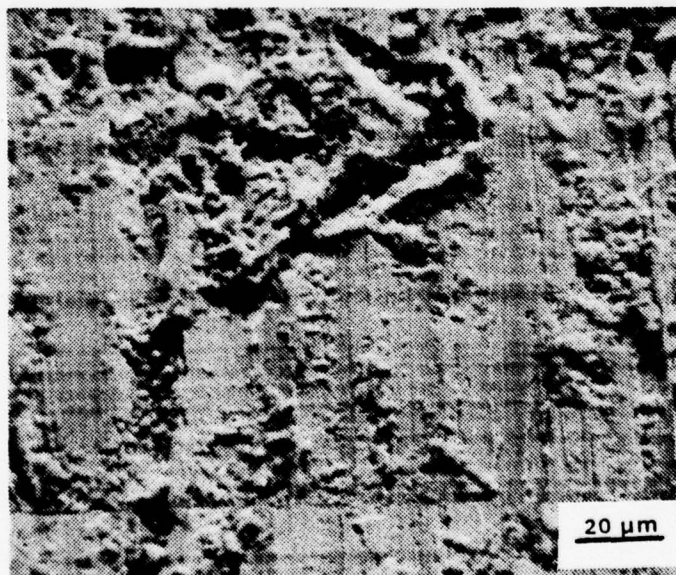
conditions, for short periods, was illustrated in Figure 41(b). Microscopic examination of the cleaned surfaces of the proximate couples exposed at different velocities for short periods of time revealed more severe metal removal and pitting corrosion on the PCS surface than observed on specimens exposed under static conditions (for the same period of time), Figure 44. Additionally, the degree of attack varied with velocity, with the PCS half of the couple exposed at 10 ft/sec (3.02 m/sec) suffering the most severe attack.

In order to obtain a more accurate picture of what happened on the surface of the proximate couples, specimens exposed for 24 hours at 5 ft/sec (1.52 m/sec) and 10 ft/sec (3.02 m/sec) were closely examined, Figures 45 through 48. Several features of the corrosion product formation became immediately obvious. As the velocity was increased, the corrosion product assumed a more compact nature and started to crack (Figure 46(a)). This was a common feature regardless of couple composition. The PCS corrosion products also assumed a darker color, going from orange at 5 ft/sec (1.52 m/sec) to a dark red-brown at 10 ft/sec (3.02 m/sec). Finally, in addition to being more compact with increasing velocity, the film was also more adherent.

Differences in topology of the corrosion products at different velocities are informative relative to the operative mechanisms of corrosion product formation. At higher velocities, the ferric hydroxide is only able to form on the PCS surface as a more compact film, is more tenacious, and is on the whole a more effective protective film. Until sufficient velocity is obtained to produce such a coherent film, the PCS surface suffers from corrosion-erosion and dissolution pitting. The average pit size observed on the PCS surface, whether coupled to 70/30

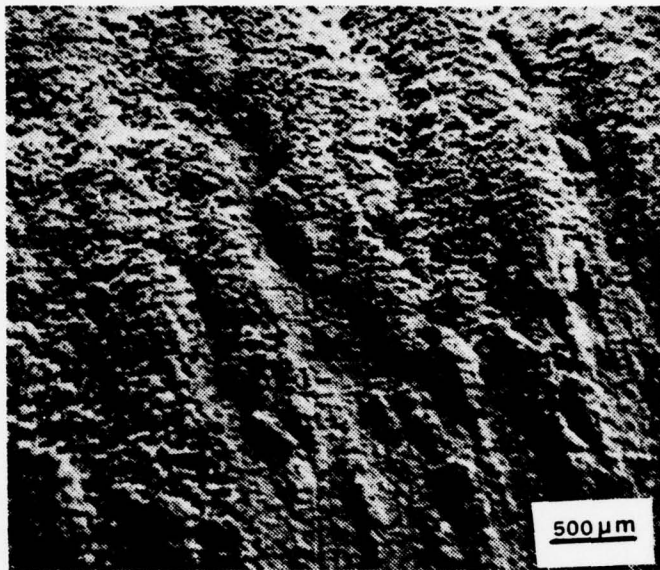


(a)

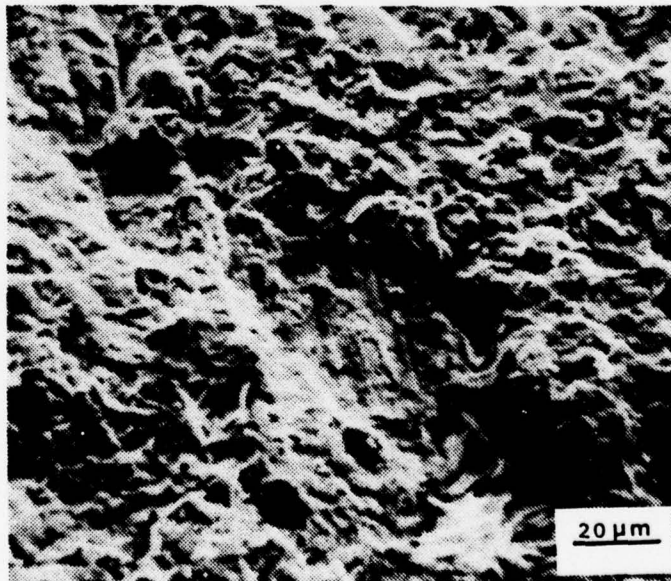


(b)

FIGURE 44: (a) CLEANED SURFACE OF PCS HALF OF 70/30 Cu-Ni/PCS PROXIMATE COUPLE, EXPOSED AT 5 ft/sec (1.52 m/sec) FOR 30 MINUTES, 600x. (b) CLEANED SURFACE OF PCS HALF OF K-MONEL/PCS PROXIMATE COUPLE, EXPOSED AT 10 ft/sec (3.02 m/sec) FOR 30 MINUTES, 600x.

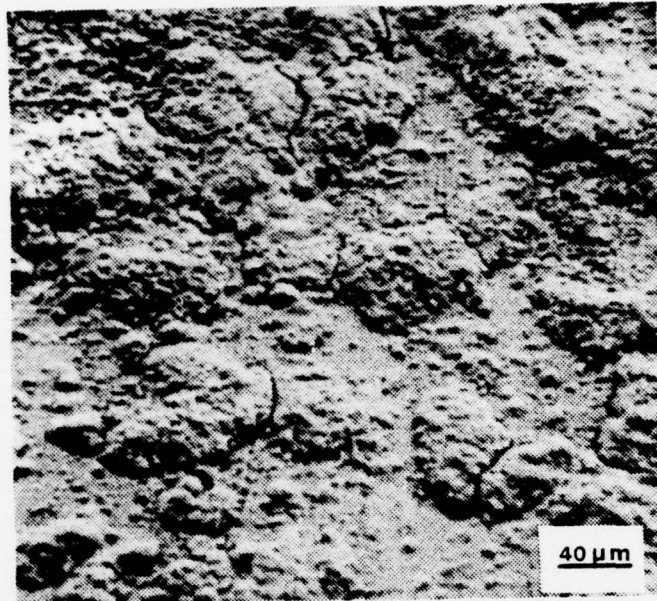


(a)

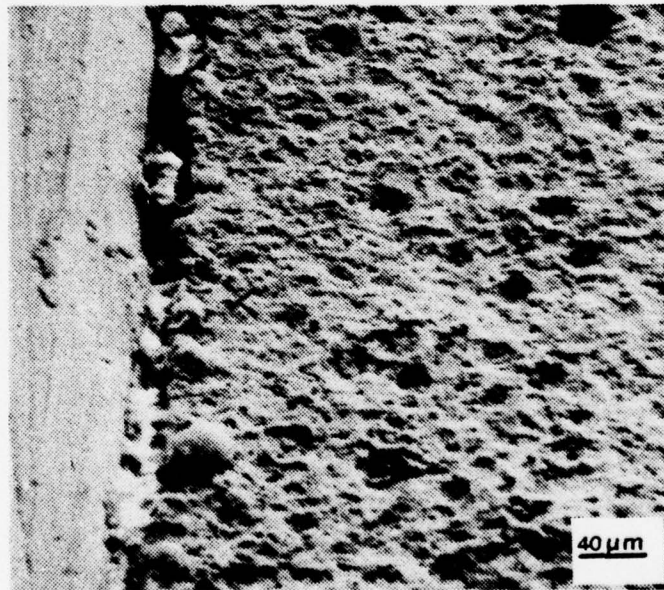


(b)

FIGURE 45: (a) SURFACE OF PCS HALF OF 70/30 Cu-Ni/
PCS PROXIMATE COUPLE EXPOSED AT 5 ft/sec (1.52 m/sec)
FOR 24 HOURS, 20x. (b) CLEANED SURFACE OF PCS HALF
OF 70/30 Cu-Ni/PCS PROXIMATE COUPLE EXPOSED AT 5
ft/sec (1.52 m/sec) FOR 24 HOURS, 600x.

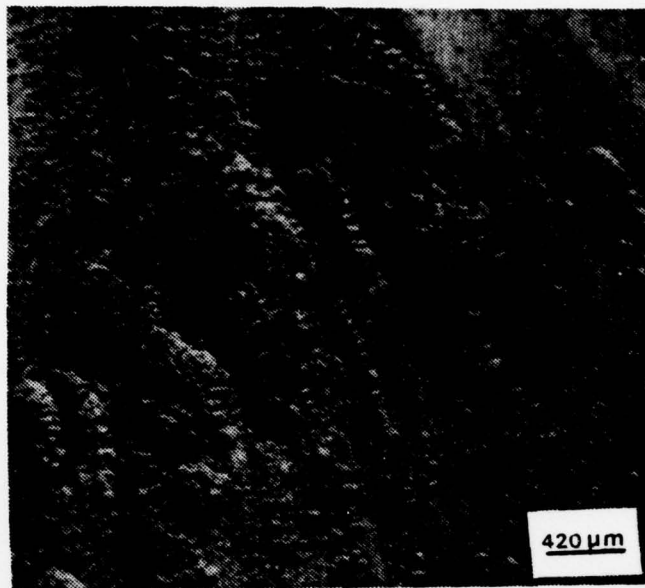


(a)

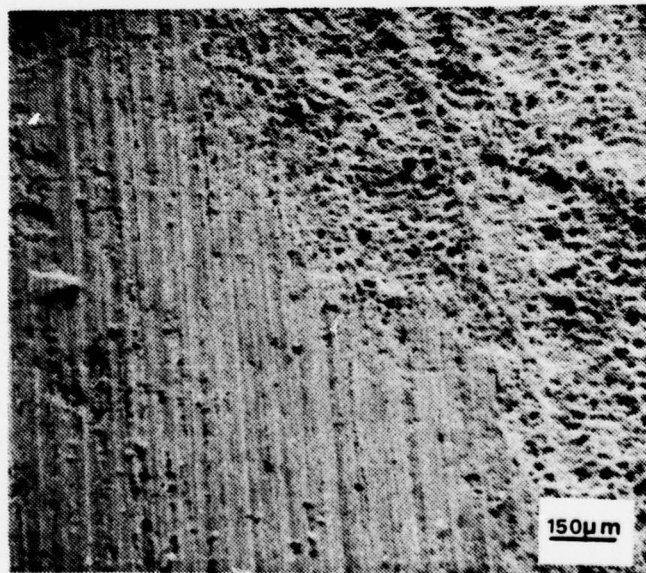


(b)

FIGURE 46: (a) SURFACE OF PCS HALF OF 70/30 Cu-Ni/PCS PROXIMATE COUPLE, EXPOSED AT 10 ft/sec (3.02 m/sec) FOR 24 HOURS, 250x. (b) CLEANED SURFACE OF INTERFACE BETWEEN 70/30 Cu-Ni and PCS IN PROXIMATE COUPLES EXPOSED AT 10 ft/sec (3.02 m/sec) FOR 24 HOURS, 235x.

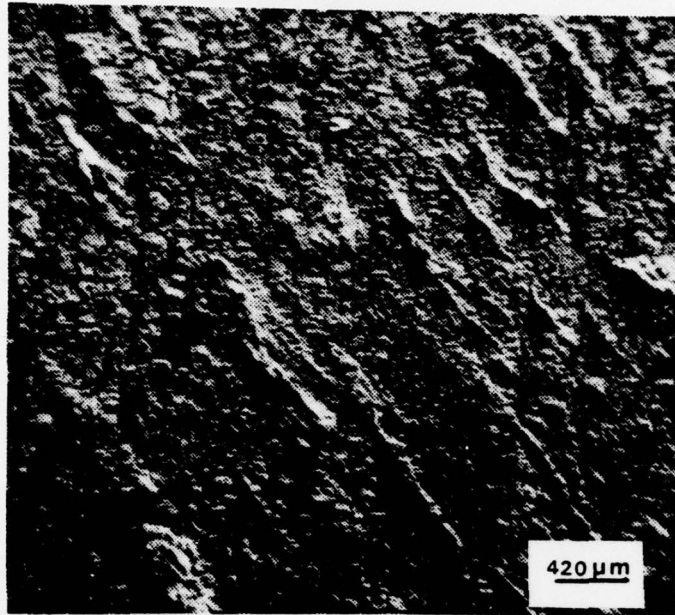


(a)

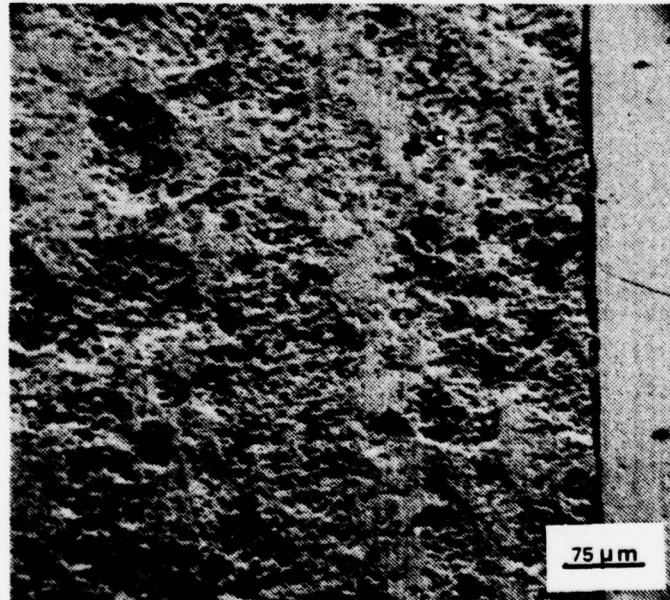


(b)

FIGURE 47: (a) SURFACE OF PCS HALF OF K-MONEL/PCS PROXIMATE COUPLE EXPOSED AT 5 ft/sec (1.52 m/sec) FOR 24 HOURS, 25x. (b) CLEANED SURFACE OF PCS HALF OF K-MONEL/PCS PROXIMATE COUPLE EXPOSED AT 5 ft/sec (1.52 m/sec) FOR 24 HOURS, 60x.



(a)



(b)

FIGURE 48: (a) SURFACE OF PCS HALF OF K-MONEL/PCS PROXIMATE COUPLE EXPOSED AT 10 ft/sec (3.02 m/sec) FOR 24 HOURS, 25x. (b) CLEANED INTERFACE OF K-MONEL/PCS PROXIMATE COUPLE EXPOSED AT 10 ft/sec (3.02 m/sec) FOR 24 HOURS, 125x.

Cu-Ni or K-Monel and regardless of whether exposed at 5 ft/sec (1.52 m/sec) or 10 ft/sec (3.02 m/sec), was 10 to 15 μm in diameter. The increased velocity did not appear to very much change the size of the pits, but did increase the number of pits per unit surface area.

D. SUMMARY OF RESULTS

1. Static vs. Dynamic Exposures

In evaluating the results of static vs. dynamic exposures, certain observed differences are worthy of note. First was the very apparent difference in the color of the corrosion product form. Irrespective of couple composition or configuration, corrosion products on PCS static specimens exhibited a bright orange color. As the velocity was increased to 5 ft/sec (1.52 m/sec) the corrosion product assumed a very dark red-brown appearance. This change in color is apparently due to an increasing rate of oxidation at the PCS surface due to increased oxygen provision [6]. This increase in oxygen supply is assisted by an increased level of turbulence intensity with higher velocity. Second, differences in corrosion product morphology are apparent as the velocity of exposure is varied. Couples (electrical or proximate) exposed to a static environment exhibited a very loosely adherent corrosion product film on the surface of the PCS. When the velocity is increased to 5 ft/sec (1.52 m/sec) the PCS corrosion product takes on an irregular topology and a slightly matted appearance, and after exposure at 10 ft/sec (3.02 m/sec) became very compact in nature and very adherent, Figure 39. Thirdly, the area covered by the PCS corrosion product varied slightly with velocity, with increasing velocity resulting in increased area of coverage (from about 80 percent in static exposure to about 95

percent at 10 ft/sec (3.02 m/sec)). Finally, the type of corrosive attack observed on the surface of the couple varied with velocity. Couples exposed to a static environment suffered a general type of surface corrosion with some scattered pitting, Figure 42, while the couples exposed to varying velocity condition experienced erosion-corrosion and dissolution pitting, Figures 45 through 48.

The many and varied parameters at work during the testing of the couples (electrical and proximate) created a very complex system of actions and reactions, but amid all of the corrosion and fluid dynamic variables, one particular feature on the exposed specimen surfaces remained nearly the same. Specifically, regardless of couple type or configuration, the mean diameter of the smallest observed surface pits was very nearly the same whether tested in static conditions or exposed to a dynamic environment. The number of pits and the severity of the erosion-corrosion varied with velocity, but all couples exposed for 24 hours, regardless of type, exhibited very nearly identical pit diameters (10 to 20 μm). The exact cause for the observed similarities is not known; it is possible that the pearlitic areas in the ferrite-pearlite PCS microstructure (Figure 18) were preferentially attacked. These pearlitic areas were typically 10 to 15 μm in diameter. Once a pearlite region is completely dissolved or otherwise removed, the "hole" left behind would become susceptible to further dissolution by erosion-corrosion mechanisms, particularly as the velocity increases.

2. Electrical vs. Proximate Couples

Little or no difference was noted in the corrosion product morphology and PCS surface attack between the two couple configurations, Figures 38, 39, 45 through 48, in all test conditions.

Any differences based on different cathode components in the couples (70/30 Cu-Ni/PCS and K-Monel/PCS) could not be manifested in visual observations, as the rate of attack appeared to be the same. The only real way to determine any differences would have been to evaluate weight loss data, and this was not done in the conduct of this work. It may be concluded, based on data shown in Figures 25, 26, 31 through 34, that proximate and electrical couples composed of 70/30 Cu-Ni/PCS should experience a higher rate of attack and more severe metal loss than the K-Monel/PCS couple. The SEM data presented was not convincing or conclusive in regards to this prediction, but the measured i_{couple} current densities and E_{couple} values of the two couple types were not so different as to produce an obvious visual dissimilarity for the durations of exposure studied here.

IV. CONCLUSIONS

The following conclusions have been reached as a direct result of this study:

1. Corrosion of galvanic couples is interdependent on internal (microstructural) and extended (electrochemical) variables.
2. At natural galvanic current densities, turbulent flow conditions give rise to a more compact corrosion product formation on PCS anodic members of couples. Film formation, cracking and removal is a cyclical process, dependent upon electrolyte velocity.
3. K-Monel cathodically polarizes more quickly in stagnant seawater electrolyte than does 70/30 Cu-Ni, thereby reducing the corrosion rate of a given coupled anode, in this case PCS.
4. Increases in velocity result in an obvious change in PCS corrosion product color, morphology, and rate of formation. In static conditions, the corrosion product is bright orange in color and quite loosely formed over the PCS surface. As velocity increases, the corrosion product color becomes darker orange (at relatively low velocities), than dark red-brown (at the highest velocity studied here, 10 ft/sec (3.02 m/sec)). Concurrently, the corrosion product morphology changes from an irregular topology and slightly matted condition at 5 ft/sec (1.52 m/sec) to a very compact form at 10 ft/sec (3.02 m/sec). This effect is noted regardless of couple type (70/30 Cu-Ni/PCS or K-Monel/PCS) or couple configuration (electrical or proximate).
5. As the test velocity increases the current density and hence corrosion rate (in MPY) increases in the case of both 70/30 Cu-Ni/PCS and K-Monel/PCS electrical couples.

6. As the velocity of the electrolyte is increased, the PCS half of the proximate and electrical couples suffers from increased attack in the form of erosion-corrosion. Under static condition the PCS surface suffers pitting attack; in the case of proximate couples, the pitting is concentrated somewhat more near the couple interface, rather than being completely and uniformly distributed over the PCS surface as with electrical couples.

V. RECOMMENDATIONS

The results of this study are a first cut at understanding the important interplay between velocity and hydrodynamic effects on the corrosion rate of proximate and electrical couples. Factors of interest in future investigations of the variables should focus on the following considerations:

1. Redesign of the specimen deployment scheme to get weight loss data for comparison with galvanic current density measurements.

2. Redesign of the dynamic exposure apparatus to permit testing at higher velocities for longer periods of time. The new design would include variations in the configuration of the specimen-carrying foil to produce different flow effects and should include attention to the baffling system to continue to minimize rotation of the electrolyte mass at higher velocities.

3. The data matrix could be expanded to include more metal types, couple configurations and intervals of testing in order to more realistically simulate in-service conditions.

4. More detailed characterization of the flow regime would prove enlightening. Instrumentation of not only the foil but also various points in the test tank would more accurately describe the system dynamics and the hydrodynamic effects present.

APPENDIX A

PREPARATION OF ARTIFICIAL SEAWATER

Synthetic standard seawater required during experimentation was prepared using the formula and procedure developed by Kester et. al. [35]. A concentrated stock solution was initially produced for ease in handling prior to use.

The following amounts of gravimetric and volumetric salts, combined with enough distilled water for a total weight of 1 kilogram, were used to produce the synthetic seawater solution.

A. Gravimetric Salts

salt	g/kg of solution
NaCl	23.926
Na ₂ SO ₄	4.008
KCl	0.677
NaHCO ₃	0.196
KBr	0.098
H ₃ BO ₃	0.026
NaF	0.003

B. Volumetric Salts

salt	g/kg of solution	ml/kg of solution
MgCl ₂ ·6H ₂ O	1.000	53.27
CaCl ₂ ·2H ₂ O	1.000	10.33
SrCl ₂ ·6H ₂ O	0.100	0.90

C. Distilled water to bring total weight to 1 kilogram

LIST OF REFERENCES

1. Rogers, T.H., Marine Corrosion, George Newnes Limited, p. 3-30, 1968.
2. Bosich, J.F., Corrosion Prevention for Practicing Engineers, Barnes & Noble, p. 12-90, 1970.
3. Uhlig, H.H., Corrosion and Corrosion Control, John Wiley & Sons, Inc., p. 20-214, 1971.
4. Tuthill, A.H., and Schillmoller, C.M., Guidelines for Selection of Marine Materials, The International Nickel Company, p. 17, May 1971.
5. Tomashov, N.D., Theory of Corrosion and Protection of Metals, The MacMillan Company, p. 271-324; 454-481, 1966.
6. Butler, G. and Ison, H.C.K., Corrosion and its Prevention in Waters. Reinhold Publishing Corporation, p. 132-138, 1966.
7. Monney, N.T., "Deep Ocean Corrosion-Simulation Facilities vs. In-Situ Research", Materials Protection and Performance, V. 12, No. 1, p. 10-13, Jan 1973.
8. Naval Civil Engineering Laboratory Technical Note N-907, The Effect of Environment on the Corrosion of Metals in Sea-Water - A Literature Survey, by H.A. Porte, p. 2-11, Jul 1967.
9. Fontana, M., and Green, N., Corrosion Engineering, McGraw-Hill Book Company, p. 76-80; 300-310, 1967.
10. National Association of Corrosion Engineers, NACE Standard TM-01-69, Test Method: Laboratory Corrosion Testing of Metals for the Process Industries, 1969.
11. Cornet, I., Velocity Effects in Corrosion, Paper presented at International Corrosion Forum Devoted to the Protection and Performance of Materials, San Francisco, California, 14-18 Mar 1977.
12. Syrett, B.C., "Erosion-Corrosion of Copper-Nickel Alloys in Sea Water and Other Aqueous Environments - A Literature Review", Corrosion, V. 32, p. 242-250, Jun 1976.
13. Davis, J.A. and others, Review of High Velocity Sea Water Corrosion T-7C-5 Task Group Report, Paper 101 presented at International Corrosion Forum, San Francisco, California, 14-18 Mar 1977.
14. Copson, H.R., "Effects of Velocity on Corrosion", Corrosion, V. 16, p. 86t-92t, Feb 1960.

15. Naval Engineering Laboratory Report 72/64, The Corrosion of Metals as a Function of Sea-Water Velocity, by J.L. Basil, p. 1-11, 10 Jul 1964.
16. U.S. Naval Engineering Experiment Station Report 910160A, Corrosion of Materials in High Velocity Sea Water, by J.L. Basil, p. 6, 30 Dec, 1960.
17. Danek, G.J. Jr., "The Effect of Sea-Water Velocity on the Corrosion Behavior of Metals", Naval Engineers Journal, p. 763-769, Oct 1966.
18. Bell Aerospace Company, Ocean City Research Corporation Final Report 1-35551, Cathodic Protection of Surface Effect Ships at High Speeds, by Bell Aerospace Company, p. 65, Sep 1975.
19. Davis, J.A. and Gehring, G.A. Jr., Materials Performance, V. 14, p. 32, 1975.
20. Davis, J.A. and Gehring, G.A. Jr., Corrosion/75, Paper No. 123, Toronto, Canada, 14-18 Apr 1975.
21. Davis, J.A. and Gehring, G.A. Jr., Corrosion/76, Paper No. 75, Houston, Texas, 22-26 Mar 1976.
22. Efird, K.D., Paper presented at the Corrosion Research Conference of Corrosion/76, Houston, Texas, 22-26 Mar 1976.
23. Davis, J.A., Watts, A.A. and Gehring, G.A. Jr., Paper presented at the Electrochemical Society 150th Annual Conference, Las Vegas, Nevada, 18-22 Oct 1976.
24. Cornet, I., Barrington, E.A. and Behrsing, Journal of the Electrochemical Society, V. 108, p. 947, 1961.
25. Beck, T.R., Corrosion/76, Paper No. 77, Houston, Texas, 22-26 Mar 1976.
26. Heitz, E., Werk Stoffe u Korrosion, V. 15, p. 63, 1964.
27. Kievits, F.J., Ysseling, F.P. Van de Berg, P.J.A. and Wisse, W., Institute of Metals International Conference, Proceedings, London, England, p. 345, 1970.
28. Ross, T.K., Wood, G.C. and Mahmud, I., Journal of the Electrochemical Society, V. 113, p. 334, 1966.
29. Ross, T.K. and Jones, D.H., Journal of Applied Chemistry, V. 12, p. 314, 1962.
30. Ross, T.K. and Hitchen, B.P.L., Corrosion Science, V. 1, p. 65, 1965.
31. Todd, J.M. and Perkins, A.J., "Corrosion of Zinc Anodes in Seawater", Naval Engineers Journal, p. 65-72, Aug 1976.

32. Luebke, W.H., A Scanning Electron Microscope Study of the Effects of Anode Velocity and Current Density on the Corrosion of Ship Hull Zinc in Synthetic Seawater, MSME-Mechanical Engineer Thesis, Naval Postgraduate School, Jun 1976.
33. Wright, P.W., A Scanning Electron Microscope Study of the Corrosion of Sacrificial Hull Anodes under Simulated Ship Service Conditions, MSME-Mechanical Engineer Thesis, Naval Postgraduate School, Dec 1976.
34. Cambridge Scientific Instrument Limited, Operating Instructions for Stereoscan Scanning Electron Microscope, Manual No. TL1116-OM-96118-000Z, Issue 1, Section 1.1.
35. Kester, D.R., Duedall, I.W., Conners, D.N. and Pytkowicz, R.M., "Preparation of Artificial Seawater", Limnology and Oceanography, V. 12, p. 176-178, Dec 1967.
36. Beckwith, T.G. and Buck, N.L., Mechanical Measurements, Addison-Wesley Publishing Company, p. 411-437, 1973.
37. Thermo Systems Incorporated, Anemometry, p. 1-14, 1973.
38. Rogers, T.W., The Marine Corrosion Handbook, McGraw-Hill Company of Canada Limited, p. 239-240, 1960.
39. Shreir, L.L. and others, Corrosion, V. 1, Newnes-Butterworths, p. 170-175, 1976.
40. Gerischer, H., "Metal and Semiconductor Electrode Processes", The Surface Chemistry of Metals and Semiconductors, H. Gatos, editor, p. 177-204, 1960.
41. Petrocelli, J.V., "Electrochemistry of Dissolution Processes", The Surface Chemistry of Metals and Semiconductors, H. Gatos, editor, p. 326-356, 1960.
42. Ailor, W.H., Handbook on Corrosion Testing and Evaluation, John Wiley and Sons, p. 174, 1971.
43. Price, J.M., A Potentiokinetic Determination of Corrosion Rates in Artificial Seawater-Hypochlorite Solutions, MS-Physics Thesis, Naval Postgraduate School, Jun 1976.

INITIAL DISTRIBUTION LIST

	No. Copies
1. Defense Documentation Center Cameron Station Alexandria, Virginia 22314	2
2. Library, Code 0412 Naval Postgraduate School Monterey, California 93940	2
3. Department Chairman, Code 59 Department of Mechanical Engineering Naval Postgraduate School Monterey, California 93940	2
4. Professor A.J. Perkins, Code 59Ps Department of Mechanical Engineering Naval Postgraduate School Monterey, California 93940	6
5. Professor T. Sarpkaya, Code 59S1 Department of Mechanical Engineering Naval Postgraduate School Monterey, California 93940	1
6. Mr. Tom Christian, Code 59 Department of Mechanical Engineering Naval Postgraduate School Monterey, California 93940	1
7. Mr. George Bixler, Code 59 Department of Mechanical Engineering Naval Postgraduate School Monterey, California 93940	1
8. LT. Gary A. Storm COMNAVACTSUK, Box 84 FPO, New York 09510	3